UNIVERSITI TEKNOLOGI MARA

DEEP CONVOLUTIONAL NEURAL NETWORK-BASED ENHANCEMENT OF DIGITAL BREAST TOMOSYNTHESIS IMAGES

NUR ATHIQAH HARRON

PhD

April 2026

UNIVERSITI TEKNOLOGI MARA

DEEP CONVOLUTIONAL NEURAL NETWORK-BASED ENHANCEMENT OF DIGITAL BREAST TOMOSYNTHESIS IMAGES

NUR ATHIQAH HARRON

Thesis submitted in fulfilment
of the requirements for the degree of
Doctor of Philosophy
(Electrical Engineering)

Faculty of Electrical Engineering

April 2026

CONFIRMATION BY PANEL OF EXAMINERS

I certify that a Panel of Examiners has met on 15th January 2026 to conduct the final examination of Nur Athiqah Harron on her Doctor of Philosophy thesis entitled "Deep Convolutional Neural Network-Based Enhancement of Digital Breast Tomosynthesis Images" in accordance with Universiti Teknologi MARA Act 1976 (Akta 173). The Panel of Examiners recommends that the student be awarded the relevant degree. The Panel of Examiners was as follows:

Mohd Hanapiah Abdullah, PhD
Associate Professor
Faculty of Electrical Engineering
Universiti Teknologi MARA
(Chairman)

Zakaria Hussain, PhD
Associate Professor
Faculty of Electrical Engineering
Universiti Teknologi MARA
(Internal Examiner)

Syed Sahal Nazli Alhady Syed Hassan, PhD
Associate Professor
School of Electrical and Electronic Engineering
Universiti Sains Malaysia
(External Examiner)

PROFESSOR DR HJH ZURAEDA IBRAHIM
Dean
Institute of Postgraduate Studies
Universiti Teknologi MARA
Date: 7 April 2026

AUTHOR'S DECLARATION

I declare that the work in this thesis was carried out in accordance with the regulations of Universiti Teknologi MARA. It is original and is the result of my own work, unless otherwise indicated or acknowledged as referenced work. This thesis has not been submitted to any other academic institution or non-academic institution for any degree or qualification.

I hereby acknowledge that I have been supplied with the Academic Rules and Regulations for Post Graduate, Universiti Teknologi MARA, regulating the conduct of my study and research.

Name of Student	:	Nur Athiqah binti Harron
Student I.D. No.	:	2021981929
Programme	:	Doctor of Philosophy (Electrical Engineering) – EE950
Faculty	:	Electrical Engineering
Thesis Title	:	Deep Convolutional Neural Network-Based Enhancement of Digital Breast Tomosynthesis Images
Signature of Student	:	……..
Date	:	April 2026

ABSTRACT

Digital Breast Tomosynthesis (DBT) has emerged as a powerful imaging modality for early breast cancer detection, particularly in women with dense breast tissue. DBT captures multiple projection images over a limited angular range, enabling a quasi-3D reconstruction of the breast. However, this limited-angle acquisition introduces image artifacts, most notably blurring and low contrast in the reconstructed slices, which can obscure critical diagnostic features such as microcalcifications, which are early indicators of breast cancer. As a result, diagnostic accuracy is compromised, and the workload on radiologists increases significantly due to the need to manually examine a large number of slices. To address these challenges, this research presents a novel deep learning-based image enhancement framework designed to enhance the visibility of microcalcifications in DBT images. The study is divided into two main phases. In the first phase, a hybrid blur detection model, referred to as the Convolutional Neural Network–Support Vector Machine–Blur Factor (CNNSVM-BF), is developed by combining features extracted from a lightweight Convolutional Neural Network (CNN) with a handcrafted Laplacian-based Blur Detection (LbBD) algorithm. These hybrid features are classified using a Support Vector Machine (SVM), which enables the accurate detection of blurry slices and allows for the exclusion of low-quality images from subsequent analysis. This selective approach not only reduces computational burden but also mirrors the practical workflow of radiologists who often ignore visibly blurry slices. In the second phase, non-blurry (sharp) slices are subjected to a microcalcification contrast enhancement pipeline that includes two steps; first, an Unsharp Masking Very Deep Super Resolution (UMVDSR) model is applied to improve global image clarity. Second, a newly proposed Microcalcification Contrast Enhancement (McCE) algorithm is introduced as a post-processing step, specifically designed to enhance the contrast and visibility of microcalcification regions, enabling better lesion detectability while preserving anatomical structures. The proposed Deep CNN-based enhancement framework is evaluated using publicly available Breast Cancer Screening Digital Breast Tomosynthesis (BCS-DBT) dataset, as well as a custom dataset collected at the Advanced Medical and Dental Institute Digital Breast Tomosynthesis (AMDI-DBT). The results demonstrate substantial improvements in both microcalcification visibility and overall image quality, achieving a peak signal-to-noise ratio (PSNR) of 47.6454 and a structural similarity index measure (SSIM) of 0.9995. Compared to baseline methods, the proposed approach exhibits a significant improvement in image clarity and microcalcification detectability. These quantitative results, supported by qualitative assessments from expert radiologists, confirm the statistical significance of the enhancement and underscore the potential integration of the proposed intelligent system into clinical CAD workflows for more accurate and early breast cancer diagnosis. In conclusion, the proposed Deep CNN-based enhancement framework holds promise for integration into computer-aided diagnosis systems, supporting early detection of breast cancer in clinical practice.

ACKNOWLEDGEMENT

In the name of Allah S.W.T, the Most Gracious, the Most Merciful. I am truly grateful for His blessings, which have granted me the strength, health, and opportunity to embark on and complete this long and challenging PhD journey.

First and foremost, I would like to express my deepest gratitude to my supervisor, Prof. Ir. Ts. Dr. Siti Noraini Sulaiman, for her unwavering support, patience, guidance, and encouragement throughout the completion of this study. Her flexibility, compassion, and willingness to pass on knowledge have allowed me to grow both academically and personally. I am sincerely thankful for her insightful comments, constructive feedback, and constant motivation, which have been invaluable to the success of this research.

My heartfelt appreciation also extends to my co-supervisory team: Assoc. Prof. Dr. Muhammad Khusairi Osman, Assoc. Prof. Dr. Noor Khairiah A. Karim, and Assoc. Prof. Ir. Dr. Iza Sazanita Isa, for their expertise, thoughtful feedback, and guidance. Their contributions have greatly enriched the quality and depth of this work.

I am also indebted to the staff of the Advanced Medical and Dental Institute (AMDI), especially Suzana Ismail, for their invaluable assistance, technical support, and the provision of essential facilities. My special thanks go to my colleagues and friends from the Advanced Control System and Computing Research Group (ACSCRG) and the Centre for Electrical Engineering Studies, UiTM Pulau Pinang, for their collaboration, ideas, and encouragement, which have helped me advance my research.

To my beloved husband, Halim b. Wasoh, thank you for your unwavering support, patience, and understanding throughout my daily struggles. My deepest love and appreciation also go to my children, Sofiyyah, Umar, Zahra, and Aqeb, who have been constant sources of inspiration, strength, and joy in my life.

This thesis is lovingly dedicated to the beautiful memory of my late mother, and to my father, Hj. Harron b. Osman, whose vision, sacrifice, and encouragement have shaped who I am today. I am eternally grateful for their love and support. A special note of thanks is due to my dear sister, Nurhafizah, for her kindness, companionship, and assistance during conferences.

Finally, I dedicate this work to my family members and friends for their continuous encouragement and prayers, with special appreciation to the truly wonderful friends I have been blessed with: Aini Hafizah, Siti Azura, Anith Nuraini, Dayang Suhaida, Syafiqah Aqilah, Nur Najiha, and Nurul Huda.

Thank you for your support, encouragement, ideas, and comments for the accomplishment of this project. This victory is dedicated to all of you. Alhamdulillah.

TABLE OF CONTENTS

LIST OF TABLES

LIST OF FIGURES

LIST OF SYMBOLS

Symbols

C	Box Constraint
E(i,j)	Enhanced Output Image
I(i,j)	Original Input Image
Th	Threshold
γ	Kernel Scale
μx	X Image Means
μy	Y Image Means
σx	X Standard Deviations
σxy	Covariance
σy	Y Standard Deviations

LIST OF ABBREVIATIONS

Abbreviations

AUC	Area Under the ROC Curve
BF	Blur Factor
CLAHE	Contrast-Limited Adaptive Histogram Equalization
CNN	Convolutional Neural Network
dB	Decibels
DBT	Digital Breast Tomosynthesis
DBToR	DBT Reconstruction CNN
FN	False Negative
FP	False Positive
FPR	False Positive Rate
FWHM	Full Width at Half Maximum
GAN	Generative Adversarial Network
HaarPSI	Haar Wavelet-Based Perceptual Similarity Index
HE	Histogram Equalization
McCE	Microcalcification Contrast Enhancement
PSNR	Peak Signal-to-Noise Ratio
RMSE	Root Mean Square Error
ROC	Range of Operating Characteristics
ROI	Region of Interest

SSIM	Structural Similarity Index Measure
SVM	Support Vector Machine
TN	True Negative
TP	True Positive
TPR	True Positive Rate
UM	Unsharp Masking
VDSR	Very Deep Super Resolution

CHAPTER 1
INTRODUCTION

1.1 Research Background

Breast cancer is one of the most common and deadly cancers affecting women globally. Early detection through effective screening significantly improves treatment outcomes and survival rates. Mammography has long been the standard screening tool for breast cancer; however, its effectiveness is limited, especially in cases where breast tissue is dense or when overlapping structures obscure lesions. This limitation is especially pronounced in dense breast tissue but affects all breast types to some extent.

Digital Breast Tomosynthesis (DBT) is an advanced breast cancer screening and diagnostic modality that acquires multiple low-dose X-ray projections over a limited angular range. These projections are reconstructed into quasi-three-dimensional cross-sectional images, offering improved visibility of overlapping dense tissues compared to conventional mammography [1]. This capability is particularly valuable for evaluating fibroglandular tissue in women with dense breasts, a common diagnostic challenge in breast imaging. However, DBT images are frequently affected by blurring artifacts during reconstruction caused by the limited-angle acquisition process. These artifacts can obscure early-stage cancer indicators, such as microcalcifications, thereby degrading the overall diagnostic performance [2].

Since DBT relies on X-ray acquisition, optimizing image quality while minimizing radiation exposure is a constant trade-off. Blurring artifacts often obscure subtle abnormalities and are more pronounced in dense breast tissue, making accurate detection more challenging [3]. Traditional image restoration methods, such as total variation-based iterative techniques and higher-order derivative models, have attempted to correct this [4]. However, these approaches often demand high computational resources and are sensitive to variations in noise, beam hardening, and X-ray scatter. Additionally, they typically require the estimation of a blur kernel, an ill-posed task that can introduce new artifacts if inaccurately defined [5]. Figure 1.1 illustrates a DBT image with blurring, an image in which most of the breast region is affected, and microcalcifications in the posterior lower breast that were not identified remain undetected.

Furthermore, blur detection has emerged as a critical and compelling area in medical imaging, particularly in modalities such as DBT, where image quality directly impacts diagnostic accuracy. A key challenge in blur detection lies in identifying discriminative features that can reliably differentiate between blur (distorted) and non-blur (sharp) image regions. Most conventional approaches address this issue through a two-stage process: initially segmenting image components using gradient-based empirical data, followed by applying a binary classifier to separate blurred from sharp regions [6]. Unlike general image recognition tasks, which often involve multiple degradation factors (e.g., noise, blur), blur detection focuses specifically on blur-related distortions, necessitating robust feature extraction that can manage the significant variance introduced by diverse image content. Convolutional Neural Networks (CNNs), known for their ability to learn hierarchical feature representations, have demonstrated superior performance over traditional handcrafted techniques, such as HOG or SURF, in this domain [7].

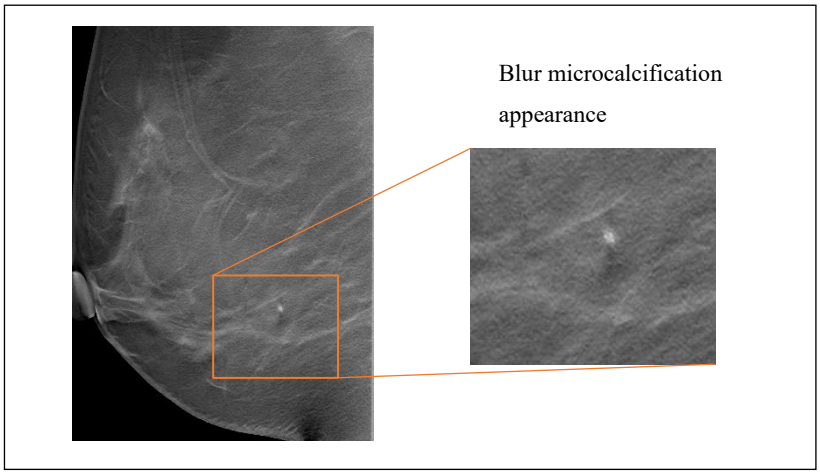

Figure 1.1 An Example of a DBT Blurring Image with Microcalcification

Recent advances in artificial intelligence and deep learning have transformed the field of image processing and computer vision. CNNs have outperformed traditional methods across a wide range of tasks, including denoising[8], deblurring [9], [10], super-resolution[11], object detection[12], and segmentation[13]. These models excel due to their ability to learn complex feature hierarchies directly from raw input data without the need for handcrafted features. When trained on large datasets, such as ImageNet, CNNs can develop robust and generalizable representations of visual data, often surpassing conventional feature-based methods in accuracy and efficiency [14].

The motivation for this study stems from the persistent challenge of poor image quality in DBT and the critical need for reliable enhancement methods. According to the [15] World Health Organization (WHO), breast cancer accounted for 2.3 million new cases and 670,000 breast cancer-related deaths globally in 2022, highlighting the importance of improved diagnostic tools. In Malaysia alone, a summary of the Malaysia National Cancer Registry 2017-2021 reported that breast cancer is the most commonly diagnosed cancer among females, starting at age 40, with nearly 16,430 women at risk [16].

Within DBT workflows, radiologists manually examine numerous image slices per patient, a laborious and time-consuming process that increases fatigue and the risk of oversight, especially when abnormalities are subtle or appear only in a few slices [17]. Clinically, radiologists interpret large volumes of medical images under time and workload constraints. Increased imaging utilization has been associated with heightened interpretation demand and risk of burnout, leading clinicians to adjust reading strategies by focusing on diagnostically informative, higher-quality image slices and deprioritizing suboptimal or blurred images that contribute little diagnostically but add interpretation time [18]. Poor image quality is also recognized as a factor in increased cognitive load and diagnostic error, which further motivates radiologists to emphasize clearer image slices when possible to maintain efficiency and accuracy in clinical practice [19]. Effective blur detection would exclude or enhance low-quality slices, thereby improving reading efficiency and diagnostic focus. Additionally, Artificial Intelligence Computer-Aided Diagnosis (AICAD) systems that incorporate Deep CNN for image enhancement help reduce reading times without significantly compromising sensitivity, specificity, or recall rates, with reductions in reading times ranging from 14 to 40 percent [14]–[16]. However, a huge number of datasets with uncertain or poor-quality images increases the computational load and reduces screening throughput due to reader fatigue. Accordingly, ensuring that only high-quality images are included is essential for achieving optimal performance in computer-aided diagnosis (CAD) systems.

Despite its clinical importance, automated blur detection and restoration in DBT remain relatively under-researched, particularly when employing deep learning-based approaches. Addressing this gap, the current study proposes a hybrid CNNSVM model for both blur detection and microcalcification contrast enhancement in DBT images. The model aims to enhance image clarity by utilizing CNNs for deep feature extraction

and a Support Vector Machine (SVM) classifier for precise blur classification. Specifically, this hybrid model integrates two complementary feature sets: (1) a Laplacian-based blur factor and (2) high-level visual features extracted by the CNN. This fusion enables robust and accurate detection of blurry slices. Following blur detection, a deep CNN-based local contrast enhancement model is applied exclusively to non-blurry images to boost microcalcification visibility. Since microcalcification clusters are critical indicators of early-stage breast cancer, enhancing their contrast can significantly improve detection accuracy and clinical decision-making. The final model will be evaluated through standard performance metrics, including the Receiver Operating Characteristic (ROC) curve and precision-recall analysis. Additionally, radiologists will perform qualitative validation of the enhanced images to ensure clinical relevance and usability.

In summary, this research presents a novel Deep CNN-based enhancement framework consisting of a two-stage pipeline for DBT imaging that reduces dependence on blur kernel estimation, enhances image quality in dense tissues, and improves the accuracy of microcalcification detection. By automating blur detection and tailoring enhancement to diagnostically relevant slices, the proposed approaches also reduce the radiologist's workload, ultimately contributing to more efficient and accurate breast cancer diagnosis.

1.2 Problem Statement

DBT has emerged as a widely used modality for early breast cancer diagnosis due to its ability to generate quasi-three-dimensional images and reduce tissue overlap, which is a standard limitation in traditional mammography. However, DBT acquires projection data over a limited angular range to minimize patient radiation exposure. This constrained acquisition introduces blurring and low-contrast artifacts in the reconstructed slices, particularly in the z-direction, where out-of-plane structures appear as smeared features due to tube motion [2], [20]. Figure 1.2 compares the reconstructed DBT image and the reference image. Note that the effect of challenging image blurring on lesion detectability is observable.

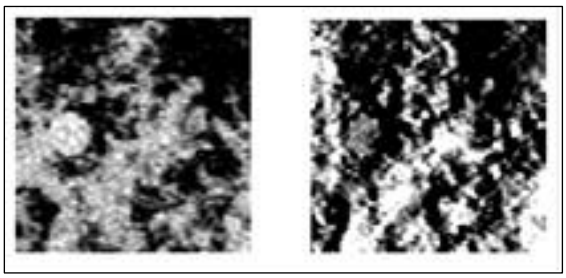

Figure 1.2 Reference Image (left) and DBT Image (right) [21].

These artifacts significantly hinder the visibility of small and subtle lesions, such as microcalcifications, especially in women with extremely dense fibroglandular tissue. As a result, it becomes difficult to distinguish malignant features in blurry, low-contrast DBT images, leading to reduced diagnostic confidence and an increased number of false negatives [20]. Consequently, minimizing or eliminating blur and contrast-related artifacts is essential for improving lesion detectability and overall diagnostic accuracy in DBT-based screening [22]. In routine clinical practice, radiologists frequently exclude severely blurred DBT slices from interpretation and concentrate on visually clearer slices. While this practice helps mitigate diagnostic uncertainty, it is subjective, time-consuming, and dependent on individual experience. This highlights a fundamental problem: there is currently no reliable, automated, and objective mechanism to identify and manage blurry DBT slices prior to diagnostic interpretation. Developing such a mechanism is challenging because blur in DBT is not uniform; it varies across slices, anatomical regions, and tissue compositions, making image quality assessment a complex, content-dependent problem.

Existing blur detection techniques primarily rely on handcrafted features derived from gradient, frequency, or edge-based statistics, followed by conventional classifiers. These approaches typically require extensive feature engineering, are sensitive to image content variations, and exhibit limited generalization when applied to complex medical images such as DBT [6]. As a result, their effectiveness in accurately detecting blur across heterogeneous DBT datasets remains inadequate. Recent advances in deep learning, particularly Convolutional Neural Networks (CNNs), have demonstrated superior performance in learning hierarchical and content-aware representations directly from raw image data. CNN-based methods have consistently outperformed traditional handcrafted approaches such as HOG or SURF in various image analysis tasks [7]. However, despite their success in general image processing, the application of CNN-based blur detection specifically tailored to DBT images

remains insufficiently explored, particularly in the context of dense breast tissue and microcalcification visibility.

Furthermore, while image enhancement techniques have been proposed to improve DBT image contrast, existing studies often treat blur detection and contrast enhancement as independent problems [20], [23]–[25]. There is a lack of integrated frameworks that first identify diagnostically unreliable (blurry) slices and then selectively enhance clinically relevant features, such as microcalcifications, in diagnostically usable slices. This gap limits the effectiveness of current DBT enhancement strategies and their alignment with real-world radiological workflows. Motivated by these challenges, this thesis addresses the following core research problems: (i) How to automatically and robustly detect blurred DBT slices in a content-aware manner without relying on handcrafted features. (ii) How to enhance microcalcification visibility in DBT images while preserving surrounding anatomical structures, particularly in dense breast tissue. (iii) How to integrate blur detection and enhancement into a unified, clinically relevant framework that supports radiologists' diagnostic decision-making.

The central hypothesis of this research is that a deep CNN-based approach can learn discriminative blur-sensitive features directly from DBT images and, when combined with targeted microcalcification contrast enhancement, can significantly improve image quality and diagnostic utility. By automatically filtering or flagging blurred slices and selectively enhancing diagnostically relevant structures, the proposed framework is expected to reduce false negatives and improve radiologist confidence. Accordingly, this research proposes a novel deep CNN-based framework for automated blur detection and microcalcification contrast enhancement in DBT images. The effectiveness and clinical relevance of the proposed approach are validated through quantitative evaluation and expert assessment by experienced radiologists, ensuring its practical applicability in DBT-based breast cancer screening workflows.

1.3 Research Objectives

The primary aim of this study is to design a new deep CNN-based enhancement framework that can perform blur detection and microcalcification contrast enhancement tasks, specifically for distinguishing microcalcifications in DBT images. To achieve this

aim, the work will be divided into several stages and carried out systematically with associated research objectives that have been identified as follows: -

i) To develop a hybrid deep feature–based blur detection method for DBT images by combining discriminative features learned from a custom-designed CNN with a Support Vector Machine (SVM) classifier, for blurry detection of DBT images.
ii) To enhance blur detection robustness and generalization by integrating explicit blur-related descriptors (blur factors) with CNN-extracted deep features, in (i).
iii) To model a new CNN-based microcalcification contrast enhancement technique that selectively enhances clinically significant microcalcification regions while preserving surrounding anatomical structures in DBT images.
iv) To comprehensively validate the proposed framework through quantitative performance evaluation using standard image quality and classification metrics, complemented by qualitative assessment from expert radiologists to demonstrate clinical relevance, diagnostic reliability, and practical applicability.

1.4 Research Scope and Limitation

This research focuses on the enhancement of DBT images using deep CNNs to improve image quality and diagnostic accuracy in breast cancer detection. Specifically, the research focuses on detecting blurring artifacts and enhancing microcalcification contrast in DBT images. The scope of this study includes:

i) Image acquisition and data collection:

The algorithm developed in this study was trained using a publicly available DBT dataset referenced in [26], which can be accessed via the Cancer Imaging Archive at https://rb.gy/ygnho7. In addition to this public dataset, the proposed methodology was tested on clinical DBT images obtained from the Advanced Medical and Dental Institute (AMDI), Universiti Sains Malaysia (USM), Bertam, under ethical approval. All images were collected retrospectively, and no individual patient interaction, such as interviews or clinical assessments, was conducted before, during, or after image acquisition.

All DBT images used in this study were in the standard Digital Imaging and Communications in Medicine (DICOM) format, which includes essential metadata for maintaining image integrity and diagnostic context. The specific patient selection criteria and data preprocessing steps are described in detail in Chapter 3, Methodology.

ii) Method Selection:

To address the challenges identified in DBT image quality, this study adopts a methodological approach grounded in recent advancements in artificial intelligence and image processing. First, the limitations of existing blur detection and contrast enhancement techniques in DBT imaging are critically examined to identify performance gaps and clinical shortcomings. Building on these insights, a hybrid model is designed that leverages CNNs for deep, data-driven feature extraction and SVMs for accurate blur classification. This hybrid approach combines the strengths of both methods, enabling robust classification performance across varying tissue densities and image conditions. To further enhance blur detection accuracy, a Laplacian-based blur factor is integrated with CNN-extracted features, creating a complementary feature set that improves model sensitivity to subtle degradations. In the subsequent stage, a CNN-based local contrast enhancement model is developed specifically to improve the visibility of microcalcifications in non-blurry DBT slices, thereby supporting the early detection of breast cancer in patients with dense breast tissue. The final output flags blurry images and enhances diagnostically relevant regions, enabling clinicians to identify early signs of breast cancer with improved efficiency and consistency.

iii) Evaluation and analysis:

The proposed model will undergo a comprehensive evaluation to assess its effectiveness, reliability, and clinical relevance. Quantitative validation will be conducted using standard performance metrics widely adopted in medical image analysis, including the Receiver Operating Characteristic (ROC) curve, Area Under the Curve (AUC), precision-recall (PR) curve, accuracy, sensitivity, specificity, and F1-score. These metrics will provide a detailed understanding of the model's performance in both blur detection and microcalcification contrast enhancement tasks, particularly under varying conditions of breast density and image quality. The evaluation will be performed on both public and clinical datasets to ensure robustness and generalizability.

In addition to quantitative analysis, qualitative validation will be carried out through expert review by certified radiologists. These experts will assess the enhanced DBT images for diagnostic quality, clarity, and the visibility of microcalcifications, comparing original and processed slices. Their feedback will be used to evaluate the clinical usability of the system and to identify any potential artifacts or distortions introduced during the enhancement process. This two-tier evaluation approach, combining statistical performance metrics with expert human judgment, ensures that the developed model is not only technically sound but also clinically meaningful.

iv) Model development platform:

The proposed automated framework is developed using MathWorks: MATLAB© version R2022b (MATLAB) software, utilizing its Image Processing and Deep Learning Toolboxes to implement the whole framework. The computer hardware used is equipped with a graphics processor and memory with a maximum capacity of 12GB and 32GB, respectively.

v) Limitations:

To maintain methodological focus and clinical relevance, the scope of the study is intentionally defined with specific boundaries and limitations. This study is limited to the analysis of two-dimensional reconstructed DBT slices and does not model full three-dimensional volumetric relationships or inter-slice consistency. The blur detection framework addresses motion- and reconstruction-induced blur associated with limited-angle DBT acquisition, while other degradation sources such as quantum noise, detector artifacts, and compression effects are not considered. The microcalcification contrast enhancement model is applied only to diagnostically acceptable (non-blurry) slices, and severely blurred images are excluded from enhancement. Model development and evaluation are conducted using a limited number of public and institution-specific DBT datasets, which may affect generalisability across different scanners, vendors, and patient populations. Finally, the proposed framework functions as a decision-support tool and does not perform lesion classification or autonomous cancer diagnosis.

1.5 Thesis Layout

This thesis is organized into five chapters, each of which systematically addresses a critical phase of the research. Chapter 1 provides an introduction to the study, establishing the context and motivation for the research by presenting the background, problem statement, research objectives, scope, and overall significance. This chapter frames the need for an automated image processing approach to enhance diagnostic accuracy in DBT, particularly in the detection of microcalcifications within dense breast tissue.

Chapter 2 delivers a comprehensive literature review, critically analyzing current methods for blur detection, image contrast enhancement, and deep learning applications in medical imaging. The review identifies key gaps in existing techniques, such as reliance on manual interpretation and limitations in traditional kernel-based deblurring methods, thereby substantiating the need for a hybrid CNNSVM model tailored to DBT images.

Chapter 3 outlines the methodology employed in the study. It describes the datasets used, including publicly available and clinically obtained DBT images, the framework development environment, and the detailed design of the proposed hybrid model. The chapter explains how CNNs are employed for deep feature extraction, how blur factors are integrated, and how the SVM is used for classification. It also discusses the contrast enhancement strategy for microcalcification visibility and elaborates on the evaluation framework used to measure model performance.

Chapter 4 presents the experimental results and analysis. This chapter evaluates the model's performance using quantitative metrics, including ROC curves, precision-recall analysis, sensitivity, specificity, and qualitative validation conducted by expert radiologists. Comparative results with existing methods are discussed to demonstrate the effectiveness and clinical relevance of the proposed approach.

Finally, Chapter 5 concludes the thesis by summarizing the key findings and contributions of the research. It reflects on the strengths and limitations of the developed framework and offers recommendations for future work. The chapter highlights how the proposed model can aid radiologists in enhancing early breast cancer detection by facilitating the efficient preprocessing of DBT images.

CHAPTER 2
LITERATURE REVIEW

2.1 Introduction

Breast cancer remains the most frequently diagnosed cancer among women worldwide. The World Health Organization (WHO) estimates that in 2022 there were approximately 2.3 million newly diagnosed cases and ~670,000 deaths globally, reinforcing the need for continued advances in screening and diagnostic imaging [27]. According to Department of Statistics Malaysia data, cancer was the fourth leading cause of death in 2022, rising from 10.5% of all deaths in 2021 to 12.6% in 2022. Deaths attributed to neoplasms have increased significantly since 2001, from 5,231 to 16,545 deaths in 2023, reflecting an upward trend in cancer mortality. The age-standardised annual cancer mortality rate in Malaysia was estimated at 86.3 deaths per 100,000 population in the latest GLOBOCAN report [28]. Screen-film mammography and full-field digital mammography are the principal modalities for screening and diagnosis of breast cancer to reduce the breast cancer mortality rate. The sensitivity of breast cancer detection is limited by the presence of overlapping tissue and structures, despite the ability of the methods to successfully detect the early signs of breast cancer, which makes these modalities less accurate for screening or diagnosis of breast cancer [29].

Breast cancer, if detected earlier during a breast cancer screening program, can offer the best chance to treat the disease at an earlier stage and improve the chance of successful treatment. Recently, due to the execution of well-structured breast cancer screening programs worldwide, the evidence of the breast cancer mortality rate in selected countries has been decreasing [30]. The decrease in the annual death rate has been attributed to research aimed at improving early detection methods and treatment. Medical imaging plays an important role in decreasing breast cancer death with contributions to early detection during screening, diagnosis, image-guided biopsy, and treatment planning.

This chapter provides a comprehensive review of existing literature relevant to breast cancer detection, with a particular focus on DBT imaging. It begins with an overview of breast cancer screening and diagnostic methods, followed by an in-depth exploration of DBT technology, its conventional diagnostic approaches, and the

associated challenges. Current research in DBT image analysis is then discussed, highlighting both conventional image processing and deep learning techniques. In addition, the chapter examines various blur image detection techniques, including both traditional and deep learning-based approaches, which are crucial for ensuring image quality in DBT analysis. A dedicated section is also included on microcalcifications in DBT images, focusing on methods for enhancing their visibility, which is essential for early diagnosis. The chapter concludes with a summary of key findings and the identification of research gaps that guide the direction of the current study.

2.2 Breast Cancer Screening and Diagnosis

Breast cancer is the leading cause of cancer death among women around the world. In 2022, there were 2.3 million women diagnosed with breast cancer and 685,000 deaths globally reported by the WHO [27]. Breast cancer affects women at any age after puberty in every country around the world, with a higher incidence in later life. In Malaysia, breast cancer is one of the top five most common cancers, accounting for 29,453 cases in the 5-year prevalence cases as reported in the GloboCan 2020 [31]. Since it is a heterogeneous disease, assessing the tumour pathologically is crucial for prognosis and treatment.

Diagnostic radiography is critical in the detection and treatment of breast cancer since early detection is seen as the best hope for reducing breast cancer mortality. Because breast cancer is a progressive disease, annual mammography screening can save lives. The probability of successfully treating the disease increases up to 30% when detected at the initial stage, whereas treatment at an advanced stage is less effective and prone to severe human physical discomfort [32]. Moreover, substantial clinical trial indicates that early detection and diagnosis of breast cancer can provide patients with more flexible treatment options and improved life quality and survivability. Therefore, related topics such as novel imaging modalities for breast tomography [33] are receiving increasing attention.

Mammography screening of the breast image from the craniocaudal and mediolateral oblique perspectives, whereas diagnostic mammography images the breast in greater detail if symptoms such as changes in the breast architecture or abnormal findings are observed on screening mammographic images. Until recently, screen-film mammography (FM) was considered the gold standard for use in breast cancer

screening programmes, but digital mammography (DM) has gained universal acceptance due to the greater spatial resolution needs. However, numerous studies have demonstrated the inadequate performance of this technology, and as a result, its use is being restricted [34]–[36].

During mammography interpretation, identifying and describing calcifications is a complicated process. Radiologists are searching for a lesion with very different characteristics that can be divided into two broad categories: calcification clusters and soft tissue findings. The calcifications of interest for detecting breast cancer are small (as little as 0.2 mm) and relatively high in contrast. The shape of the calcification and the distribution of the calcification cluster are important biomarkers for malignancy. Soft tissue lesions are of different types: masses (with various shapes and margin descriptors, such as spiculated, smooth, obscured, irregular), architectural distortions (abnormal configuration of the fibroglandular tissue), and asymmetries (dense tissue patterns in one breast with no correspondence on the contralateral breast) [2].

Despite widespread use, traditional screening methods are not without drawbacks. False negatives (where cancer is missed) and false positives (where benign conditions are mistakenly identified as malignant) can lead to anxiety, unnecessary biopsies, or delayed treatment. Dense breast tissue further complicates interpretation by masking potential abnormalities. Overall sensitivity is limited by the presence of dense fibroglandular breast tissue, which might disguise the presence of an underlying malignancy [37], [38]. Similarly, the presence of overlapping fibroglandular tissue, which might mimic the appearance of malignancy, reduces specificity. Above all, the visual distinction between malignant and benign lesions is ambiguous, and as a result, measuring breast lesions with discriminative characteristics provides significant challenges. Although the bulk of mammography services in Malaysia have transitioned from film to digital, quality assurance remains a key challenge [39].

As a result, when interpreting screening mammography, comparing to past images is critical for enhancing both sensitivity and specificity [40]–[43] and provides additional information not obtained by alternative contemporaneous imaging, such as DBT. Additionally, radiologist fatigue, variability in interpretation, and technical limitations of 2D imaging contribute to diagnostic inconsistency. These limitations have driven the demand for more advanced imaging techniques that provide greater clarity and diagnostic confidence.

2.3 Digital Breast Tomosynthesis (DBT)

DBT mammography is one technology being developed to improve the detection and characterization of breast lesions, especially in women with nonfatty, less dense breasts. Multiple projection images are reconstructed using DBT, allowing for the visual review of thin breast sections. This technology can potentially reveal cancers that are hidden or concealed by normal tissue surrounding the lesion. DBT involves acquiring multiple projection exposures by a digital detector from a mammographic X-ray source that moves over a limited arc angle [44]. These projections are reconstructed into one mm-thick slices using algorithms such as filtered back projection (FBP) or iterative reconstruction. This layer-by-layer visualization enables radiologists to detect and characterize lesions that overlapping tissues in standard mammography may obscure. Figure 2.1 shows the DBT system and an example of projected images.

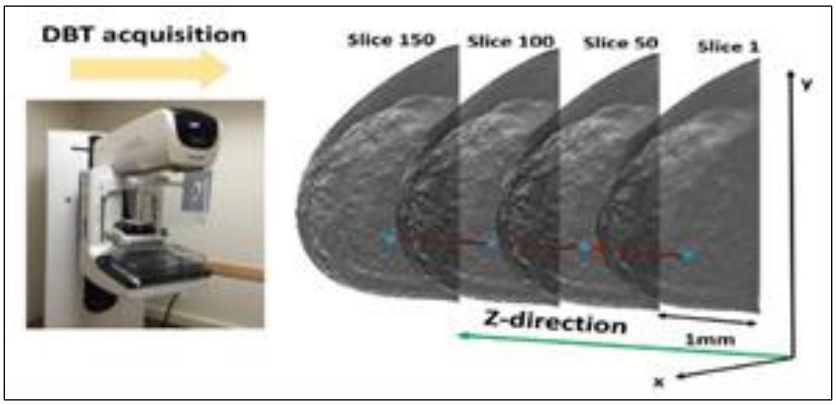

Figure 2.1 Digital Breast Tomosynthesis and a Series of Exposures Result in Multiple Projection Image Datasets [45]

The advent of computer reconstruction algorithms has enabled the development of derivative technologies, including tomosynthesis. In a conventional Digital Mammogram, a compressed breast is subjected to ionizing radiation [46]. The energy that passes through the breast is converted into an electrical signal by a detector, which generates the clinical image. The x-ray tube, the breast, and the detector are stationary (Figure 2.2). The image that is produced in any one projection, such as a craniocaudal (CC) or mediolateral oblique (MLO) view, is a two-dimensional representation of three-dimensional space. Each pixel represents the average of the information acquired across the full thickness of the breast. A three-dimensional representation of the breast would

be similar to those obtained through Computed Tomography, Magnetic Resonance Imaging, or ultrasound scanning [44].

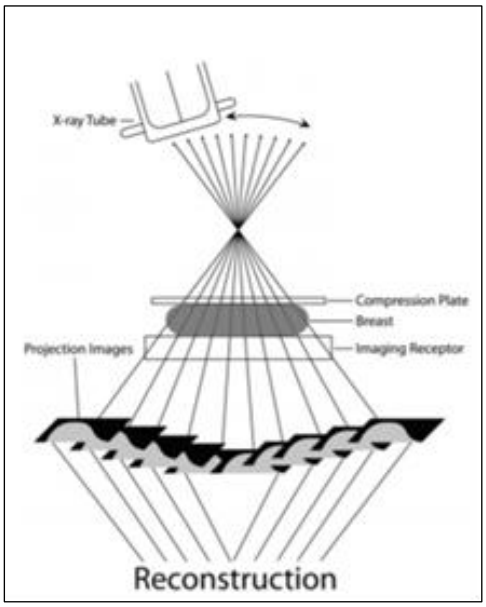

Figure 2.2 Digital Breast Tomosynthesis system. The X-ray tube moves through a Narrow Arch While the breast is in Compression. A Series of Exposures Results in Multiple Projection Image Datasets. Each Exposure Is a Fraction of the Dose of a Conventional Mammographic View. Projection Image Datasets Are Reconstructed Into Multiple Thin-Slice Images (E.G., 1-Mm Thickness) For Interpretation by the Radiologist [44]

This approach reduces the effect of overlapping tissue and improves lesion visibility, especially in dense breasts. The shift toward DBT and other computer-aided diagnostic tools marks a significant evolution in breast cancer screening. Large clinical studies have shown that adding DBT to digital mammography can reduce recall rates while increasing cancer detection, including invasive cancers, supporting DBT's clinical value in screening workflows [47]–[49]. DBT improves lesion visibility, enhances localization accuracy, and facilitates the identification of architectural distortions and subtle masses.

2.3.1 Diagnosis with DBT

In the diagnostic workflow of DBT, the breast is imaged using multiple low-dose X-ray projections acquired at different angles across a limited arc of rotation. These projection images are then reconstructed into a set of thin slices, typically 1 mm thick, forming a three-dimensional (3D) volume of the breast. This tomographic

reconstruction enables radiologists to examine the breast tissue slice by slice, thereby minimizing the issue of tissue overlap that commonly hampers interpretation in conventional 2D mammography. As a result, DBT significantly enhances the visibility of lesions, especially in women with dense breast tissue [50].

The conventional diagnostic approach involves manual interpretation by radiologists who scroll through the reconstructed DBT slices using specialized workstations. During this assessment, radiologists evaluate lesion characteristics, including shape, margin definition, density, and spatial distribution. These observations are systematically categorized according to the Breast Imaging Reporting and Data System (BI-RADS), a standardized classification system that guides clinical decision-making and reporting consistency [51]. DBT is often interpreted in conjunction with Full-Field Digital Mammography (FFDM), which provides high-resolution 2D images to complement the volumetric data from DBT, thereby offering a more comprehensive diagnostic perspective.

Despite its clinical advantages, the conventional interpretation of DBT is time-consuming and labour-intensive. Each DBT scan can produce between 40 and 100 slices per breast, depending on the acquisition protocol and breast thickness [52]. Radiologists must examine each slice meticulously, which increases their cognitive workload and contributes to diagnostic fatigue. This prolonged reading time can potentially compromise diagnostic accuracy, especially in high-volume screening environments.

Furthermore, while DBT improves the visualization of mass lesions and architectural distortions, certain features remain diagnostically challenging. Low-contrast lesions and subtle microcalcifications, for instance, may still be complex to detect due to their faint appearance and small size. These limitations underscore the need for adjunctive tools, particularly computer-aided detection (CAD) systems and deep learning-based algorithms, to assist radiologists by pre-analyzing DBT volumes, flagging suspicious regions, and potentially reducing the incidence of oversight errors. As radiology continues to adopt artificial intelligence (AI) in clinical practice, the role of conventional DBT diagnosis is shifting towards a synergistic model in which human expertise is augmented by machine intelligence. This evolution is crucial to maintaining diagnostic efficiency and accuracy in the face of increasing imaging complexity and case volumes.

2.3.2 Issues and Challenges in the Diagnosis with DBT

DBT has emerged as a transformative imaging modality that addresses several limitations of conventional two-dimensional (2D) mammography, particularly in women with dense breast tissue. By enabling quasi-three-dimensional visualization, DBT reduces tissue overlap, enhances lesion conspicuity, and improves the detection of architectural distortions and masses. Despite these advantages, DBT has not yet achieved its full diagnostic potential. Its clinical effectiveness is hindered by multiple unresolved challenges, including the substantial interpretive burden, technical deficiencies in image reconstruction, interpretive variability among radiologists, and, most critically, the persistence of blurry slice artifacts and the limited visibility of microcalcifications. These limitations represent fundamental barriers to early and accurate breast cancer detection, directly motivating the need for advanced image enhancement and detection methods.

One of the most critical technical issues in DBT is the persistence of blurry slice artifacts. These artifacts degrade spatial resolution and impair the visualization of subtle lesions. They arise from multiple factors, including the limited angular range of X-ray acquisition, focal spot motion during continuous scanning, and patient-induced motion during breast compression. Continuous-motion acquisition systems, although efficient, introduce focal spot motion blur, which amplifies spatial unsharpness and disproportionately diminishes the visibility of small, clinically significant features such as microcalcifications [53]. Additionally, reconstruction algorithms can generate ripple and out-of-plane artifacts, which obscure fine anatomical details and may mimic pathological findings, creating the risk of both false positives and false negatives [54]. Importantly, blurry slices are not superficial aesthetic degradations; they actively compromise diagnostic performance by concealing small abnormalities and forcing radiologists to expend additional cognitive effort when reviewing adjacent slices for confirmation. Recent DBT-focused learning-based studies demonstrate that blur can be mitigated directly in reconstructed volumes using data-driven coarse-to-fine strategies, resulting in improved lesion visibility across multiple viewing directions. These findings confirm the feasibility of incorporating automated blur handling into DBT imaging pipelines, while also highlighting the importance of clinically practical and computationally efficient solutions suitable for routine screening workflows [20].

A second, closely related limitation concerns the detection of microcalcifications, which are among the earliest indicators of ductal carcinoma in situ (DCIS). While DBT markedly improves the detection of masses and distortions, it remains less effective for microcalcifications. Thin-slice reconstructions, although useful for reducing tissue overlap, often compromise spatial resolution and contrast for small calcifications, which are frequently better visualized in 2D mammography [55]. Studies demonstrate that calcifications can appear fragmented across multiple slices, suffer from diminished conspicuity, and are susceptible to increased noise, particularly when reconstructed with traditional filtered backprojection (FBP) algorithms [54]. To compensate for these limitations, radiologists frequently rely on synthetic 2D views or adjunct full-field digital mammography (FFDM), underscoring the insufficient standalone capability of DBT for microcalcification detection [56]. The clinical risk here is significant: blur artifacts combined with poor calcification conspicuity may obscure the earliest manifestations of breast cancer, thereby undermining DBT's role in early detection.

Beyond image quality issues, DBT introduces practical and infrastructural challenges. The high volume of data generated, often comprising dozens to hundreds of slices per breast, increases interpretation time and contributes to radiologist fatigue. On average, reviewing DBT datasets takes nearly twice as long as interpreting standard mammograms [57], [58], which reduces throughput and efficiency in screening programs. Furthermore, diagnostic accuracy remains dependent on the reader's expertise, and inter-observer variability continues to be a concern when evaluating subtle abnormalities such as architectural distortions and calcifications [56]. At the systems level, DBT requires significant computational resources for image reconstruction and storage. Algorithms such as FBP and simultaneous algebraic reconstruction technique (SART) are computationally intensive, prone to noise amplification and edge distortions, and demand robust infrastructure for processing and archiving large datasets [59]. These factors create barriers to widespread adoption, particularly in resource-constrained healthcare settings.

In summary, while DBT represents a significant advance over 2D mammography, its diagnostic performance is constrained by three interlinked challenges: (i) the heavy interpretive workload, (ii) the persistence of blurry slice artifacts, and (iii) the reduced visibility of microcalcifications. Blurring not only undermines overall image clarity but also directly compromises the detection of

calcifications, which are critical for identifying early-stage breast cancers such as DCIS. Together, these challenges highlight the urgent need for advanced image processing techniques that can suppress blur, enhance microcalcification contrast, and support radiologists in managing the interpretive burden. Recent advances in deep learning, hybrid machine learning approaches, and model-based reconstruction algorithms provide promising avenues for mitigating these limitations and enabling DBT to realize its full potential as a frontline modality for breast cancer screening and diagnosis.

2.4 Recent Advances in DBT Image Analysis

DBT has transformed breast imaging by enabling three-dimensional visualization of tissue structures. Recent advances in digital imaging, data processing, and artificial intelligence have opened new frontiers in the analysis of DBT images. While conventional diagnostic methods rely heavily on radiologist interpretation, current research is increasingly focused on automated techniques to enhance accuracy, efficiency, and consistency in breast cancer diagnosis.

Modern DBT research explores various domains, including image enhancement, lesion segmentation, classification, microcalcification detection, and image quality assessment. These efforts are driven by the growing need to manage the large volume of DBT data, reduce diagnostic errors, and support radiologists in decision-making. Traditional image processing techniques have been used to enhance image quality and extract salient features, while deep learning models have emerged as powerful tools for automated lesion detection and classification. Figure 2.4 illustrates a typical DBT image analysis pipeline, encompassing key stages from raw image acquisition to clinical decision support.

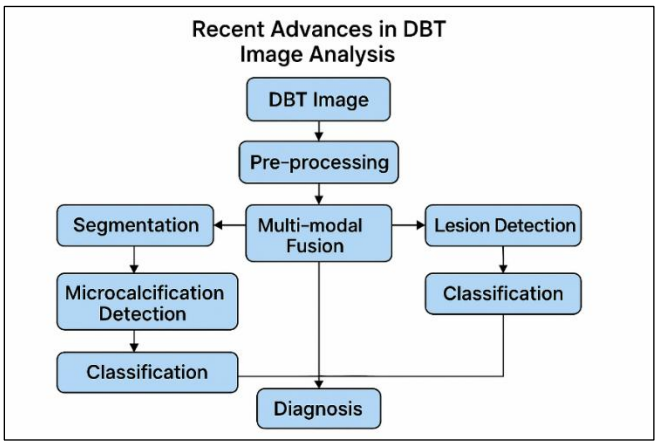

Figure 2.3 Recent Advances in DBT Image Analysis Pipeline

2.4.1 DBT Image Processing

Image processing forms the foundation of DBT analysis by improving image quality and preparing data for interpretation or further computational analysis. As DBT involves the acquisition of multiple low-dose projections and their subsequent reconstruction into volumetric slices, pre-processing and enhancement steps are essential to ensure diagnostic accuracy and consistency. One of the primary goals of DBT image processing is to reduce noise. Since each slice is generated from low-dose acquisitions, the resulting images often contain quantum noise. Techniques such as Gaussian filtering, median filtering, and bilateral filtering have been applied to smooth out noise while preserving lesion edges [59]. Additionally, artifact suppression methods are implemented to reduce the impact of motion blur or reconstruction streaks, which can obscure critical diagnostic features.

Contrast enhancement techniques, such as histogram equalization and Contrast-Limited Adaptive Histogram Equalization (CLAHE), are commonly used to improve the visibility of soft tissue structures. These methods help emphasize differences between dense and fatty tissue, thereby improving lesion detectability [55]. Intensity normalization is another common step, particularly important when combining images from different machines or patient studies for model training. Methods such as z-score normalization and min–max scaling are typically applied to ensure standardized intensity levels across datasets [60]. In clinical applications, radiologists are often overwhelmed by the sheer number of slices produced during DBT. To address this, research has proposed automated slice selection algorithms based on edge density,

entropy, or anatomical landmarks to isolate diagnostically significant slices, reducing review time without compromising diagnostic value [61].

Moreover, segmentation plays a crucial role in delineating regions of interest (ROIs), such as masses or architectural distortions. Traditional image segmentation methods such as thresholding, region growing, morphological operations, and watershed algorithms have been widely used. While deep learning segmentation is gaining popularity, these conventional approaches continue to serve as important baselines or components in hybrid models [62]. Finally, handcrafted feature extraction methods, including texture analysis (e.g., Gray-Level Co-occurrence Matrix, Local Binary Patterns), shape descriptors, and statistical measures, have been extensively employed in earlier DBT studies [55], [60]. These features are often used in classical machine learning models or combined with deep learning features in multi-feature fusion frameworks. A summary of the key DBT image processing techniques, their objectives, and representative methods is presented in Table 2.4.

Table 2.1
DBT Image Processing Techniques

Author(s)	**Technique**	**Purpose**	**Example Methods**
Sechopoulos et al. (2013) [59]	Noise Reduction	Minimize image noise due to low-dose acquisition	Gaussian filter, Median filter, Bilateral filter
Tagliafico et al. (2015) [55]	Contrast Enhancement, Feature Extraction	Improve visibility of tissues and lesions Extract visual descriptors for lesion analysis	Histogram Equalization, CLAHE, GLCM, LBP, Shape descriptors, Statistical features
Bernardi et al. (2016) [52]	Slice Selection	Reduce the number of slices to aid the radiologist's efficiency	Entropy-based filtering, ROI-based selection
Wang et al. (2018) [60]	Segmentation	Identify and isolate regions of interest	Thresholding, Watershed, Region Growing, Morphology Ops

2.4.2 Deep Learning Approaches for DBT Images

In recent years, deep learning has emerged as a powerful tool for advancing the analysis of DBT images. By leveraging large datasets and multilayer neural networks, deep learning models have demonstrated remarkable capabilities in lesion detection,

classification, segmentation, and microcalcification analysis tasks. These methods offer significant advantages over traditional approaches, particularly in their ability to automatically extract and learn complex, hierarchical features from raw imaging data. Deep learning models provide a significant advantage over traditional approaches by automatically learning hierarchical features directly from raw DBT data. Unlike conventional methods that rely on handcrafted features, CNNs can extract complex patterns and contextual relationships within the breast tissue. This capability is especially beneficial in DBT, where the 3D volumetric nature of the data presents challenges for manual feature engineering. As a result, deep learning has enabled more accurate and efficient analysis across various tasks such as lesion detection, classification, and microcalcification identification.

Deep learning has been widely applied to the identification of suspicious regions within DBT volumes. CNN-based architectures such as Faster R-CNN, YOLO, and RetinaNet have been adapted for lesion detection tasks, demonstrating high sensitivity in identifying masses and architectural distortions [63]. These models are capable of processing multiple DBT slices simultaneously or integrating spatial features across slices, thereby enhancing contextual awareness and improving detection accuracy. For image-level diagnosis, models such as ResNet, DenseNet, and VGGNet have been utilized to classify DBT images into benign or malignant categories. These networks automatically learn discriminative features from the imaging data, and their depth allows them to capture intricate structures within breast tissue. Multi-branch architectures that combine DBT with full-field digital mammography (FFDM) inputs have also been explored, resulting in improved diagnostic performance [58].

Given the volumetric nature of DBT, 3D-CNNs and multi-view CNN architectures have been developed to capture spatial relationships across slices better. These models, such as 3D-ResNet and hybrid multi-view networks, exploit the inter-slice continuity of breast structures, yielding more robust and accurate analysis. However, 3D features may introduce extra noise due to the fuzzy microcalcifications in slices that are far away from the focus slices [65]. Detecting microcalcifications in DBT remains a challenging task due to their small size and subtle contrast. However, patch-based deep learning approaches, utilizing architectures such as U-Net and attention-enhanced U-Net variants, have shown promising results. These models focus on fine-grained features and have demonstrated effectiveness in accurately localizing microcalcifications within 3D DBT volumes [66].

The scarcity of large, annotated DBT datasets has motivated the use of weakly supervised learning and transfer learning strategies. Pre-trained models (e.g., trained on ImageNet) are often fine-tuned on smaller DBT datasets to reduce the need for extensive manual annotation while maintaining competitive performance [67]. These approaches have facilitated the development of accurate models even with limited domain-specific data. To enhance clinical trust and interpretability, explainable AI techniques such as Gradient-weighted Class Activation Mapping (Grad-CAM) and saliency maps are increasingly incorporated into DBT analysis. These tools visualize the regions of interest influencing the model's decision, allowing radiologists to better understand and validate the AI system's outputs [64].

The CNN-based methods for DBT image analysis have also demonstrated notable improvements in denoising [23], [25], [68], deblurring [21], and enhancing contrast resolution [69]. However, due to the scarcity of publicly available DBT datasets, many studies are constrained to using physical or simulated breast phantoms for model training and evaluation. Table 2.2 summarizes several key studies that have employed both conventional and deep learning techniques for blur detection and quality enhancement in DBT and related imaging modalities. These explainability techniques not only support clinical integration but also highlight the importance of image quality in diagnostic accuracy. As deep learning models are highly sensitive to input quality, issues such as blur and noise can significantly impact performance. This leads to a growing focus on blur image detection, which is explored in detail in the following section (Section 2.5), as a critical step in ensuring reliable DBT analysis.

Table 2.2
Studies on the Deep Learning Approach in DBT images

Author(s)	**Image Type (Dataset)**	**Contributions**	**Method**	**Finding Assessment**	**Performance Measure**
Classification					
Ricciardi et al. (2021) [70]	DBT image (Private)	CAD system to classify DBT images	DBT-DCNN	increased sensitivity and a significant reduction of false positives (FP) (use pre-processing denoising for each series of images)	Accuracy and a sensitivity of (90% ± 4%; 96% ± 3%)
Zhang et al. (2020) [71]	DBT images (Private)	full-volume 3D DBT images binary	2D CNN (leverage AlexNet pre-trained	Results support the natural assumption that the tissue separation available in DBT z-	Performance 0.854 auROC, which is 28.80%

Author(s)	Image Type (Dataset)	Contributions	Method	Finding Assessment	Performance Measure
		negative/positive classification	on ImageNet)	slices is an invaluable asset in diagnosis. *only malignant cases are labeled as positive	higher than the baseline method
Mendel et al. (2019) [72]	DBT images (Private)	malignant and benign classification	ImageNet pre-trained VGG19 for feature extraction in FFDM and DBT images	Features were selected from the VGG19 model after each max pooling layer. Average pooling was performed for feature dimension reduction. To avoid redundant features, Leave-One-Out Step-wise feature selection was performed to obtain the most frequently selected features. Then, the Leave-One-Out Support Vector Machine (SVM) classifier was used to estimate the likelihood of malignancy.	The best AUC in mass/architectural distortion and calcification detection is for DBT z-Stack slice images in CC and MLO view (AUC = 0.98 ± 0.01 and AUC = 0.97 ± 0.03, respectively)
Yousefi et al. (2018) [73]	DBT images (Private)	CAD framework for mass detection in DBT	DCNN & MI-RF	The model learns complex patterns automatically from 2D slices of DBT data and uses all the information obtained from the slices to analyze DBT images	81% accuracy, and 86% sensitivity
Yeh et al. (2018) [74]	DBT images (Private)	classifying breast cancer		automatic computer-aided diagnosis (CAD) system for DBT image analysis	
Rodriguez-Ruiz et al. (2018) [46]	Reconstructed images (Private)	artifact suppression, higher resolution, and less noise	shallow network (CNN) and filtered back-projection method	employed a CNN model to classify calcification using reconstructed images when employing different DBT reconstruction algorithms (filtered back projection and enhanced multiple parameter iterative reconstruction)	AUC of the CNN model trained with images that are reconstructed using the filtered back projection method is 0.857
Samala et al. (2018) [75]	DBT images (Private)	classifying DBT images as mass or normal	Two-stage transfer learning (pre-trained AlexNet,	Rather than using the CNN directly as a classifier, the CNN at the second stage is used for feature extraction. Then, a feature selection method and a random	AUC of 0.90 with pruning the model and an AUC of 0.89 without pruning.

Author(s)	Image Type (Dataset)	Contributions	Method	Finding Assessment	Performance Measure
				forest classifier are applied to the extracted features for classification.	
Kim et al. (2016) [76]	DBT reconstructed volume (Private)	classifying masses and FPs	Concatenated 3D CNN and lateral view VOI	Discover hidden or latent bilateral feature representation of masses in self-taught learning.	The proposed model performed better (AUC = 0.847) than the handcrafted feature classifier (AUC = 0.826).
Object Detection and Segmentation					
Zheng et al. (2021) [77]	DBT images (Private)	A framework for clustered MCs false positives reduction in the detection of clustered MCs	3D context-aware CNN	This strategy can effectively incorporate the extra information about the MCs of adjacent slices and avoid the influence of anisotropic resolution. *Performance of this model is much better than Samala's 2D CNN, but not as well as 3D ResNet-18.	Accuracy of 92.68% for FPs reduction, sensitivity of 90%
Fan et al. (2020) [1]	DBT images (Private)	CAD framework for mass detection and segmentation	3D-Mask RCNN	Results showed that the Mask RCNN achieved better performance than the Faster RCNN in terms of fewer FPs/lesion, whereas an inverse result was observed for the breast-based evaluation, which showed fewer FPs/breast for the Faster RCNN compared with the Mask RCNN.	Sensitivity was 90% with 0.8 false positives (FPs) per lesion.
Buda et al. (2020) [26]	DBT images (Public) https://www.cancerimagingarchive.net	model for the detection of abnormalities in DBT	Single-phase Deep learning	trained the first single-phase detection model for this dataset that will serve as a baseline for future development.	Sensitivity of 65% at two false positives per breast
Lai et al. (2020)	DBT images (Private)	method that employed the U-Net to	U-Net	In the post-processing stage, segmentation was predicted from the U-Net, in which less than	AUC = 0.859.

Author(s)	Image Type (Dataset)	Contributions	Method	Finding Assessment	Performance Measure
		segment DBT images		50 voxels in volumes were removed as volumetric constraints.	
Lotter et al. (2019) [78]	FFDM images (Private)	classification (mass, calcifications, focal asymmetry, architectural distortion, and normal)	three-stage model: pre-trained ResNet model, RetinaNet, multiple-instance learning (MIL)	ROI extracted from the stage two model using z-Stack	AUC = 0.945
Denoising, Reconstruction					
Gao et al. (2021) [23]	Breast phantoms (Digital & physical) (Private)	Denoising DBT images	DNGAN (DCNN with adversarial)	improved the contrast-to-noise ratio (CNR) and detectability index (d') of the simulated MCs in the validation phantom DBTs. *Only tested the denoiser on a small set of human subject DBTs.	CNR improved 0.097
Wu et al. (2020) [67]	Breast phantoms	improve the contrast and in-depth resolution of DBT reconstruction images	UNet and ROI loss	improve the contrast and in-depth resolution of microcalcifications novel ROI loss function for adding attention to the region of microcalcifications *ROI loss only led to slightly worse overall RMSEs and SSIMs compared to L2 loss. There was no substantial visual difference in the glandular reconstructed using the two losses.	SSIM 0.0.724 ± 0.098
Teuwen et al. (2021) [79]	phantom projections and breast CT	DBT reconstruction from projection views	DBToR is a CNN-based model that uses the L2 loss function	The DBToR — containing a couple of reconstruction blocks — takes projection images and the breast thickness as initial inputs.	SSIM 0.89 ± 0.01
Aditya et al. (2020) [80]	Virtual phantoms	search a simulated mass and a smaller simulated micro-calcification	CNN	The case of the filtered noise shows how a CNN can approximate the ideal observer for a search task, achieving a statistical efficiency of	Efficiencies: 88% for the microcal, 90% for the mass

Author(s)	Image Type (Dataset)	Contributions	Method	Finding Assessment	Performance Measure
		embedded in filtered noise and single slices DBT-virtual phantoms		0.77 for the microcalcification and 0.78 for the mass.	
Su et al. (2020) [81]	phantom projections	Solve the DBT reconstruction problem	DIR-DBTnet	The network structure contains three parts: the reconstruction module, the denoising module, and the multiplier update module. The denoising module employed a CNN to generate denoised images. In the experimental study, simulated DBT sinogram-label pairs data were used.	FWHMs 12.9mm Full Width at Half Maximum
Sahu et al. (2019) [25]	DBT images (Private)	denoising the DBT projections	GAN	The model contains a generator that learns the distribution of data and a discriminator, which predicts the label of input images (fake or real). The proposed model takes patches (200 × 200) of DBT projection images.	The proposed GAN model has the best performance in terms of HaarPSI (0.383) compared with the MSE loss CNN (0.367), KSVD (0.295), and BM3D (0.2851) models.
Choi et al. (2018) [21]	DBT images (Private)	method to reduce the blurring artifact in DBT images	DRCNN	The lesion detectability of the DBT image is improved significantly after applying the proposed DRCNN *While the proposed network improves the visibility of the lesion, it was observed that the original fine structures presented in the reference images were not recovered fully	-

2.5 Blur Image Detection Techniques

Image blur is one of the critical factors that can degrade the diagnostic quality of medical images, particularly in modalities like DBT, where multiple low-dose projections are combined to reconstruct 3D volumes. Blur can arise from various sources, including patient motion, limited acquisition angles, or hardware limitations, and can obscure important anatomical features or lesions. Consequently, detecting and correcting blur is essential to maintaining diagnostic integrity and optimizing the performance of automated analysis systems.

Blur detection techniques can generally be categorized into two main approaches: conventional image processing methods and deep learning-based techniques. Conventional methods rely on mathematical or statistical analysis of image characteristics, such as Tenegrad and Laplacian variance, that capture edge sharpness [82] and wavelet transforms [83]. More recently, deep learning approaches such as blur image identification with an ensemble CNN [84], GAN-based deblurring [85], and a multi-scale feature learning CNN model for defocus blur estimation [86] have been proposed, demonstrating improved accuracy and robustness.

More recent studies [87] have also evaluated deep-learning–based blur detection directly on large-scale clinical breast imaging data across multiple vendors, indicating increasing maturity of automated blur screening methods and motivating the need for DBT-specific extensions. Table 2.3 presents a concise summary of key studies related to blur detection in related medical imaging modalities. It highlights the methods used, data types, and reported outcomes, offering a snapshot of the current research landscape. Most of these studies demonstrate the advantages of CNNs in capturing complex blur patterns, although their reliance on simulated or non-clinical data remains a limitation. Importantly, few studies have directly addressed the detection and enhancement of blur specific to microcalcifications in extremely dense breast tissue, an area this thesis aims to explore.

Table 2.3
Summary of Key Studies Related to Blur Detection Techniques

Author(s)	Method	Modality	Technique	Key Findings
Nowakowska et al. (2024) [87]	CNN blur classifier	Digital mammography	Deep learning	Automated blur screening feasible on clinical data
Choi et al. (2022) [20]	Two-phase CNN deblurring	DBT images	Deep learning	Reduced blur and improved lesion visibility in DBT
Karaali, Harte, & Jung, (2022) [86]	Multiscale CNN	Natural images	Deep Learning	Multi-scale feature learning improves defocus blur estimation accuracy.
Wang, Li, & Zhang, (2019) [84]	Ensemble CNN	Natural images	Deep Learning	Robust blur classification using pruned AlexNet & GoogleNet with ensemble fusion.
Kupyn et al. (2018) [85]	DeblurGAN	Natural/ Medical	Deep Learning	GAN-based image restoration with improved clarity
Tong et al. (2004) [83]	Wavelet Transform	General imaging	Conventional	Multiscale edge loss detection
Pech-Pacheco et al. (2000) [82]	Laplacian Variance	General imaging	Conventional	Effective but limited by noise sensitivity

2.5.1 Conventional Blur Image Detection Techniques

Conventional blur detection techniques rely on the analysis of low-level image features, such as gradients, frequency components, and edge sharpness, to determine the presence and severity of blur. These methods are typically model-agnostic, computationally efficient, and interpretable, making them useful as baseline techniques or in hybrid systems. A commonly used method is the Laplacian variance technique, which computes the variance of the Laplacian of an image. A non-blurry image tends to have higher Laplacian variance due to the abundance of high-frequency components [88]. Similarly, edge-based approaches, such as the Tene grad and Brenner gradient methods, measure the sharpness of edges by calculating gradient magnitude or differences between adjacent pixel intensities. These approaches are simple to implement and have been employed in real-time image quality assessment pipelines [72].

Another category involves frequency-domain analysis, where blur is detected by observing the suppression of high-frequency components in the image's Fourier transform. Recent work by [90] applied a hybrid time-frequency representation using discrete wavelet transforms (DWT) to enhance the sensitivity of edge detection in medical images. Wavelet-based methods are particularly advantageous for multiscale analysis, as they allow the decomposition of images into different frequency bands while preserving spatial information. The Cumulative Probability of Blur Detection (CPBD) metric, though initially developed for natural images, has also been adapted for radiological image assessment, offering a probabilistic interpretation of perceptual blur [74].

Despite their interpretability and low computational cost, conventional methods face limitations in handling complex medical images, such as DBT, where blur characteristics can be subtle and confounded by noise or anatomical structures. Additionally, most of these methods are handcrafted and are not well-suited to variations in acquisition settings or tissue density. As a result, while they are still valuable for initial screening or integration into hybrid models, they are increasingly being supplemented or replaced by data-driven approaches in modern DBT analysis pipelines.

2.5.2 Deep Learning Approaches for Blur Image Detection

Deep learning has become the preferred strategy for image blur detection due to its ability to automatically learn discriminative features from large-scale datasets. Unlike conventional approaches that rely on handcrafted blur metrics, deep neural networks, particularly CNNs, are capable of modelling complex and subtle blur patterns that are otherwise difficult to capture. This has led to significant improvements in both global and local blur detection across various imaging contexts, including medical imaging applications. In particular, CNNs excel in feature learning and representation, thereby reducing the dependence on handcrafted feature design and increasing recognition performance accuracy [75].

Two primary tasks are commonly associated with blur detection: blur–non-blur classification and blur estimation. The first distinguishes between non-blur and blur regions, while the second estimates the blur kernel or the strength of defocus. Estimation strategies directly construct discriminative blur features, thereby enhancing the ability

to differentiate between varying levels of blur [86], [93]–[99]. Early deep learning methods often integrated CNNs with traditional techniques, utilizing convolutional networks as patch-level feature extractors to complement older classifiers. For instance, Park et al. examined the efficiency of defocus detection features by combining deep and handcrafted features to classify image patches, particularly those with sparse and sharp edges [100].

Subsequent developments refined these approaches to address limitations in patch-level analysis. Huang et al. [6] implemented a six-layer CNN to generate patch-level blur maps, later combining outputs across multiple scales to improve global detection. Similarly, Zeng et al. [101] proposed a local blur metric derived from deep features and their principal components, while Kim et al. [102] introduced a neural network with long residual skip-connections and multiscale reconstruction loss functions to learn blur kernels explicitly. In another direction, Shen et al. [92] employed a semantic segmentation approach for detecting blur regions. However, the method remained sensitive to blur boundary sharpness and texture flattening, indicating the need for additional contextual information and larger annotated datasets. More recently, Wang et al. [103] presented the Hierarchical Edge-guided Region-complemented Network (HER-Net), which improved detection by refining boundary accuracy and better localizing blurred regions.

The performance of CNNs for blur classification has also been benchmarked against conventional methods. A recent study [104] directly compared deep convolutional neural networks with the Laplacian method. While the CNN approach showed lower sensitivity than the Laplacian method, it outperformed in specificity, proving more accurate in identifying non-blurry images. This suggests that CNNs are particularly adept at capturing global image context, even when local blur signals are subtle. Furthermore, methods such as visualizing CNN attention maps (e.g., Heatmap activation) [105] provide insights into how these networks identify blur-related features, thereby improving model interpretability.

Despite these advancements, a major limitation in applying deep learning to DBT blur detection is the scarcity of annotated datasets specific to DBT volumes. To address this, researchers have employed simulated blur generation on existing datasets or applied transfer learning from natural image quality assessment (IQA) tasks. More recently, semi-supervised and self-supervised approaches have been proposed to reduce reliance on labelled data, as demonstrated by Chen et al. (2021), making these methods

more feasible for medical imaging contexts. The potential for pattern recognition in an image based on a collection of images is related to the amount of a priori knowledge about the object provided. Researchers must struggle with a range of unknown characteristics when extracting features from images [105]–[107]. Researchers apply several data enhancement strategies to limit the impact of uncertainty.

On the other hand, visual input alone is insufficient for many recognition tasks. In some prediction or recognition cases, image data is not the sole criterion; the diagnosis should be made by combining image data with structured data. Additionally, the actual physical sizes could not be objectively reflected by different images [108]. Classification of features based on a single feature is easily influenced by the object's area, angle, scale change, noise interference, and other variables, resulting in a loss in classification accuracy.

To overcome these limitations, some researchers have proposed hybrid approaches that combine CNNs with other machine learning models to boost classification. Several studies [109], [110] explored the integration of CNNs with SVMs, leveraging CNNs for feature extraction and SVMs for classification. In these frameworks, the final fully connected layer of the CNN is replaced with an SVM classifier, allowing the system to retain the CNN's hierarchical feature extraction capability while benefiting from SVM's efficiency and robustness in classification tasks [110]. This hybrid CNNSVM strategy has been shown to enhance classification accuracy and reduce computational cost, making it particularly attractive for medical imaging tasks such as blur detection in DBT.

Nonetheless, even with these methodological improvements, computational complexity remains a major barrier. Deep multi-stream architectures require a large number of parameters, high GPU memory capacity, and extensive processing time, limiting their routine deployment in clinical practice. Table 2.4 provides a structured overview of previous research on blur detection using deep learning approaches, highlighting their methodological frameworks, strengths, and limitations. Each method is holistically assessed to highlight trade-offs: for example, ensemble and GAN-based methods demonstrate high accuracy but low efficiency and limited interpretability. At the same time, hybrid CNNSVM approaches strike a more balanced profile. This analysis provides the rationale for developing lightweight yet effective blur detection frameworks tailored to DBT imaging.

Nevertheless, challenges remain in achieving model generalizability across different DBT systems and ensuring interpretability for clinical adoption. Addressing this gap, the present study proposes a custom five-layer CNNSVM model specifically tailored to DBT blur detection. By integrating CNN-based feature learning with handcrafted structured data, this model aims to balance performance with computational efficiency, achieving robust detection of global blur in DBT while remaining clinically practical.

Table 2.4
Comparative Evaluation of Deep Learning–Based Blur Detection Methods Across Accuracy, Computational Efficiency, and Interpretability

Author(s)	**Method / Model**	**Key Findings / Contribution**	**Overall Evaluation (Accuracy, Efficiency, Interpretability)**
Versaci et al. (2017) [106]	Adaptive fuzzy contrast enhancement	Image enhancement method, supportive of blur detection tasks	Moderate accuracy (fuzzy preprocessing); High efficiency; Moderate interpretability
Shakeri et al. (2017) [108]	Fuzzy clustering with adaptive histogram equalization	Enhanced image preprocessing to improve blur detection	Moderate accuracy; High efficiency; Moderate interpretability
Samek et al. (2017) [105]	CNN interpretability using visualization techniques	Improved understanding of blur-related activations	N/A accuracy (focus on interpretability); High efficiency; High interpretability (CNN visualization)
Park et al. (2017) [100]	Combined deep and handcrafted features	Unified multi-scale and handcrafted feature approach, improved patch classification	Moderate accuracy (deep + handcrafted); High efficiency; Moderate interpretability
Zeng et al. (2018) [101]	Local blur metric from CNN feature learning	Accurate local blur detection, dependent on principal component analysis	Moderate accuracy (local blur metric with PCA + CNN); High efficiency; Moderate interpretability
Kim et al. (2018) [69]	Residual skip-connections and multiscale reconstruction	Robust kernel estimation, improved contextual blur detection	High accuracy (residual skip-connections); Moderate efficiency; Low interpretability
Huang et al. (2018) [6]	Multi-scale discriminative deep feature learning	Patch-level blur maps combined across scales for enhanced blur detection	Moderate-High accuracy (multi-scale CNN features); Moderate efficiency; Low interpretability

Author(s)	Method / Model	Key Findings / Contribution	Overall Evaluation (Accuracy, Efficiency, Interpretability)
Zhao et al. (2019) [95]	Deep ensemble networks with diversity boosting	Improved robustness, reduced overfitting, but computationally costly	High accuracy (robust ensemble networks); Low efficiency (costly computation); Low interpretability

Author(s)	Method / Model	Key Findings / Contribution	Overall Evaluation (Accuracy, Efficiency, Interpretability)
Tang et al. (2019) [93]	DeFusionNet: recurrently fusing multi-scale deep features	Improved discriminative blur detection, strong multi-scale feature learning	High accuracy (multi-scale fusion); Low efficiency (computationally heavy ensemble); Low interpretability (complex model)
Szandala (2020) [104]	CNN for blur vs. the Laplacian method	CNN has higher specificity, Laplacian has higher sensitivity	Moderate accuracy (CNN vs Laplacian); High efficiency; Moderate interpretability
Shen et al. (2020) [92]	Semantic segmentation for blur region extraction	Good detection, but sensitive to blur boundary sharpness and texture size	High accuracy (pixel-level blur maps); Moderate efficiency (semantic segmentation requires training); Moderate interpretability (sensitive to blur boundaries)
Veluchamy & Subramani (2020) [107]	Fuzzy dissimilarity histogram equalization	Improved contrast for downstream blur analysis	Moderate accuracy; High efficiency; Moderate interpretability
Zhang et al. (2021) [109]	Feature fusion with guided training	Enhanced classification performance in blur-like contexts	High accuracy (feature fusion); Moderate efficiency; Low interpretability
Khairandish et al. (2022) [110]	Hybrid CNN-SVM segmentation for MRI	Improved tumor detection, applicable to blur classification	High accuracy (CNN-SVM hybrid); High efficiency; Moderate interpretability
Karaali et al. (2022) [86]	Deep multi-scale feature learning	Accurate defocus blur estimation with multi-scale features	High accuracy (multi-scale features); Moderate efficiency; Low interpretability
Jiang et al. (2022) [99]	MA-GANet: Multi-attention GAN	Improved blur detection with adversarial learning and attention mechanisms	High accuracy (multi-attention GAN); Low efficiency (adversarial training is costly); Low interpretability
Zhao et al. (2022) [97]	Image-scale-symmetric cooperative network	Better cooperative feature learning, effective on large datasets	High accuracy (cooperative multi-scale learning); Moderate efficiency; Low interpretability
Huang et al. (2023) [94]	Multi-scale convolutional feature approximation	Enhanced blur detection accuracy using hierarchical features	High accuracy (multi-scale feature approximation); Moderate efficiency; Low interpretability
Wang et al. (2023) [103]	HER-Net: hierarchical edge-guided and region complemented	Improved boundary refinement and pixel-level blur accuracy	High accuracy (HER-Net refined boundaries); Moderate efficiency; Low interpretability

The combined evaluation of deep learning–based blur detection methods (Table 2.6) highlights a consistent trade-off between accuracy, computational efficiency, and interpretability. High-capacity models, such as ensemble networks [95], [96] and multi-attention GANs [99], achieve state-of-the-art accuracy but suffer from low efficiency and poor interpretability due to their architectural complexity. While these approaches demonstrate technical promise, their computational overhead makes them impractical for clinical deployment in DBT, where rapid processing and manageable infrastructure are critical.

Conversely, lightweight or hybridized methods, such as patch-level CNNs with handcrafted features [6], [100], [101] or CNNSVM frameworks [110], achieve a more balanced performance profile. Although their accuracy is sometimes moderate compared to heavy deep models, these approaches offer significantly higher efficiency and maintain acceptable levels of interpretability. Importantly, CNNSVM hybrids [110] demonstrate the potential to retain CNN's strong feature extraction ability while leveraging SVM's classification efficiency, thereby reducing computational burden without sacrificing diagnostic robustness.

This synthesis highlights that the optimal strategy for DBT blur detection is not to adopt the most complex or highest-accuracy architecture, but rather to develop a balanced model that integrates deep feature learning with efficient classification. Hence, the hybrid CNNSVM model proposed in this study addresses the identified gaps by prioritizing both computational feasibility and interpretability, while maintaining sufficient accuracy to detect blur in DBT images reliably.

2.6 Microcalcification Enhancement in DBT Images

Microcalcifications are tiny calcium deposits within breast tissue that frequently serve as early indicators of breast cancer, particularly ductal carcinoma in situ (DCIS). Their identification is of critical importance in breast cancer screening, as they are often the earliest radiographic markers of malignancy at a stage where treatment outcomes are most favorable. Despite this importance, the reliable detection of microcalcifications in DBT remains a significant challenge due to their extremely small size (typically 0.1–1 mm), low contrast against glandular tissue, and the masking effect of overlapping anatomical structures, particularly in women with dense breasts [95].

While DBT reduces tissue overlap compared to conventional 2D mammography, its limited angular range and sparse acquisition sampling can lead to blurred or poorly resolved calcifications in reconstructed slices [112]. Traditional reconstruction methods, such as filtered backprojection (FBP), often make this problem worse by smoothing out fine details, making microcalcifications harder to see. As a result, researchers have focused on developing better ways to detect and enhance these small features to improve diagnosis.

Conventional CAD pipelines dominated early detection systems. These methods primarily employed handcrafted features such as morphological descriptors, intensity thresholds, and texture metrics to isolate calcifications. Although conceptually straightforward, they frequently suffered from high false-positive rates and sensitivity to image noise, limiting their clinical robustness [64]. With the advent of deep learning, CNNs have emerged as powerful alternatives capable of automatically learning discriminative features directly from DBT data. For instance, Lotter [78] demonstrated the feasibility of an end-to-end deep-learning pipeline trained on DBT volumes to detect microcalcifications, achieving encouraging sensitivity while reducing false detections via attention-based feature filtering.

Nevertheless, challenges persist. Dense breast tissue continues to obscure subtle calcifications, and progress is hampered by the limited availability of annotated DBT datasets containing microcalcification cases. These limitations not only hinder algorithm training and benchmarking but also constrain the generalizability of proposed models. As such, enhancing the visibility of microcalcifications through advanced contrast enhancement remains a critical pre-processing step for both human readers and AI-driven diagnostic systems.

2.6.1 Microcalcification Contrast Enhancement

Contrast enhancement is fundamental to the reliable detection of microcalcifications in DBT. By increasing the distinction between calcifications and surrounding parenchyma, enhancement methods improve conspicuity and reduce the risk of missed diagnoses [113]. Traditional enhancement techniques such as histogram equalization, unsharp masking, and high-pass filtering have been widely applied due to their simplicity and low computational cost. However, these methods often indiscriminately amplify noise and may generate over-saturated images that obscure

clinical interpretation [114]. To address these drawbacks, more sophisticated image processing strategies such as contrast-limited adaptive histogram equalization (CLAHE) and multiscale filtering have been explored, demonstrating greater efficacy in enhancing subtle structures in mammographic imaging [100]–[102].

In DBT, the challenge is compounded by the volumetric nature of the data, where calcification appearance may vary across slices. To address this, recent research has shifted toward deep learning-based contrast enhancement, which enables networks to learn enhancement functions directly from data. CNNs trained on patch-level DBT samples have demonstrated the ability to selectively emphasize subtle intensity differences associated with calcifications, while simultaneously leveraging spatial context across slices [118]. DBT-specific microcalcification computer-aided detection (CADe) has recently advanced through deep learning architectures that exploit cross-slice contextual information and attention mechanisms to improve the detection of microcalcification clusters [119]. In parallel, recent studies [120] have explicitly targeted microcalcification visibility by optimizing DBT reconstruction and enhancement strategies for lesion detectability rather than solely for pixel-wise fidelity. These developments indicate a shift toward task-driven DBT enhancement, while also revealing the lack of integrated frameworks that jointly address image quality degradation and microcalcification visibility.

Building upon this, advanced architectures such as U-Net variants and residual learning frameworks have been tailored for contrast enhancement tasks. These models integrate attention mechanisms to highlight microcalcification-specific features while suppressing background clutter, resulting in improved sensitivity [121], [122]. In parallel, generative adversarial networks (GANs) have begun to show promise for producing sharper, high-fidelity enhancement outputs that preserve fine calcification detail without introducing significant artifacts [25], [123]. Recent work has also explored pre-reconstruction deep learning to suppress DBT-specific artifacts, such as ripple and distortion effects, using cycle-consistent frameworks with attention mechanisms, demonstrating measurable improvements in artefact characteristics relevant to diagnostic readability [124]. Recent studies have demonstrated that super-resolution convolutional neural networks can be effectively adapted to tomosynthesis imaging to improve image quality. Gomi et al. [125] proposed a projection-based convolutional neural network with super-resolution to enhance digital chest tomosynthesis images, reporting improved spatial resolution and visual clarity without

introducing diagnostically misleading artifacts. Although their work focused on chest tomosynthesis rather than breast imaging, it provides strong evidence that CNN-based super-resolution frameworks are well-suited for limited-angle tomosynthesis modalities, where image blur and resolution loss are inherent. These findings motivate the exploration of super-resolution–based enhancement strategies for DBT, particularly for improving the visibility of fine structures such as microcalcifications.

Table 2.5 Combined evaluation of microcalcification enhancement methods in DBT. Each study is holistically assessed across three key dimensions: accuracy, computational efficiency, and clinical applicability. The table highlights a consistent trade-off across existing microcalcification enhancement techniques in DBT. Traditional methods, such as histogram equalization [103] and CLAHE [104]–[106], remain computationally efficient but frequently suffer from noise amplification and limited clinical robustness, particularly in the context of subtle calcifications within dense breasts. Machine learning–based approaches [105] and early CNN models [107] improved contrast discrimination and detection accuracy, but dataset limitations and lack of DBT-specific optimization often constrained their effectiveness. More advanced architectures, including U-Net variants with attention [110], [111], have demonstrated superior capacity to selectively enhance fine structures, though they remain computationally demanding and risk overfitting on limited training data. GAN-based methods [63], [106] represent the cutting edge of enhancement by producing sharp, high-fidelity outputs, yet their high resource demands and limited interpretability reduce their immediate clinical applicability.

Despite these advances, significant limitations still exist. The main one is the lack of annotated DBT datasets with microcalcification cases, especially in dense breast groups. This limits both algorithm development and the benchmarking of enhancement performance across imaging platforms. As a result, there is an ongoing need to create enhancement methods that are resilient to variations in breast density and can be applied universally across different imaging systems. Addressing these gaps motivates this study, which introduces a CNN-based contrast enhancement model specifically designed for DBT images of dense breasts with suspected microcalcifications. Taken together, these findings suggest that the most promising strategy for DBT is neither reliance on lightweight but noisy traditional methods nor wholesale adoption of computationally heavy generative models, but rather a balanced framework that integrates robust pre-processing, efficient deep learning enhancement, and targeted

post-processing. By addressing the limitations noted in the literature, particularly noise amplification, dense tissue masking, and computational burden, this integrated approach aims to provide a clinically feasible, high-performance solution for microcalcification detection in DBT.

Table 2.5
Combined Evaluation of Microcalcification Enhancement Methods in DBT

Author(s)	**Accuracy**	**Computational Efficiency**	**Clinical Applicability**	**Overall Evaluation (Accuracy, Efficiency, Applicability)**
Mohideen & Thangavel (2015) [114]	Moderate (contrast improved but noise amplified)	High (lightweight histogram method)	Low (limited clinical robustness)	Moderate accuracy (contrast improved but noise amplified); High efficiency (lightweight histogram method); Low applicability (limited clinical robustness)
Sahu et al. (2019) [25]	High (GAN-based denoising preserved fine detail)	Low-Moderate (GANs require significant resources)	High (applied directly in the DBT context, promising for clinical use)	High accuracy (GAN-based denoising preserved fine detail); Low-Moderate efficiency (GAN resource intensive); High applicability (applied directly to DBT, strong clinical promise)
Karakaya (2023) [116]	High (machine learning enhanced detection accuracy)	Moderate (ML adds computational cost)	Moderate (tested on mammograms, potential for DBT)	High accuracy (ML-enhanced detection); Moderate efficiency (computational overhead); Moderate applicability (tested on mammograms, potential DBT use)
Kavitha & Kangaiammal (2023) [117]	High (contrast enhancement effective for subtle structures)	Moderate (higher than basic HE)	Moderate (experimental validation, not fully clinical)	High accuracy (subtle structure visibility improved); Moderate efficiency (higher than basic HE); Moderate applicability (experimental, not clinical)
Singh et al. (2023) [118]	High (direct comparative evaluation FFDM vs DBT)	High (clinical retrospective study)	High (relevant clinical findings on calcification visibility)	High accuracy (clinical evaluation, FFDM vs DBT); High efficiency (retrospective study); High applicability (direct calcification diagnostic relevance)

Author(s)	Accuracy	Computational Efficiency	Clinical Applicability	Overall Evaluation (Accuracy, Efficiency, Applicability)
Lian & Wang (2023) [122]	High (attention + fusion improved fine structure visibility)	Moderate (complex U-Net variant)	Moderate (promising for enhancement, limited DBT focus)	High accuracy (multi-layer fusion attention U-Net); Moderate efficiency (complex DL model); Moderate applicability (promising for enhancement, limited DBT focus)
Ouyang et al. (2023) [121]	High (attention-based U-Net improved local features)	Moderate (deep learning requires GPU resources)	Moderate (validated on segmentation, adaptable to calcifications)	High accuracy (attention-based U-Net); Moderate efficiency (GPU-dependent); Moderate applicability (validated for segmentation, adaptable to calcifications)
Gaona et al. (2024) [123]	High (GAN-based augmentation improved classification)	Low (GANs are computationally heavy)	Moderate (mass classification, adaptable to calcifications)	High accuracy (GAN-based augmentation improved classification); Low efficiency (computationally heavy); Moderate applicability (mass-focused, adaptable to calcifications)

2.6.2 Research Gaps and Opportunities

Despite notable progress in DBT image analysis, substantial research gaps remain in both the detection of blurred slices and the enhancement of microcalcifications, which are vital for early breast cancer diagnosis. These gaps not only constrain DBT's full clinical potential but also highlight areas where further innovation is urgently required.

A first and fundamental gap lies in the limited visibility of microcalcifications in DBT images, particularly in extremely dense breast tissue. While DBT reduces tissue overlap compared to 2D mammography, its restricted angular range, reconstruction artifacts, and reduced spatial resolution often obscure the subtle intensity differences that characterize calcifications. Recent work confirms that blurring in reconstructed slices can mask these small but critical features, directly affecting diagnostic sensitivity [53]. Although deep learning–based methods have shown promise for lesion detection and contrast enhancement, most efforts have concentrated on masses or architectural distortions rather than calcifications, leaving a significant diagnostic gap.

Closely related to this is the challenge of detecting and suppressing blur slices in DBT volumes. Each DBT exam produces dozens to hundreds of slices, but a considerable portion may be degraded by acquisition-related blur caused by focal spot motion, patient movement, or reconstruction limitations. These low-quality slices increase the radiologist's workload, reduce interpretive confidence, and may obscure subtle lesions such as microcalcifications. Despite its clear clinical relevance, systematic approaches for blur slice detection in DBT remain limited, with most prior work focusing on natural images or global blur metrics rather than DBT-specific slice-level blur classification. This gap highlights the need for dedicated frameworks that can identify and filter diagnostically suboptimal slices before enhancement or analysis.

A third limitation is the lack of publicly available, annotated DBT datasets containing microcalcifications. The absence of large, diverse, and well-curated datasets has restricted the development of robust and generalizable machine learning models. Many existing studies rely on small institutional cohorts, phantom experiments, or simulated cases, which fail to capture the heterogeneity of real-world patient presentations. This limitation is further compounded by the absence of benchmarking across models, making it difficult to compare methods or draw consistent conclusions [126].

Fourth, there is a lack of integration across the diagnostic pipeline. Most existing research treats blur detection, contrast enhancement, and lesion identification as independent tasks. This compartmentalized approach risks introducing inconsistencies and inefficiencies, particularly when diagnostic performance depends on the interplay of image quality, feature visibility, and lesion detectability. An end-to-end framework that jointly incorporates image quality assessment, enhancement, and microcalcification detection has not yet been systematically explored, despite its potential to deliver more reliable and clinically robust results.

Finally, the issue of explainability and interpretability of deep learning models remains largely unresolved. For successful adoption in clinical practice, radiologists require transparent and justifiable outputs, including visual cues and quantitative confidence measures that support AI-driven decisions. However, current approaches rarely integrate interpretability tools such as saliency mapping, attention weighting, or uncertainty quantification into microcalcification detection pipelines. This lack of explainability not only reduces trust in AI systems but also limits their practical deployment in high-stakes screening environments [127]. To consolidate these findings,

Table 2.6 summarizes the main gaps, their clinical implications, and opportunities for future work.

Table 2.6
Research Gaps and Opportunities in DBT Image Analysis

Research Gap	**Why It Matters**	**Research Direction**
Insufficient visibility of microcalcifications in DBT reconstructions	Restricted angular range, blur artifacts, and low spatial resolution obscure subtle calcifications, especially in dense breasts	Develop specialized enhancement models to improve calcification contrast while minimizing blur selectively
Lack of blur slice detection in DBT	Blurry slices caused by motion, focal spot trajectory, or reconstruction degrade interpretive quality and may obscure microcalcifications.	Design robust slice-level blur detection frameworks to filter suboptimal slices before enhancement and diagnosis.
Lack of publicly available, annotated DBT datasets with microcalcifications	Most studies rely on small, simulated, or phantom datasets, limiting generalizability and benchmarking.	Curate and share annotated DBT microcalcification datasets to enable robust, comparable deep learning model development.
Limited integration across the diagnostic pipeline (blur detection, contrast enhancement, lesion identification)	Treating tasks in isolation introduces inconsistencies and inefficiencies, affecting diagnostic robustness.	Develop end-to-end pipelines integrating blur detection, enhancement, and microcalcification detection for reliable and efficient DBT analysis.

In summary, the literature identifies four key gaps that hinder DBT's diagnostic potential: (i) inadequate microcalcification visibility, (ii) no blur slice detection frameworks, (iii) lack of annotated calcification datasets, and (iv) fragmented pipeline development. The proposed study addresses these issues by introducing a two-stage pipeline: UMVDSR-based and McCE algorithm (postprocessing) enhancement, augmented with integrated blur slice detection. This design aims to improve diagnostic precision, workflow integration, and transparency in DBT imaging.

2.7 Summary

This chapter has provided a comprehensive overview of the current landscape in DBT image analysis, focusing on challenges and advances in breast cancer screening, image enhancement, and lesion detection. Beginning with the clinical context of breast

cancer diagnosis, the chapter explored the significance and evolution of DBT as a 3D imaging modality, offering improved detection accuracy over traditional 2D mammography, particularly in dense breast tissues. The discussion detailed conventional and advanced diagnostic techniques for DBT, highlighting persistent challenges such as limited contrast resolution, image blurring, and difficulty in identifying subtle abnormalities, including microcalcifications.

Recent research has increasingly shifted toward the use of deep learning for both image processing and lesion detection, with promising results in tasks such as blur detection, denoising, and automated lesion classification. However, the effectiveness of these models is heavily dependent on image quality issues, such as noise and blur, which can significantly impact performance, as noted in Sections 2.4 and 2.5. A focused review of blur detection techniques underscored the transition from conventional, handcrafted methods to data-driven deep learning approaches, which offer superior sensitivity and adaptability. This naturally leads to the critical importance of contrast enhancement, especially for microcalcifications that often appear faint or obscured in DBT slices. Section 2.6 emphasized the clinical relevance of these small calcifications and the role of both traditional and deep learning-based enhancement methods in improving their visibility.

Together, the insights from this literature review not only frame the current capabilities and limitations of DBT image analysis but also reinforce the motivation behind this study: to develop a deep learning-based approach for blur detection and contrast enhancement tailored to improving microcalcification visibility in DBT images of extremely dense breast tissue. The following chapter will present the methodology used to achieve this goal.

CHAPTER 3
METHODOLOGY

3.1 Introduction

This chapter presents the methodology used to develop and evaluate the proposed framework for detecting blur in Digital Breast Tomosynthesis (DBT) images, enhancing microcalcification contrast, and improving automated detection performance. The workflow is divided into three main stages: blur detection, image enhancement, and microcalcification detection. Each stage is designed to address specific limitations in DBT imaging and contribute to the overall goal of improving diagnostic accuracy. In the first stage, a comprehensive blur detection framework is employed to differentiate between blurry and non-blurry DBT images reliably.

The process begins with the Laplacian-based Blur Detection (LbBD) algorithm, which extracts handcrafted statistical features to provide an initial quality assessment. This is followed by deep learning based approaches, including a Convolutional Neural Network (CNN) constructed from scratch and an enhanced CNNSVM hybrid model, which leverages convolutional feature extraction with the classification strength of a Support Vector Machine (SVM). To further improve detection accuracy, a hybrid feature strategy is also explored, combining CNN-extracted features with additional handcrafted descriptors derived from the LbBD method. This ensures that only high-quality images are processed in the subsequent stages, thereby avoiding the amplification of noise and artifacts during enhancement.

The second stage focuses on microcalcification contrast enhancement using a hybrid deep learning approach that combines Very Deep Super Resolution (VDSR) with an Unsharp Masking (UM) pre-processing step and a Microcalcification Contrast Enhancement (McCE) post-processing algorithm. This approach aims to improve the visibility of delicate structures while minimizing background noise, thereby aiding both human interpretation and computer-aided detection systems. The adoption of a VDSR-based enhancement strategy in this study is further motivated by prior tomosynthesis research [125] demonstrating that convolutional neural network–based super-resolution can significantly improve image quality in limited-angle acquisition systems without compromising diagnostic fidelity.

The methodological contribution of this research lies in the design of a cascaded, content-aware DBT enhancement framework that integrates automated blur detection with targeted microcalcification contrast enhancement. Unlike existing DBT studies that treat image quality assessment and enhancement as independent tasks, this work introduces a sequential decision-driven pipeline, where diagnostically unreliable slices are first identified and excluded before enhancement is applied. Furthermore, the proposed methodology introduces a novel hybrid feature fusion strategy (CNNSVM-BF) that combines deep CNN representations with explicit blur quantification, and a task-specific CNN-based enhancement model (UMVDSR-McCE) tailored for microcalcification visibility in dense breast tissue.

The methodology presented in this chapter is organized as follows: Section 3.2 outlines the overall research design, describing the sequential stages of the proposed framework. Section 3.3 presents the dataset characteristics and the pre-processing steps applied before analysis. Section 3.4 details the proposed blur detection approaches, including learning-based, deep learning, and hybrid methods. Section 3.5 describes the image enhancement framework developed to improve microcalcification visibility in DBT images. Section 3.6 explains the performance evaluation procedures used to assess the effectiveness of each stage in the framework. Finally, Section 3.7 provides a summary of the chapter.

3.2 Research Design

A DBT-based breast cancer screening typically generates a large number of images for each patient. However, many of these DBT images may suffer from blurriness or insufficient quality for reliable diagnosis. In current clinical practice, there are no standardized metrics for quantifying image blurriness; instead, assessments generally rely on the radiologist's qualitative judgment, which can be subjective and prone to variability. To address this limitation, this study proposes a novel quantitative approach for evaluating and enhancing DBT images using a deep learning–based framework. The research methodology is structured into four sequential phases, as illustrated in Figure 3.1: (i) DBT image collection and acquisition, (ii) classification of DBT images into blurry and non-blurry categories, (iii) microcalcification local contrast enhancement of non-blurry DBT images, and (iv) performance validation and evaluation. This design ensures that only diagnostically reliable images are processed

in the enhancement stage, thereby minimizing noise amplification and improving the accuracy of subsequent microcalcification detection.

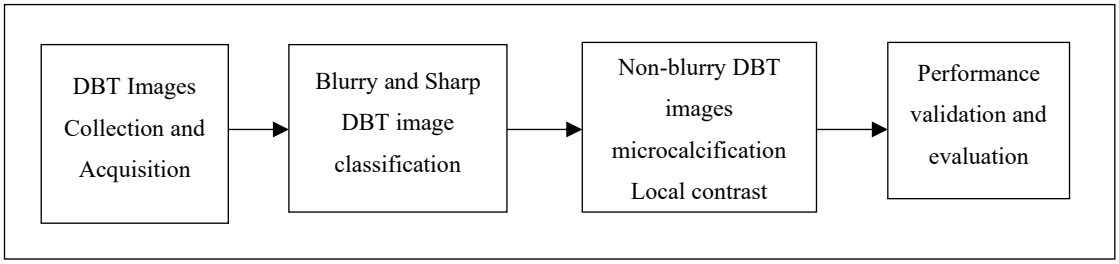

Figure 3.1 Block Diagram of Research Methodology

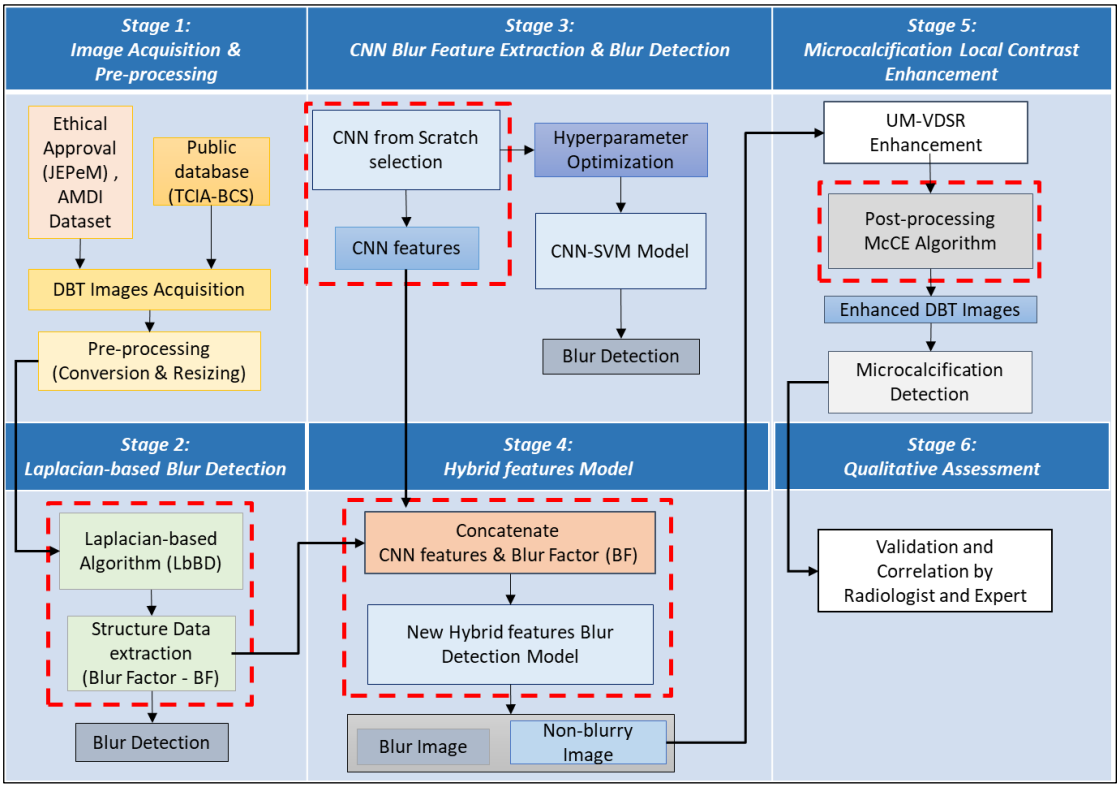

Figure 3.2 Overall Flow of Research Activities Involved in This Study. Red Blocks Indicate the Main Contributions in This Study

To implement each component of the methodology outlined in the block diagram, the research is structured into six distinct stages. The overall workflow of the study is illustrated in Figure 3.2. The process begins with Stage 1, which focuses on DBT image acquisition, including obtaining ethical approval, sourcing datasets, and conducting pre-processing steps such as conversion and resizing. This stage is described in detail in Section 3.3. Stages 2 to 5 address the proposed quantitative methods, while Stage 6 focuses on qualitative expert assessment.

In Stage 2, a newly developed LbBD algorithm is employed to classify DBT images into blurry and non-blurry categories. During this process, structural data referred to as the blur factor (BF) is extracted from the LbBD output. Stage 3 involves the development of CNN architectures from scratch for automated blur feature extraction. Multiple CNN models are evaluated to identify the most effective architecture for extracting discriminative features. The best-performing CNN features are then integrated into a CNNSVM hybrid model to perform blur or non-blur classification of DBT images, with performance comprehensively assessed. Stages 2 and 3 correspond to Research Objective 1 (RO1), with detailed methodology provided in Sections 3.4.1 to 3.4.3.

Stage 4 introduces a novel hybrid feature model for blur detection, in line with Research Objective 2 (RO2). Here, the structural BF data obtained in Stage 2 are combined with the automated CNN features from Stage 3 to enhance the classification accuracy of blurry and non-blurry DBT images. Both feature sets serve as complementary class descriptors. The methodology for this stage is described in Section 3.4.4.

Following Stage 4, only non-blurry DBT images are retained for further processing, while blurry images are excluded. Stage 5 focuses on the microcalcification local contrast enhancement of non-blurry DBT images, particularly for cases involving extremely dense breast tissue. This stage introduces a new enhancement pipeline that combines the UMVDSR model with a post-processing McCE algorithm. The aim is to improve the visibility of microcalcifications for subsequent detection tasks. Stage 5 corresponds to Research Objective 3 (RO3), and its methodology is explained in Section 3.5. Collectively, Stages 2 to 5 form a cascaded deep CNN-based framework that integrates blur detection with targeted contrast enhancement.

Stage 6 involves both quantitative and qualitative evaluation of the proposed framework. Statistical performance metrics are used to assess system performance, while a structured expert evaluation is conducted with radiologists and subject matter experts in medical imaging and image processing. Enhanced images are rated using a subjective scoring system (1 to 5) to assess visual quality and diagnostic usefulness. This stage addresses Research Objective 4 (RO4), with its methodology described in Section 3.6. Overall, the methodology is designed to align with the study's research objectives, with performance metrics discussed at the end of each stage.

3.3 Image Acquisition and Pre-processing

The dataset serves as the foundation for the analysis and results presented in this thesis. For this study, a comprehensive collection of DBT images was curated to ensure both the reliability and validity of the findings. The dataset comprises DBT images obtained from the Advanced Medical and Dental Institute (AMDI) of Universiti Sains Malaysia (USM) and a publicly available dataset accessible online. This section describes the data acquisition process and the pre-processing steps undertaken to ensure that the images are suitable, consistent, and relevant to the research objectives.

3.3.1 Image Acquisition and Data Collection

Two datasets were used in this study, namely, the Breast Cancer Screening Digital Breast Tomosynthesis (BCS-DBT) dataset [26], as well as a custom dataset collected at the Advanced Medical and Dental Institute Digital Breast Tomosynthesis (AMDI-DBT) for training and testing the proposed methods. The acquisition processes for both datasets are outlined below.

a) Public Dataset – (BCS-DBT)

The public online DBT dataset was primarily employed for initial analysis and model development in the formulation of the blurry–non-blurry image classification approach. This dataset was obtained from The Cancer Imaging Archive (TCIA) under the Breast Cancer Screening Digital Breast Tomosynthesis (BCS-DBT) collection (DOI:10.7937/E4WT-CD02), accessible at
https://www.cancerimagingarchive.net/collection/breast-cancer-screening-dbt/.

The dataset comprises 22,032 reconstructed DBT volumes from 5,610 studies involving 5,060 patients, collected at Duke Health System between 2014 and 2018. Patients were divided into four groups:

i) 5,129 normal studies
ii) 280 studies requiring additional imaging without biopsy
iii) 112 benign biopsied studies
iv) 89 studies with confirmed cancer

Two experienced radiologists annotated all cases containing masses or architectural distortions. As this research focuses on BI-RADS categories 4 to 6, with visible masses or architectural distortions and biopsy recommendations, only two groups of patients were selected, as highlighted in the yellow box in Figure 3.3. From the overall dataset, 201 patients with 396 DBT images were selected: 223 images from the benign group and 173 images from the cancer group.

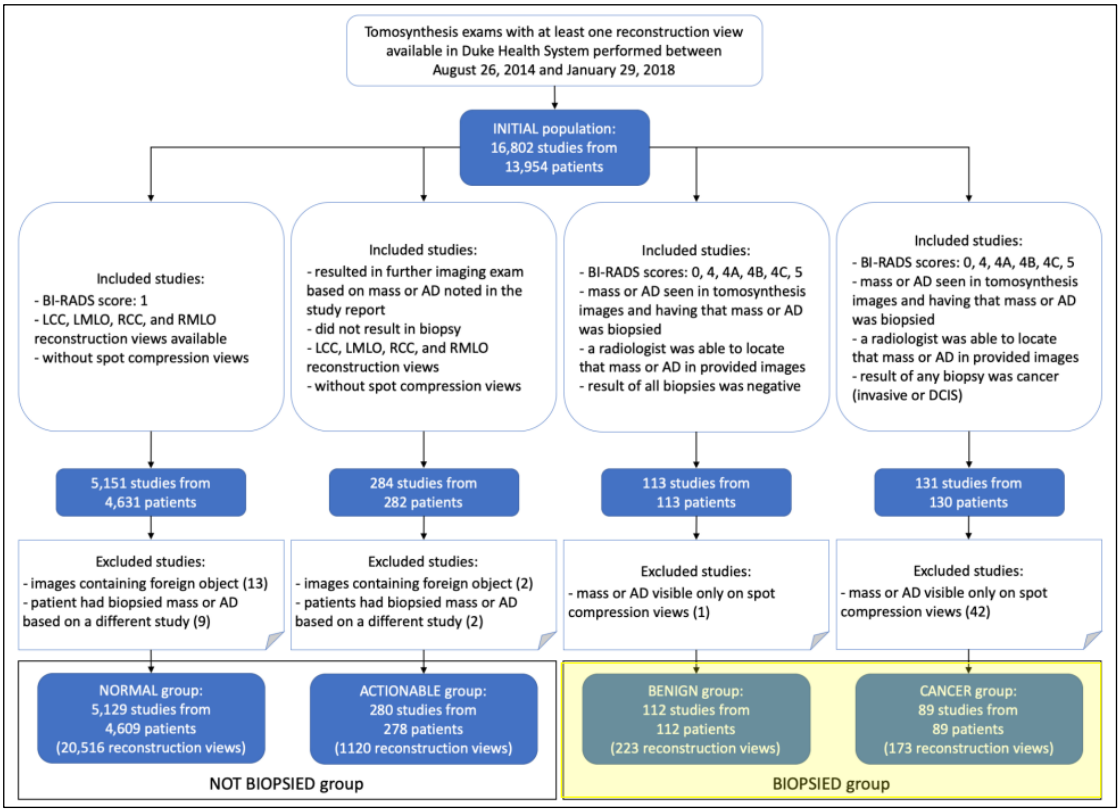

Figure 3.3 Patient Flowchart [26]

b) Advanced Medical and Dental Institute Dataset (AMDI-DBT)

The second dataset comprises DBT images obtained from AMDI, USM Bertam. Before data collection, ethical approval was granted by the Human Research Ethics Committee of USM (JEPeM) under code USM/JEPeM/21090622, approved on 13 December 2021 and valid until the end of 2023 (Appendix 1). In line with the approval, DBT images acquired between 2010 and 2023 were included without the need for patient interviews. All images were de-identified, anonymised, and securely stored in compliance with ethical regulations. Ethical approval is crucial for research involving

human subjects, particularly in medical imaging, to ensure patient confidentiality and compliance with regulatory standards.

The Imaging Unit, with assistance from a trained radiographer, extracted the DBT images from the Picture Archiving and Communication System (PACS) according to the specifications required in this study.

Inclusion criteria:

i) Female patients aged 25 years or older
ii) Suspicious abnormality on DBT, unilateral or bilateral
iii) BI-RADS category 4, 5, or 6 with biopsy recommended
iv) DBT images containing calcifications or microcalcifications

Exclusion criteria:

i) Images with significant artifacts or distortions
ii) Patients with prior breast surgery affecting breast anatomy (e.g., lumpectomy, mastectomy, reconstruction)
iii) Pregnant or lactating patients

A total of 2,643 DBT images from 12 subjects meeting these criteria were retrospectively collected between early 201~~2~~0 and March 2023.

c) Dataset Split

According to the Pareto principle, each dataset was split into 80% training and 20% validation sets. While the Pareto principle endorses the 80:20 divide, it is primarily a heuristic seen in deep learning applications[128]. The split was performed using a MATLAB script (splitarraydatastore), which takes an image list as input and randomly assigns the images into the specified proportions. The dataset distribution is summarised in Table 3.1.

Table 3.1
Total Number of DBT Images and Split Fraction for Both Datasets

Dataset	No. of Images	Split Fraction	
		Training 80%	Validation 20%
BCSDBT	396	316	80
AMDI-DBT	2643	2115	528
Total	3039	2431	608

3.3.2 Image Pre-processing

The pre-processing stage began with the original input images, which were converted from DICOM-type files into bitmap-type (.bmp) files. The standard biomedical imaging file format, DICOM, includes essential metadata for retaining key image information and was used for acquiring both datasets. However, this format cannot be directly used as input for deep learning models due to limited compatibility with standard training pipelines. For this reason, all images were converted to .bmp format, which is readily processed in MATLAB without significant information loss.

Following format conversion, all DBT images were resized to a standard resolution to ensure uniformity of input dimensions, reduce computational cost, and minimise memory usage during training. Image sizes across both datasets varied in height and width, although each dataset was internally consistent. In Stage 2, the choice of image size was particularly critical because it directly influenced the variance values in the Laplacian-based blur detection (LbBD) algorithm. Image resizing experiments, involving stepwise reductions from 25% to 10% of the original size, were conducted to determine the optimal scale without compromising detection accuracy.

For Stages 2 to 4 (blur detection and classification), all images were resized, as determined through preliminary experiments (Section 3.4.1). This resolution was found to balance computational efficiency with the preservation of diagnostically relevant features, such as microcalcifications and subtle tissue structures. For Stage 5 (microcalcification local contrast enhancement), the original full-resolution DBT images were used to ensure that no fine structural details were lost before enhancement. This approach maximised the potential for contrast improvement, particularly in

extremely dense breast tissue, and preserved the highest possible fidelity for both automated detection and expert visual assessment.

Figure 3.4 shows examples of non-blurry and blurry DBT images containing microcalcifications before and after resizing. The resizing preserved the visibility of microcalcification clusters and important structural cues, while the original resolution was retained for enhancement in Stage 5 to maintain full diagnostic value.

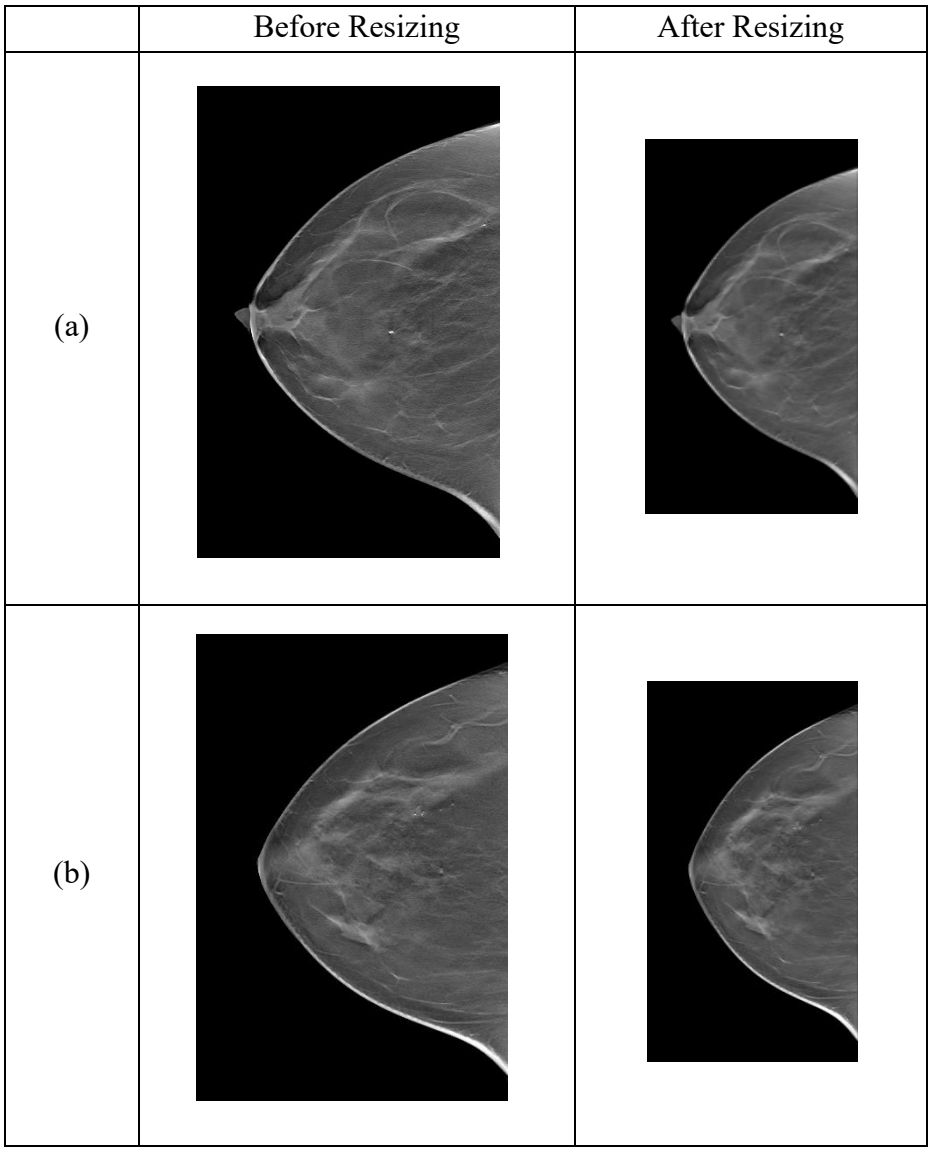

Figure 3.4 Examples of DBT Images with Microcalcifications Under Different Conditions Before and After Resizing. (a) Non-blur DBT Image with Microcalcifications, (b) Blur DBT Image with Microcalcifications

From a deep learning perspective, reducing the image dimensions lowers the computational complexity, allowing the CNN to process more images per batch while reducing GPU memory demands. This enables faster convergence during training

without significantly compromising feature representation. From a clinical perspective, the chosen resolution preserves the visibility of delicate microcalcification clusters and subtle structural variations that are diagnostically important in DBT images. Excessive downscaling risks blurring these small details, which could degrade classification and detection accuracy, while excessively high resolutions can lead to overfitting and prolonged training times.

By adopting the resized resolution for early stages and reverting to the original resolution for enhancement, this study ensures that both automated CNN feature extraction and expert visual inspection can be performed effectively, maintaining diagnostic integrity while optimising computational performance in the earlier stages.

3.4 Detection of Blurry DBT Images

This study introduces a novel hybrid feature approach termed Convolutional Neural Network–Support Vector Machine–Blur Factor (CNNSVM-BF), designed specifically for the detection of blur in DBT images. The method integrates two distinct yet complementary sources of information: automated deep features extracted through a custom-developed CNNSVM model and handcrafted structural features in the form of BF computed from the LbBD algorithm. In the initial stage of processing, the BF values are calculated using the Laplacian operator, providing a quantitative representation of image sharpness. Following this, a CNN developed from scratch is applied to extract deep, high-level features that characterise blur in DBT images. Unlike conventional blur detection approaches that rely solely on handcrafted metrics or end-to-end deep classifiers, this study adopts a hybrid feature learning paradigm, where explicit blur descriptors are integrated with learned deep representations to improve robustness and interpretability.

The need for this dual-feature approach arises from a key limitation in the current research landscape, as no publicly available image quality dataset includes DBT images annotated for blur detection. Consequently, expert radiologists were engaged to manually classify the available DBT datasets into two groups: blurry images and non-blurry images. This expert-driven annotation process not only served as the ground truth for model training but also provided a baseline for evaluating the effects of image blur on subsequent microcalcification detection tasks. The hybrid CNNSVM-BF approach leverages CNN-derived image features alongside the handcrafted BF metric to

strengthen the representation of global blur characteristics, thereby enhancing classification accuracy while reducing computational demands. The overall methodology is structured as an integrated pipeline, as illustrated in Figure 3.5, commencing with the computation of the Blur Factor from the LbBD algorithm, followed by CNN-based feature extraction, and blur classification using the CNNSVM model. Finally, the combination of CNN features with BF values forms a hybrid feature vector for final blur detection. This sequence forms a cohesive framework for addressing the challenges of automated blur detection in DBT imaging.

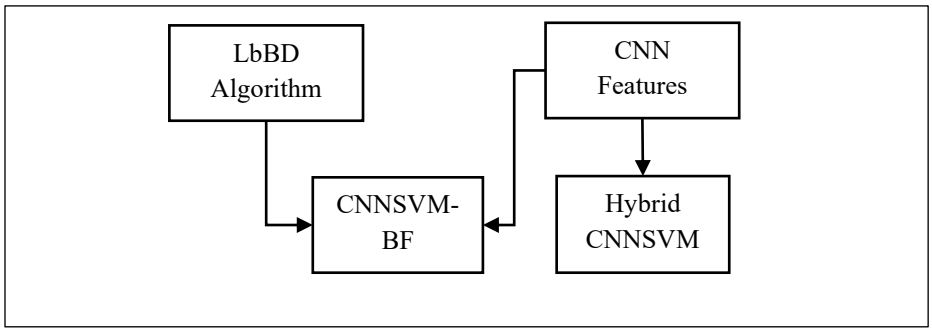

Figure 3.5 Four Main Components of Blur Detection Methodology

3.4.1 Proposed Laplacian-based Blur Detection (LbBD) Algorithm and Blur Factor

There are numerous approaches to quantify image blurriness. Nevertheless, one of the most widely adopted and computationally efficient methods is the variance of the Laplacian technique, which yields a single floating-point value representing the degree of image sharpness or blur [129]. Despite its practicality, there are currently no standardised quantitative parameters in clinical radiology for determining the level of blurriness in DBT images. In routine practice, radiologists typically rely on subjective visual assessment, which can vary significantly between observers. This underscores the need for a robust, objective, and reproducible metric for blur quantification in clinical imaging workflows.

In this study, the LbBD algorithm was developed to assign a numerical blurriness level referred to as the Blur Factor (BF) to each DBT image before classification into “blurry” or “non-blurry” categories. The Laplacian operator was applied to emphasise grey-level discontinuities and suppress regions with gradually varying intensity, thereby facilitating the detection of edges. This second-order

derivative filter generates an output where object boundaries and fine structures appear as grey edge lines against a dark background [130], enabling the identification of both external and internal edges within the breast tissue. The LbBD algorithm begins by reducing the resolution of the input images by 25%, 20%, 15%, and 10% to calculate an optimal variance measure representing the total number of edges. The Laplacian operator is then convolved with the reduced-resolution image, and the variance of the resulting response is computed. A high variance value in an in-focus image indicates many edge responses, while a low variance implies fewer detected edges, suggesting that the image is likely blurred.

Therefore, an image can be considered blurry if it contains a relatively small number of detectable edges. The selection of a suitable threshold is highly dependent on the specific domain, and an inappropriate choice can lead to incorrect labeling of images. For instance, an image with no significant blurriness might be incorrectly classified as “blurry,” whereas a genuinely blurred image might be labeled as “non-blurry.” To mitigate this, each image’s intensity variance was plotted along an axis with two distinct centers, corresponding to the blurry and non-blurry classes, and the optimal threshold was determined analytically. The decision boundary between classes was then defined using the weighted mean of these class centers. However, relying solely on a direct thresholding approach proved inadequate due to its excessive sensitivity to threshold selection.

Finally, all calculated BF values and their associated blur statuses were systematically tabulated for subsequent use in the hybrid CNNSVM-BF framework. The complete operational workflow of the LbBD algorithm is depicted in Figure 3.6, while Figure 3.7 outlines the primary computational steps used to generate the BF table. Together, these components provide a robust quantitative foundation for integrating Laplacian-based structural analysis with deep learning features in the blur detection process for DBT images.

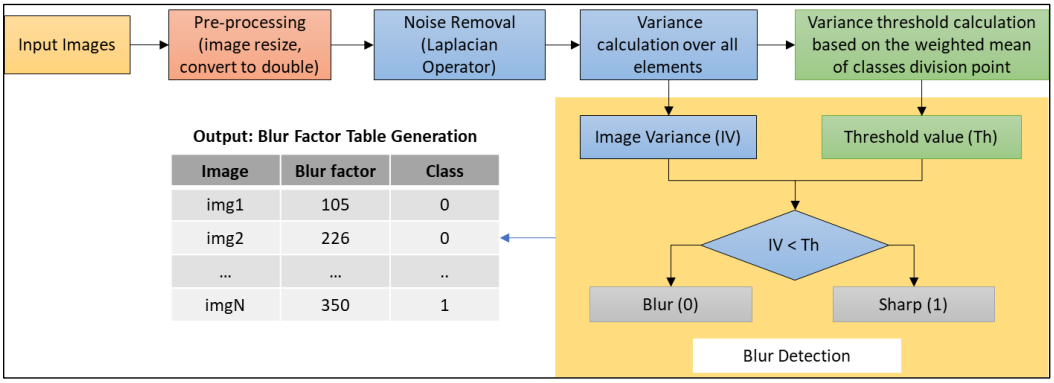

Figure 3.6 Flowchart of the LbBD Implementation

Algorithm 1 Laplacian Blur Factor Algorithm

1 **Input:** DBT images **Im**
2 **Output:** Blur factor **bf**
3 **for** *k=1 to numberOfImages* **do**
4 Read input image
5 Resize image
6 Convert image to double (multidimensional matrix)
7 Find Laplacian variance using Laplacian filter and variance function
8 Initialize Threshold value Th
9 **if** *Iv< Th* **then**
10 Label image = 0 (Blurry)
11 Denote variance value as blur factor
12 **else**
13 Label image = 1 (Non-Blurry)
14 Denote variance value as blur factor
15 **end if**
16 **end for**
17 Tabulate all the blur factor and status for each input image

Figure 3.7 Pseudocode for Laplacian-based Blur Detection (LbBD) Algorithm

3.4.2 Feature Extraction using CNN Constructed from Scratch

While recent advances in deep learning have significantly improved blur detection performance, existing CNN-based approaches often remain constrained by high computational complexity and hardware demands. Architectures such as AlexNet [14] and GoogleNet [131], for example, require 62,378,344 and 6,799,700 parameters, respectively, necessitating substantial GPU memory and extended training times. The challenge is further compounded when training from scratch on relatively small datasets, as many parameters increase the risk of overfitting [132], [133]. Although multi-stream networks and transfer learning approaches have shown performance

improvements, they typically incur increased parameter counts, memory usage, and computational cost.

Reducing network complexity through methods such as decreasing the number of convolutional layers, reducing the number of neurons in fully connected layers, or lowering the resolution of input images has been widely explored in the literature [134], [135]. However, such simplifications must be carefully balanced to ensure that the model retains adequate representational capacity for the target task. In this study, the classification of blurry versus non-blurry DBT images aims to maintain generalisation to unseen data. Computational efficiency gains must therefore not come at the expense of classification accuracy.

To address these constraints, this study proposes a lightweight CNN constructed entirely from scratch to perform automated blur feature extraction. By designing the architecture in-house, precise control over its complexity is achieved, ensuring compatibility with available hardware resources while maintaining strong discriminative capability. Five progressively deeper architectures were developed, designated BDCNN1 through BDCNN5, each with an increasing number of convolutional layers ranging from three to seven. All models incorporated fully connected (FC) and SoftMax classification layers. Training and validation were conducted on the combined DBT datasets described in Section 3.3 to determine the optimal trade-off between network depth and performance.

Each CNN employs a standard three-stage design: convolutional layers, pooling layers, and fully connected layers augmented with batch normalization (BN) and Rectified Linear Unit (ReLU) activation functions. For instance, the BDCNN1 architecture consists of three convolutional layers with 8, 16, and 32 filters, respectively, each with a fixed 3×3 kernel size and a stride of 1. Symmetric padding of two pixels is applied to preserve border information, preventing the premature loss of peripheral features [136]. Following [137], BN layers are introduced after each convolutional layer to accelerate convergence by normalising the distribution of feature maps within each mini-batch. ReLU activation functions are employed to introduce non-linearity, enabling the network to learn complex, high-dimensional patterns [119], while max-pooling layers downsample the spatial dimensions, retaining key features and reducing computational load.

The remaining architectures (BDCNN2 through BDCNN5) follow the same basic structure but double the number of filters at each successive convolutional block,

enabling controlled scaling of representational capacity. The architectural parameters for all models are illustrated in Figure 3.8, and the parameter counts for the deepest model, BDCNN5, are reported in Table 3.2. Even with seven convolutional layers, the total parameter count remains substantially lower than that of conventional CNNs, reducing both memory footprint and training time. The novelty of the proposed CNN design lies not in architectural depth, but in its task-specific optimisation for DBT blur characterization, balancing representational capacity with computational efficiency. Unlike transfer-learning-based solutions, the network is constructed from scratch to learn DBT-specific blur patterns that are not present in natural image datasets.

The decision to limit the architecture to seven convolutional layers was a deliberate design strategy aimed at balancing model complexity and training stability. Intense convolutional neural networks, although capable of capturing highly abstract features, often encounter the vanishing gradient problem, where the gradients propagated backward through many layers diminish in magnitude, thereby hindering effective weight updates in earlier layers. By constraining the network depth, this effect is mitigated, ensuring that gradient flow remains sufficiently strong for all layers to learn effectively.

Furthermore, limiting the number of layers reduces the total number of trainable parameters, which in turn lowers the risk of overfitting. In this phenomenon, the model memorizes training data rather than generalizing to unseen samples. This is particularly important in medical imaging tasks, where annotated datasets are typically limited. Finally, a shallower network configuration facilitates faster convergence during training, as the optimization process is less complex and more stable. Collectively, these considerations justify the adoption of a seven-layer convolutional design as a trade-off between representational capacity, generalization ability, and computational efficiency.

Stochastic Gradient Descent with Momentum (SGDM) was initially adopted with a learning rate of 0.01 and 50 training epochs to evaluate the impact of layer depth on model performance. The selection of SGDM was motivated by its well-established convergence speed and training stability in CNN optimization, as supported by both empirical and theoretical studies [120]–[122].

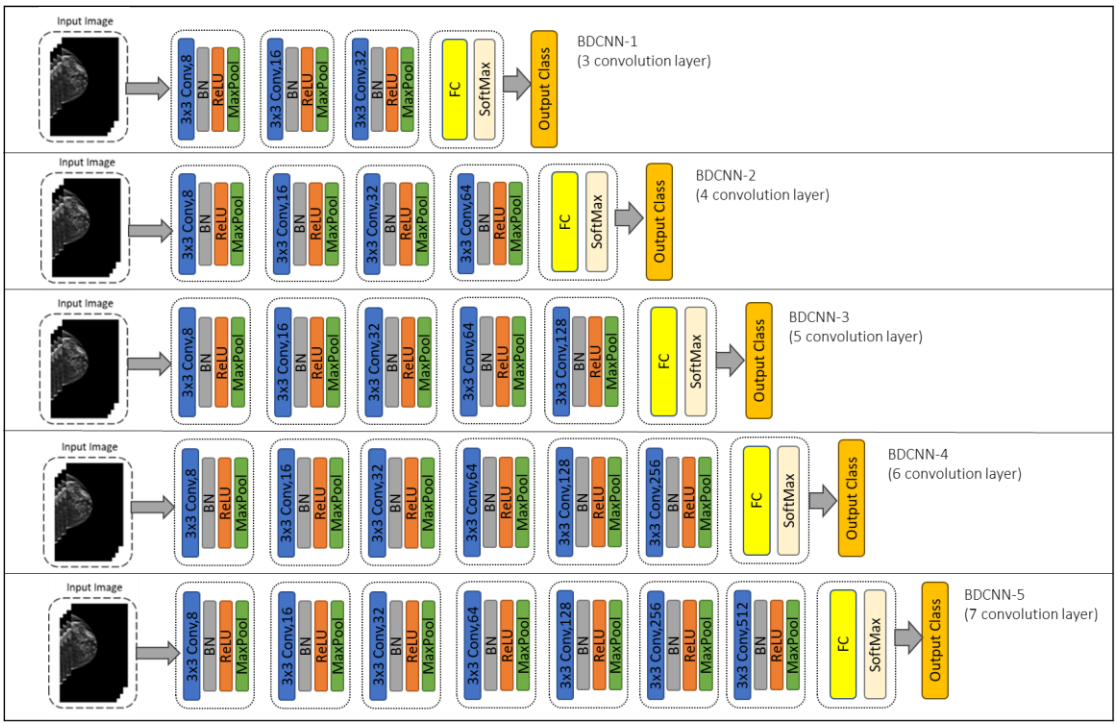

Figure 3.8 Five Models of Constructed CNN From Scratch

Table 3.2
Parameters of Constructed BDCNN5 Architecture

Layer	Layer Name	Parameter Properties	No. of Parameters
0	Input Image		0
1	Conv1	Weight 3×3×1×8 Bias 1×1×8	80
	BN1	Offset 1×1×8 Scale 1×1×8	16
	Relu1	-	0
	MaxPool1	-	
2	Conv2	Weight 3×3×8×16 Bias 1×1×16	1168
	BN2	Offset 1×1×16 Scale 1×1×16	32
	Relu2	-	0
	MaxPool2	-	
3	Conv3	Weight 3×3×16×32 Bias 1×1×32	4640

Layer	Layer Name	Parameter Properties	No. of Parameters
	BN3	Offset 1×1×32 Scale 1×1×32	64
	Relu3	-	0
	MaxPool3	-	
4	Conv4	Weight 3×3×32×64 Bias 1×1×64	18496
	BN4	Offset 1×1×64 Scale 1×1×64	128
	Relu4	-	0
	MaxPool4	-	
5	Conv5	Weight 3×3×64×128 Bias 1×1×128	73856
	BN5	Offset 1×1×128 Scale 1×1×128	256
	Relu5	-	0
	MaxPool5	-	
6	Conv6	Weight 3×3×128×256 Bias 1×1×256	294912
	BN6	Offset 1×1×256 Scale 1×1×256	512
	Relu6	-	0
	MaxPool6	-	
7	Conv7	Weight 3×3×256×532 Bias 1×1×532	1226260
	BN7	Offset 1×1×532 Scale 1×1×532	1064
	Relu7	-	0
	MaxPool7	-	
8	Fc1	Weight 2×532 Bias 2×1	1066
		Total Parameters	1622550

To further refine feature extraction and classification performance, three widely adopted optimisers, Stochastic Gradient Descent with Momentum (SGDM), Adaptive Moment Estimation (Adam), and Root-Mean-Squared Propagation (RMSProp), were systematically evaluated. Optimisers were tested across a range of hyperparameters to assess convergence speed, stability, and final accuracy. Specifically, learning rates of 0.001, 0.01, and 0.1 and training epochs of 50 and 100 were investigated while holding other parameters constant.

SGDM is among the simplest yet most effective optimization algorithms for deep learning. Unlike plain SGD, which may suffer from slow convergence and oscillations in ravine-like loss surfaces, SGDM introduces a momentum term that accumulates a moving average of past gradients. This allows the optimizer to accelerate convergence in the relevant direction while dampening oscillations across sharp curvature regions. The learning rate in SGDM is typically kept static, but the addition of momentum significantly improves stability and convergence speed in training CNNs [141].

The Adam optimizer is widely used in deep learning because it effectively combines the strengths of AdaGrad and RMSProp. Specifically, Adam computes adaptive learning rates for each parameter by maintaining exponentially decaying estimates of the first-order moment (the mean of past gradients) and the second-order moment (the uncentered variance of past gradients). This dual-moment estimation enables Adam to balance the rapid convergence benefits of RMSProp with the robustness of AdaGrad, making it highly suitable for non-stationary and sparse gradient problems [142].

RMSProp, introduced by [142], is an adaptive learning rate optimization algorithm. It maintains an exponentially decaying average of squared gradients for each parameter, which is then used to normalize the gradient updates. By dynamically adjusting learning rates in this way, RMSProp effectively addresses challenges posed by non-stationary objectives and helps stabilize training, especially in recurrent and deep neural networks. The characteristics and hyperparameter configurations for each optimizer are presented in Table 3.3. This comparative evaluation ensured that the final CNN architecture was paired with the most effective optimisation strategy for robust, efficient, and accurate blur feature extraction in DBT image analysis.

Table 3.3
Optimizer Characteristic and Hyperparameters Setting

Optimizers	Characteristics	Specifications
SGDM	Simplest deep learning optimizer. A static learning rate for all the parameters requires the duration of the whole training, and it has a fast convergence ability [31].	learning rate = 0.001/0.01/0.1, epoch = 50,100 weight decay = 0.0005, momentum = 0.9, Nesterov = False
ADAM	Adam evaluates adaptive learning rates from the first and second moments of gradients for various parameters [32].	learning rate = 0.001/0.01/0.1, epoch = 50,100 beta1 = 0.9, b eta2 = 0.999, epsilon = 1 × 10−8, amsgrad = False
RMSProp	To reduce the training time, the RMSProp learning rate decays exponentially [33]	learning rate = 0.001/0.01/0.1, epoch = 50,100 rho = 0.9, epsilon = 1 × 10−7

3.4.3 Hybrid CNNSVM

CNN and SVM represent two of the most powerful and widely adopted techniques in contemporary machine learning and computer vision, each excelling in different aspects of the classification process. CNNs, with their hierarchical architecture, are capable of automatically learning multi-level visual features directly from image data, capturing both low-level primitives such as edges and textures, and progressively abstracting them into higher-level semantic representations [14]. In contrast, SVMs are renowned for their robust theoretical foundation in structural risk minimization [143] and their ability to construct optimal separating hyperplanes in high-dimensional feature spaces, thereby enhancing generalization performance even with limited data.

In recent years, several studies [110], [144], [145] have proposed hybrid CNNSVM models that combine the strengths of both paradigms, replacing the CNN's final SoftMax classification layer with an SVM classifier. This hybridisation enables the CNN to serve purely as a powerful feature extractor, while delegating the final classification stage to the SVM, which is better equipped to handle complex, non-linear

decision boundaries in the extracted feature space. Such an approach has been shown to improve accuracy and stability, particularly in tasks where the dataset size is insufficient for optimally training deep fully connected layers [146].

In the present study, the proposed hybrid CNNSVM model employs the best-performing six-layer architecture, BDCNN4, developed in Section 3.4.2, as the deep feature extractor for DBT blur detection. Each convolutional layer in this network progressively transforms the input image into increasingly abstract feature representations: the earliest layers respond to primitive structures such as edges and blobs, while deeper layers encode more complex patterns relevant to differentiating blurry from non-blurry DBT images. This hierarchical feature learning is particularly advantageous for DBT image analysis, where subtle structural differences, such as microcalcification visibility, can be critical for clinical interpretation.

The final fully connected layer of BDCNN4 is removed, and the output of the penultimate layer is extracted as a fixed-length deep feature vector. These vectors are then used as input to an SVM classifier configured with a radial basis function (RBF) kernel, selected for its ability to capture non-linear class boundaries that are expected in the blurry–non–blurry classification space. The SVM's hyperparameters kernel scale (γ) and box constraint (C) are optimised via grid search with 5-fold cross-validation to balance classification margin maximization with tolerance for minor misclassifications.

By decoupling feature learning CNN from decision boundary optimization SVM, the hybrid CNNSVM framework harnesses the complementary strengths of both methods: the CNN contributes rich, domain-relevant image descriptors, while the SVM ensures optimal separation between blurry and non-blurry image classes. The structural overview of the proposed BDCNN4SVM hybrid model is shown in Figure 3.9, which illustrates the sequential pipeline from DBT image input, through deep feature extraction, to SVM-based classification.

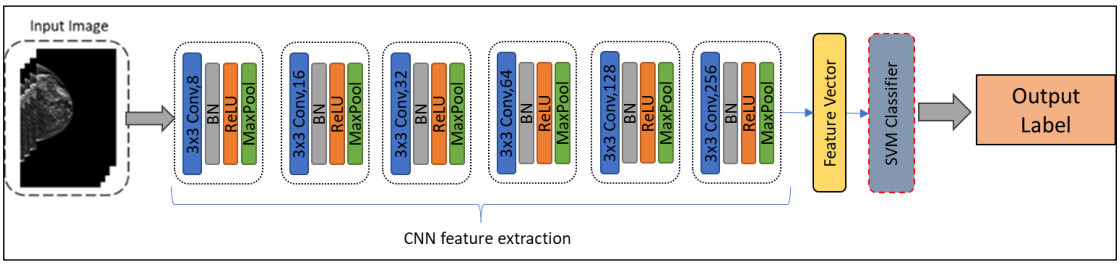

Figure 3.9 Structure of the Hybrid BDCNN4SVM Model for Enhanced Blur Detection in DBT Images

While the hybrid CNNSVM approach demonstrated superior performance, further investigations were conducted to determine whether alternative classification algorithms could yield comparable or improved results when paired with the BDCNN4 feature extractor. The integration is further evaluated against alternative classifiers, such as k-Nearest Neighbour (k-NN) and Decision Tree (DT), to assess whether the observed performance gains are unique to the SVM or consistent across other decision-making models.

The k-NN algorithm is a well-established non-parametric method in machine learning, widely used for classification due to its simplicity and effectiveness in various domains. In k-NN, each test image is classified according to the majority label among its k closest training samples in the feature space. The present study employed MATLAB's fitcknn function with default parameters, exploring k values of 3, 5, 7, and 9 to determine the most effective neighbourhood size. The Euclidean distance metric was used to compute similarity, and a kd-tree search method was employed to improve computational efficiency. To mitigate the influence of dominant classes in the neighbourhood, the option to weight neighbours according to their distance was considered, allowing closer points to exert greater impact on the classification outcome.

The DT classifier, in contrast, is a hierarchical, multi-stage decision-making model that recursively partitions the feature space into regions of homogeneous class labels. In this study, MATLAB's fitcdt function was used with default settings, configured to a maximum category level of 10, a maximum number of decision splits of 1, a minimum of one observation per leaf node, and a minimum of ten observations per branch node. The algorithm for determining the best split was set to 'allsplit,' ensuring an exhaustive search for optimal partitioning. While DTs offer interpretability and low computational cost, they are more susceptible to overfitting compared to margin-based classifiers such as SVMs.

Beyond custom-constructed architectures, a comparative study was also undertaken using well-known existing CNN models, AlexNet, ResNet18, ResNet50, VGG16, and InceptionV3 as deep feature extractors. These architectures have demonstrated state-of-the-art performance across large-scale image recognition tasks and offer varying trade-offs in network depth, parameter count, and computational complexity. Since fully connected layers generally produce the most discriminative features for classification, features from the final fully connected layer of each network were extracted and subsequently fed into a linear SVM classifier. The training

parameters were aligned with those used in the proposed BDCNN4SVM pipeline to enable fair comparison.

AlexNet consists of eight layers, five convolutional and three fully connected, and requires input images of size 227×227×3. It was the breakthrough model in the ImageNet Large Scale Visual Recognition Challenge (ILSVRC) 2012, leveraging over 14 million images for training across 1,000 classes. ResNet architectures, particularly ResNet18 and ResNet50, introduced the concept of residual learning, enabling the training of much deeper networks without degradation in accuracy; the former contains 18 layers, while the latter contains 50 layers, both with an input size of 224×224×3. VGG16 [133], though shallower than ResNet50, remains popular due to its uniform use of 3×3 convolutional kernels and a large number of filters, resulting in a high parameter count (138 million) and a substantial model size (515 MB). InceptionV3 [128] employs factorised convolutions and auxiliary classifiers, achieving competitive accuracy (78.1% top-1 on ImageNet) with an input size of 299×299×3 and a relatively compact 23.9 million parameters.

A comparative summary of these architectures is presented in Table 3.4, highlighting the trade-offs between depth, network size, and parameter count. As depth and parameter count increase, feature richness also increases; however, this comes at the cost of computational load and longer training times. This balance between architectural complexity and practical feasibility is particularly critical in medical imaging contexts such as DBT blur detection, where both accuracy and computational efficiency are essential.

Table 3.4
Selected Existing CNN Model Architectures

Model	**Image Input Size**	**Total Layers**	**Network Size (MB)**	**Parameters (M)**
AlexNet	227×227×3	8	227	61.0
ResNet18	224×224×3	18	96	25.6
ResNet50	224×224×3	50	167	44.6
VGG16	224×224×3	16	515	138.0
InceptionV3	299×299×3	48	89	23.9

3.4.4 Proposed New Hybrid Features CNNSVM Blur Detection Model

Building upon the feature extraction capabilities of the BDCNN4 architecture and the classification strength of the SVM, this study proposes a novel hybrid feature integration approach termed CNNSVM-BF. The method is designed to combine the deep, data-driven features learned by the CNN with a handcrafted, domain-specific descriptor, namely, the BF derived from the LbBD algorithm described in Section 3.4.1. This dual-feature strategy aims to exploit the complementary strengths of deep learning and traditional image processing, thereby enhancing the robustness and discriminative power of the blur detection model in DBT images.

The rationale for integrating the BF into the CNNSVM framework stems from the observation that CNN-derived features, while highly effective at capturing abstract and hierarchical representations, are not explicitly optimised for quantifying global blur characteristics. Conversely, the BF, computed as a variance-based edge descriptor from the Laplacian response, provides a direct numerical representation of blurriness that is grounded in human visual perception of edge sharpness. By combining these two complementary feature types, deep-learned representations and handcrafted structural descriptors, the CNNSVM-BF model can more effectively discriminate between non-blurry and blurry DBT images, particularly in challenging cases where deep features alone may be insufficient.

In the proposed workflow, DBT images are first processed through the BDCNN4 network to generate a deep feature vector from the final fully connected layer. In parallel, the same images undergo BF computation via the LbBD algorithm, producing a scalar blur descriptor for each image. These two outputs are then concatenated to form a hybrid feature vector, which is normalised and used as input to the SVM classifier. This fusion effectively injects global blur information into the learned feature space, allowing the classifier to leverage both high-level semantic features and explicit edge-based sharpness cues.

The advantage of this integration is twofold. First, the BF provides an additional axis of separability in the feature space, improving classification boundaries for cases where CNN features alone may produce overlapping clusters. Second, the inclusion of the BF imposes a level of interpretability to the decision-making process, as the blur score can be directly correlated with perceptual sharpness, thereby offering a quantitative justification for the classification outcome. This interpretability is

particularly valuable in clinical contexts, where explainability is a key factor in the adoption of automated decision-support tools.

To validate the effectiveness of the CNNSVM-BF approach, a comparative evaluation was conducted against both pure CNNSVM and pure CNN-FC baselines, as well as other classifier configurations described in Section 3.4.3. The assessment used identical training and validation splits (80:20) and employed the same hyperparameter settings for the SVM classifier to ensure fairness. Performance metrics, including accuracy, precision, recall, F1-score, and area under the ROC curve (AUC), were computed to assess classification efficacy. The results, presented in Section 4.3, demonstrate that the hybrid CNNSVM-BF consistently outperforms its non-hybrid counterparts across all metrics, particularly in improving sensitivity to blurry cases without sacrificing specificity in non-blurry image detection.

The hybrid approach is illustrated in Figure 3.10, which depicts the dual-stream processing pipeline, one branch extracting high-level CNN features and the other computing the BF, culminating in the feature fusion stage and final SVM classification. This architecture exemplifies how handcrafted domain knowledge, when judiciously integrated into a deep learning pipeline, can yield measurable improvements in performance while enhancing model interpretability for clinical end-users.

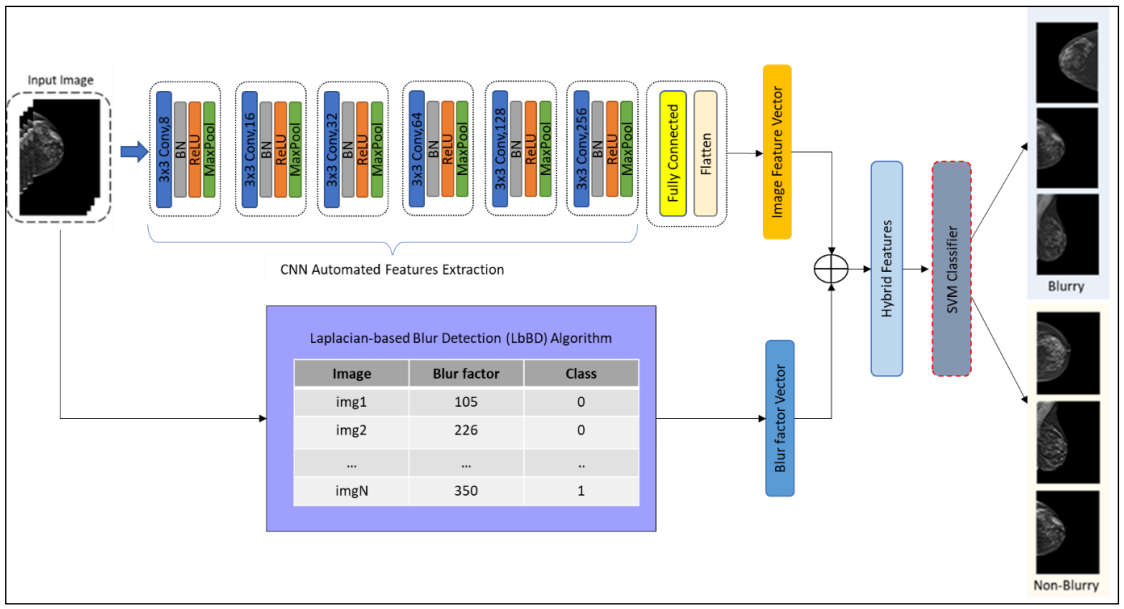

Figure 3.10 Architectural Design of Proposed CNNSVM-BF Hybrid Features Blur Detection Model

Figure 3.10 illustrates the hybrid features approach, which begins with the input of DBT images, which are simultaneously processed through two distinct yet complementary computational streams. In the deep feature extraction stream, the DBT images are fed into the optimised BDCNN4 architecture (as described in Section 3.4.2), which progressively learns hierarchical visual representations through convolutional, pooling, and fully connected layers. The output of the final fully connected layer forms a high-dimensional feature vector that encodes complex textural, structural, and contextual information relevant to blur classification.

In parallel, the handcrafted feature computation stream applies the LbBD algorithm (Section 3.4.1) to the same DBT images. This algorithm computes the BF by measuring the variance of the Laplacian response, yielding a scalar value that directly quantifies the degree of edge sharpness in the image. The outputs from both streams, the deep feature vector from the CNN and the scalar BF, are concatenated to form a hybrid feature representation. These hybrid features are then normalised to ensure feature scale compatibility before being passed into the SVM classifier. The SVM uses this enriched representation to learn an optimal hyperplane for separating non-blurry and blurry image classes, leveraging both abstract learned features and explicit edge-based sharpness cues.

This hybrid features design not only enhances classification accuracy but also increases the interpretability of the decision-making process. The BF provides a direct, quantifiable measure of blur that can be referenced in clinical assessments, thereby strengthening trust and transparency in automated DBT quality evaluation. Furthermore, this hybrid CNNSVM-BF formulation represents a key methodological contribution of this thesis, demonstrating that explicit domain knowledge (blur factor) can be synergistically integrated with deep features to improve classification performance, stability, and interpretability in DBT image quality assessment.

3.5 Proposed CNN-Based Contrast Enhancement Model for DBT Images

As outlined in Figure 3.2, Stage 5 of this research focuses on the development of a dedicated CNN-based framework for microcalcification local contrast enhancement in DBT images. The primary objective is to maximize the detectability of microcalcifications, thereby improving diagnostic accuracy in early breast cancer screening. In contrast to global contrast enhancement methods, the proposed

UMVDSR-McCE framework is designed as a selective, diagnostically driven enhancement strategy, operating exclusively on non-blurry DBT slices and focusing on microcalcification regions of interest to avoid unnecessary background amplification. This stage comprises two interdependent modules: image enhancement and microcalcification detection.

3.5.1 Microcalcification Local Contrast Enhancement: Unsharp Masking Very Deep Super-Resolution - Microcalcification Contrast Enhancement (UMVDSR-McCE)

Digital Breast Tomosynthesis has fundamentally transformed breast imaging by introducing three-dimensional reconstruction, effectively mitigating the issue of tissue overlap present in conventional two-dimensional mammography. However, while DBT provides volumetric data, the visibility of subtle high-frequency features such as microcalcifications remains strongly dependent on image quality parameters, including spatial resolution, noise levels, and artefact suppression. These tiny calcium deposits, often no larger than 0.1 mm, are clinically significant as they can represent the earliest radiographic signs of ductal carcinoma in situ or other malignant processes.

Despite the advantages of DBT, the detection of microcalcifications in dense breast tissue remains challenging. Poor image quality can obscure their presence, potentially leading to false negatives, which adversely affects clinical decision-making and patient outcomes [54]. Therefore, this study hypothesises that local contrast enhancement of DBT images targeted explicitly at microcalcification regions can improve their visual conspicuity and thus enhance both radiologist interpretation and CAD-based detection accuracy.

To address this, the proposed approach integrates Unsharp Masking Very Deep Super-Resolution (UMVDSR) as a pre-processing step, followed by a Microcalcification Contrast Enhancement (McCE) algorithm in the post-processing stage. This hybrid pipeline, referred to as UMVDSR-McCE, is designed to improve local contrast in calcification regions, suppress high-frequency noise while retaining diagnostically relevant delicate structures, and produce visually interpretable enhancement results without distorting surrounding soft tissue features. The rationale for this design is grounded in the strengths of the individual components: (i) VDSR provides a deep learning-based residual learning framework that restores high-

frequency details lost during image acquisition and reconstruction [148]. (ii) UM acts as a pre-filter to boost edge information, thereby improving the convergence and efficiency of VDSR training. By sharpening an image, the texture and finer details can be enhanced. One common method for sharpening is known as “unsharp masking,” which can be employed in various kinds of images. It should be noted that the unsharp mask technique does not introduce artifacts or add new details to the image, but it significantly enhances the appearance of existing details by increasing the acutance ofsmall-scale elements, making important details easier to perceive [149], [150] (iii) McCE applies targeted local contrast manipulation within detected calcification regions, avoiding unnecessary alterations to non-relevant areas.

The complete process flow is illustrated in Figure 3.11, where the UM pre-processed DBT image is first super-resolved using VDSR. Then, the McCE post-processing selectively enhances the calcification region of interest (ROI). Importantly, in this stage, only non-blurry DBT images identified from Section 3.4.4 are processed, ensuring that enhancement is applied to diagnostically optimal inputs.

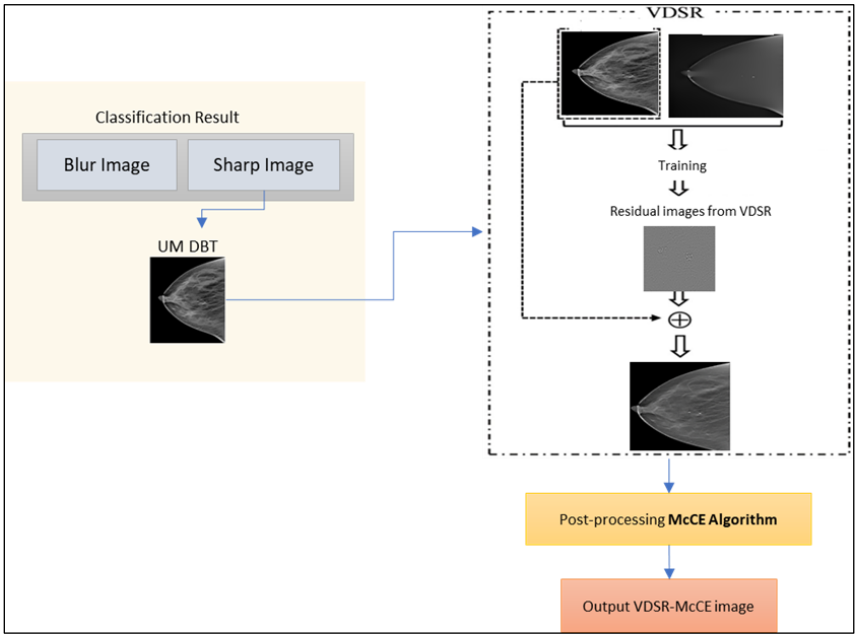

Figure 3.11 Flowchart of Microcalcification Local Contrast Enhancement: UMVDSR-McCE is Implemented by Combining Pre-Processing [Unsharp Masking (UM) with VDSR] and Post-Processing (McCE)

a) VDSR Architecture

The VDSR architecture, originally proposed by [148], is a 20-layer deep convolutional network optimised for single-image super-resolution. The network learns a direct mapping between low-resolution (LR) and high-resolution (HR) images by predicting a residual image, which captures the high-frequency details missing in the LR version. These residuals are then added back to the LR input to produce the final HR output.

Each of the 20 convolutional layers (except the first and last) employs 64 filters of size 3×3, followed by ReLU. The final layer reconstructs the residual using a 3×3×64 filter. The network's skip-connection-based residual learning approach allows for faster convergence and more stable optimisation, making it particularly suited to medical imaging, where preservation of fine details is crucial.

During training, scale factors of 2, 3, and 4 were used, and the corresponding LR images were created by bicubic downsampling of the original HR DBT projections. Data augmentation techniques such as small-angle rotations and translations were applied to increase training variability, thereby improving network generalisation. The resulting model was capable of reconstructing HR projections with enhanced microcalcification visibility, as shown in Figure 3.12.

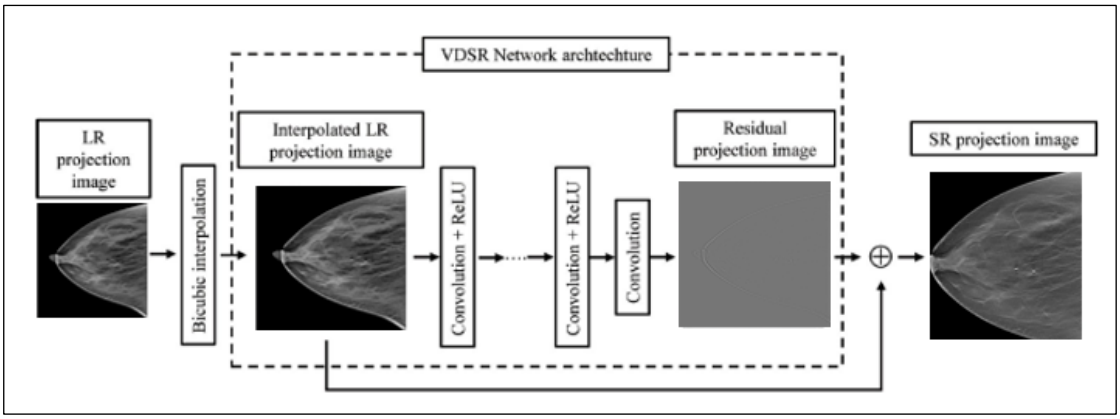

Figure 3.12 VDSR Network Architecture for DBT

b) Training dataset

For VDSR training, 200 reference DBT projections (with microcalcification) were randomly selected. Each reference image was paired with its LR counterpart, generated using bicubic interpolation at the chosen scale factors. The residual images

were computed as the difference between the HR reference and its interpolated LR version. This residual-focused learning reduces the network's complexity by focusing only on the missing high-frequency content.

c) Residual learning

Before VDSR processing, the LR images underwent Unsharp Masking with a Gaussian standard deviation of 2.5. This step enhances edge sharpness without excessively amplifying high-frequency noise, thus optimising the quality of input fed into the VDSR network. The UM pre-processing also improves the visibility of calcifications in the projection space, helping the network focus on relevant microstructural patterns.

d) Proposed McCE Algorithm

The McCE post-processing stage begins with calcification ROI segmentation using the UMVDSR-enhanced DBT image (Figure 3.13a). The most enormous contiguous blob representing the breast area is isolated using morphological filtering (Figure 3.13b). Pixels outside the breast mask are replaced with their mean background intensity (Figure 3.13c) to suppress irrelevant regions. Next, a top-hat transformation is applied to enhance bright, small-scale features such as microcalcifications while suppressing the larger background structures (Figure 3.13d). Following thresholding and binarisation, the final calcification mask (Figure 3.13e) is produced.

Local contrast enhancement is applied exclusively within the calcification mask using an edge-aware manipulation function, with the amplitude (0.4) and quantity (0.5) parameters set to their default values and retained following empirical evaluation on representative DBT images. Subsequently, unsharp masking is performed with a radius of 1.5 pixels and an amount of 1.0, also based on default function settings and empirical observation, to sharpen calcification edges while preserving surrounding tissue structures. Amplitude, quantity, and amount are dimensionless parameters. These parameter choices were found to provide a suitable balance between contrast enhancement and artefact suppression. As a result, the final enhanced DBT output remains diagnostically faithful and avoids the introduction of misleading visual artifacts. The stepwise McCE process is summarised in Figure 3.14, highlighting how

edge-preserving local contrast enhancement and targeted sharpening combine to maximise microcalcification conspicuity.

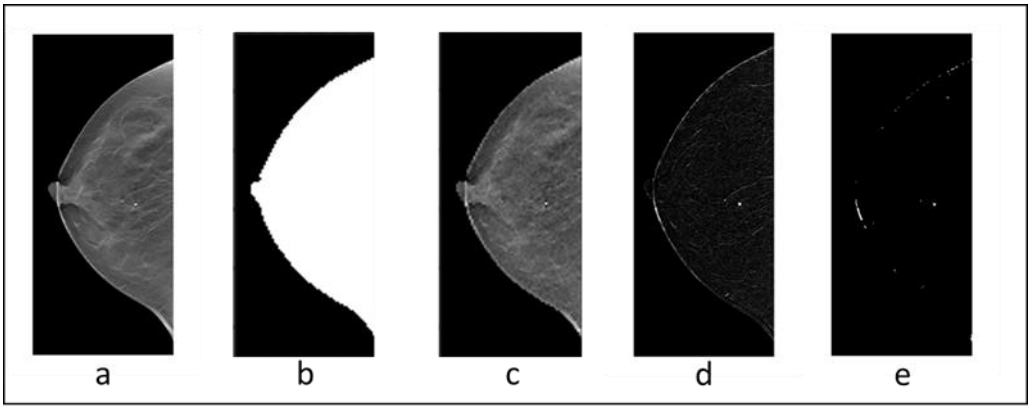

Figure 3.13 Calcification Mask Steps (a) Input image From Previous Stage (b) Breast Area Mask (c) Filtered Image in the Breast Area (d) Top-Hat Transformation (e) Final Mask with Calcification/Microcalcification

McCE Algorithm	
1	**Input:** DBT images ***Im***
2	**Output:** Enhanced images ***Is***
3	**for** *k=1 to numberOfImages* **do**
4	Read input image
5	Convert ***Im*** to gray scale image
6	Threshold set to 0: To get binary mask
7	Create breast mask of ***Im*** : Extract the large blob in the image and fill the area with hole.
8	Mask individual color channel: Extract individual red (R), green (G) and blue (B) color chanel and get the mean gray levels in R, G, and B.
9	Make outside the mask the mean of value above the threshold.
10	Create RGB image: combine separate color chanel into single true color RGB image. Output: ***rgbimg***
11	Convert RGB image, ***rgbimg*** to gray image
12	Perform morphologicalTop-hat filtering: Remove uneven background illumination from image with dark background. Output is ***I1***
13	Set McThreshold : ***McTh*** = *0.7*
14	Create calcification mask, ***cMask***: convert the **I1** to binary image using threshold value ***McTh.***
15	Create local contrast function with amplitude 0.4 and quantity 0.5
16	Reconstruct ***McLC*** image: Apply the local contrast function to calcification area, ***cMask***
17	Create Unsharp Masking function with with radius 1.5 and amount 1
18	Reconstruct ***McLCS*** image: Sharpen the calcification area, ***cMask*** using the unsharp masking function
19	**End for**

Figure 3.14 McCE Algorithm

To evaluate the performance of the proposed technique, it is compared with state-of-the-art contrast enhancement techniques such as histogram equalization (HE), Contrast Limited Adaptive Histogram Equalization (CLAHE), and contrast stretching using the DBT original dataset.

i) HE maps all input levels to one grey level [114]. The probability of all grey levels is uniformly distributed in the output image, i.e., at each grey level, we have an equal number of pixels. This technique has the disadvantage that it considers the global intensity of the image instead of the local intensity for contrast enhancement. It does not consider the input visual details of the image during enhancement. This results in the image having excessive contrast enhancement. The resulting image looks unnatural and causes visual artifacts in the image.

ii) CLAHE is an upgraded form of histogram equalization [151]–[153], which is generally used for low contrast images. CLAHE first divides the input image into multiple disjoint images that do not overlap each other [117]. After that, it performs histogram equalization on all the disjoint images. In this technique, the slope of the function is used for transformation, depending on the height of the histogram. Then, all histograms of these disjoint images are clipped to a limit. The clipping limit is used to limit the upper range of enhancement of every pixel. Histogram equalization of all sub-images is done separately. In the resultant image, all the details are very clear concerning the background. The CLAHE technique enhances both the foreground and background, which is the biggest advantage of this technique. This results in a high contrast output image.

iii) Contrast stretching in [154] is a type of normalization that performs stretching on the range of intensities. To perform stretching, this technique specifies limits of the upper pixel value on which normalization is performed; it also specifies limits of the lower pixel value for normalization of the image. The advantage of contrast stretching is that it enhances contrast in the image without distorting grey levels.

The contrast enhancement produces a processed image with higher contrast than the untreated image. Visual study of the image allows us to recognize this form of augmentation. However, visual inspection cannot provide a comprehensive and exact

characterisation. However, no parameter or approach can provide subjective and objective specialization. So, the performance is evaluated using the quality metrics PSNR and SSIM.

3.5.2 Assessing the Impact of UMVDSR-McCE Enhancement Method on Microcalcification Detectability

In alignment with the overarching objective of this study, a CNN-based framework for DBT image enhancement was developed to support diagnostic interpretation and facilitate early breast cancer detection within the breast region. Microcalcifications, minute calcium deposits that frequently manifest as early indicators of malignant lesions, play a critical role in clinical decision-making. Accurate identification of these structures is therefore essential for timely diagnosis and improved patient outcomes.

While earlier research has primarily concentrated on the recognition of microcalcifications in DBT images to assist radiologists, these efforts have often relied on conventional image processing or feature-engineering approaches, which may be less effective in challenging imaging conditions such as dense breast tissue. To address this gap, many recent studies have adopted the Faster Region-Based Convolutional Neural Network (Faster R-CNN) architecture as a robust detection paradigm. Faster R-CNN offers the advantage of integrating region proposal generation and classification into a unified deep learning framework, enabling efficient and accurate localization of microcalcifications even in cluttered or low-contrast backgrounds.

Building on this premise, the present study incorporates a modified Faster R-CNN model to evaluate the effectiveness of the proposed UMVDSR-McCE method. The aim is twofold: (i) to assess whether enhancement improves the detectability of microcalcifications in DBT images, and (ii) to compare performance against original non-blurry DBT images to quantify the added value of the proposed enhancement pipeline. For experimental evaluation, two datasets were prepared:

i) Non-blurry DBT Images (original) – comprising images classified as non-blurry during the blur detection stages (Section 3.4) and used without further enhancement.

ii) Enhanced DBT Images (UMVDSR-McCE) – comprising non-blurry images processed using the proposed local contrast enhancement method described in Section 3.5.1.

Both datasets were subjected to microcalcification detection using the Faster R-CNN model, with identical training parameters to ensure a fair comparison. Performance was evaluated in terms of detection accuracy, sensitivity, and false positive rate, thereby allowing for a comprehensive assessment of the impact of image enhancement on detection reliability. A qualitative visual inspection was also conducted to examine how well each approach highlighted microcalcifications, particularly in challenging cases involving dense glandular tissue. Representative detection results from both datasets are presented in Figure 3.15, illustrating the visual differences between original and enhanced non-blurryDBT images and their effect on detection outcomes.

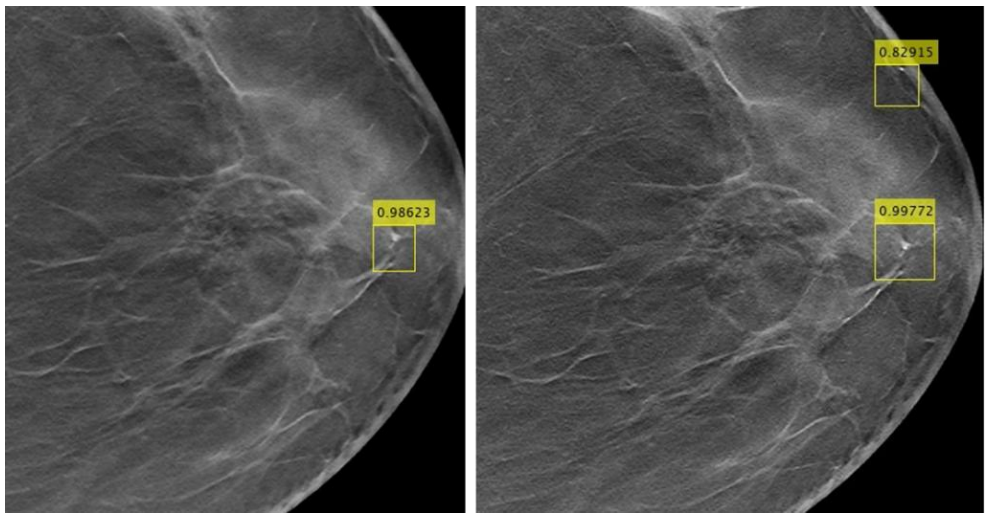

a) Original Non-blurry DBT image b) Enhanced Non-blurry DBT image

Figure 3.15 Example of Microcalcification Detection Outputs for Both Original Non-blurry and Enhanced Non-blurry (UMVDSR-McCE) DBT Images

3.6 Performance Evaluation

The evaluation of the proposed methodology is conducted in three complementary parts, reflecting the two principal contributions of this study: blur image detection and microcalcification local contrast enhancement, and incorporating both

quantitative and expert qualitative assessments. This tripartite evaluation framework ensures that the system's effectiveness is not only validated through computational metrics but also corroborated by clinical relevance and expert perception.

3.6.1 Performance of Blur Image Detection

The classification performance of the proposed CNNSVM-BF blur detection system is assessed using standard quantitative measures derived from the confusion matrix (CM). This matrix records the classification outcomes in terms of True Positives (TP), True Negatives (TN), False Positives (FP), and False Negatives (FN). From these components, the following performance metrics are calculated:

Accuracy (Equation 3.1): The accuracy of image classification is a percentage that represents the total quantity of correctly classified pixels to the number of pixels in the image. It examines an image's entire pixels correctly.

$$\text{Accuracy} = \frac{TP+TN}{TP+TN+FP+FN} \tag{3.1}$$

Precision (Equation 3.2): The true positive (TP) shows the percentage of pixels that were categorized correctly.

$$\text{Precision} = \frac{TP}{TP+FP} \tag{3.2}$$

Recall (Equation 3.3): The probability of pixel identification that logically displays typical characteristics but is classified as abnormal characteristics is known as a true negative (TN).

$$\text{Recall} = \frac{TP}{TP+FN} \tag{3.3}$$

F1-score (Equation 3.4): The ratio of predictive performance based on recall and precision, given by:

$$\text{F1-score} = \frac{2 \times \text{Precision} \times \text{Recall}}{\text{Precision} + \text{Recall}} \tag{3.4}$$

In addition, Receiver Operating Characteristic (ROC) curves are plotted to visualize the trade-off between TPR and False Positive Rate (FPR), defined as:

$$\text{FPR} = \frac{\text{FP}}{\text{FP+TN}} \tag{3.5}$$

The Area Under the Curve (AUC) is used to summarize classifier performance, with AUC = 1.0 representing a perfect classifier and AUC = 0.5 corresponding to random classification. Higher AUC values indicate superior discrimination capability between non-blurry and blurry DBT slices. Figures 3.16 and 3.17 present the metric definitions and the typical relationship between ROC curves and system performance.

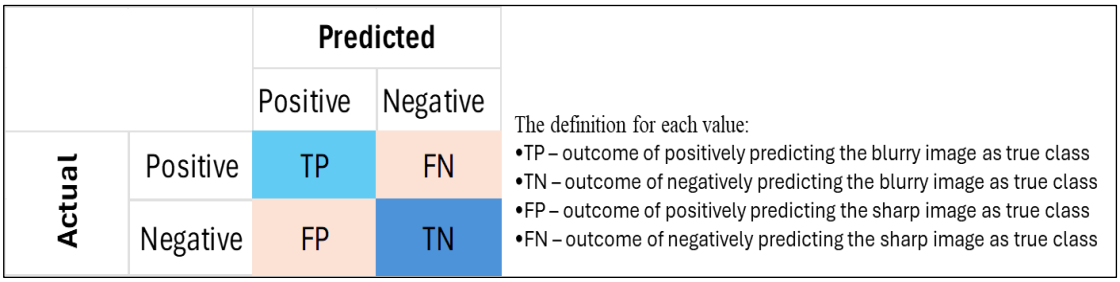

Figure 3.16 Summary of the Performance Metrics Used in CM.

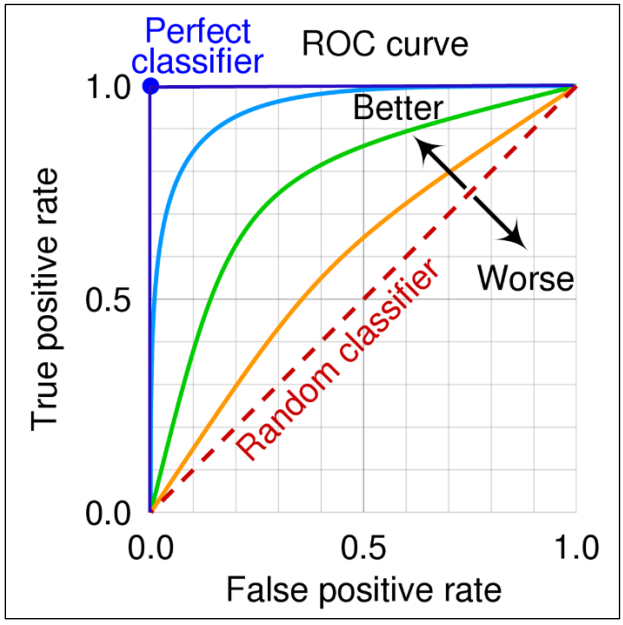

Figure 3.17 Shows Several ROC Curves and Their Relation to the System's Performance. AUCdenotes the Total Area Under Each ROC

3.6.2 Performance of Image Quality Enhancements

The quality of DBT image enhancement achieved by the proposed UMVDSR-McCE model is quantitatively evaluated using Peak Signal-to-Noise Ratio (PSNR) and Structural Similarity Index Method (SSIM), ensuring both pixel-level fidelity and perceptual image quality are assessed.

i) Peak Signal-to-Noise Ratio (PSNR)

PSNR is a standard metric for image quality, especially in enhancement or reconstruction tasks. Expressed in decibels (dB) and general interpretation in PSNR is:

- < 20 dB - Poor quality, significant distortion.
- 20–30 dB - Fair quality, but noticeable artifacts or blur.
- 30–40 dB - Good quality, close to the original, visually acceptable in most cases.
- > 40 dB - Excellent quality, almost indistinguishable from the reference image.

PSNR is derived from the Mean Squared Error (MSE) between the original input image I(i,j) and the enhanced output image E(i,j):

$$MSE = \frac{\sum (I(i,j)_{original} - E(i,j)_{filtered})^2}{\text{Image Size}}$$

The PSNR is calculated as:

$$PSNR = 10 \log_{10} \frac{256^2}{MSE}$$

MSE is the mean squared error between the reference and test images. A higher PSNR generally indicates closer similarity to the reference, although in medical imaging, high PSNR does not always equate to improved diagnostic quality, since enhancement may intentionally alter pixel values. Higher PSNR values typically indicate greater similarity between enhanced and reference images, although for contrast enhancement tasks, modest PSNR reduction may occur due to intended structural sharpening.

ii) Structural Similarity Index Method (SSIM)

SSIM is a perception-based model that evaluates image similarity based on luminance, contrast, and structural information. It is calculated as:

$$SSIM(x,y) = \frac{(\mu x2 + \mu y2 + C1)(\sigma x2 + \sigma y2 + C2)}{(2\mu x\mu y + C1)(2\sigma xy + C2)}$$

Where μx,μy are image means, σx,σy are standard deviations, σxy is the covariance, and C1, C2 are stability constants. SSIM values closer to 1.0 indicate higher structural similarity and perceptual fidelity. Unlike PSNR, SSIM is more sensitive to structural changes, making it especially relevant in medical imaging where lesion visibility is critical.

By employing PSNR and SSIM together, the evaluation captures both quantitative accuracy and qualitative visual fidelity, offering a balanced and clinically meaningful assessment of the enhancement process.

3.6.3 Expert Evaluation

The expert evaluation designed to validate the proposed DBT image enhancement system was both methodologically rigorous and clinically informed. It involved domain experts, including radiologists, biomedical engineers, image processing specialists, and radiographers, who were tasked with evaluating the visual and diagnostic performance of the system through structured image analysis tasks. The review was designed to collect subjective assessments of image clarity, blur detection accuracy, and microcalcification enhancement performance through a structured visual analysis process. Therefore, the evaluation form was segmented into four main sections, each tailored to assess a specific functional component of the enhancement framework.

Section A comprised a total of 10 image pair comparisons, with each pair consisting of two DBT slices extracted from the same volumetric dataset. Experts were required to identify which image was more suitable for cancer diagnosis. This section specifically targeted the system's capacity to reduce redundancy by automatically identifying and discarding slices with limited diagnostic value, thus enhancing workflow efficiency and interpretability for clinicians. Section B evaluated the effectiveness of the proposed blur detection method and contained 10 individual DBT images.. Experts were asked to categorize each image as either "blur" or "non-blur" based on visual perception without any prior indication of ground truth. This assessment provides insight into the model's performance in replicating human perception of image clarity, with the ultimate aim of identifying and discarding suboptimal slices prior to further enhancement or diagnostic analysis.

Section C assessed the enhancement of microcalcification visibility using a blind comparison approach. The evaluation involved 20 comparison sets, each comprising enhanced DBT images generated by three distinct models, including the proposed method. The experts were blinded to the model identities and were asked to choose the image set that best enhanced microcalcification visibility while preserving background tissue and anatomical structures. This allowed for an unbiased comparative analysis of the proposed method's enhancement performance against conventional alternatives.

Finally, Section D gathered qualitative feedback from radiologists regarding the overall usefulness, potential impact, and clinical integration of the proposed DBT enhancement pipeline. Experts rated various aspects of the system on a Likert scale and

provided open-ended comments on their expectations, including improved detection accuracy, time savings, standardization, and integration with computer-aided diagnosis (CAD) systems. The complete expert evaluation form, detailing the structure and content of the assessment, is provided in Appendix 3.

Overall, this multi-faceted evaluation framework not only confirmed the technical robustness of the proposed enhancement model but also validated its clinical viability through direct expert feedback on 50 curated DBT image samples. All responses were treated confidentially, and assessors were instructed to perform the evaluation independently to maintain the integrity of the data. The expert feedback collected serves as an essential component in validating the practical value of the developed system and in refining its performance based on real-world clinical insights. Further details and findings from the expert assessment are discussed in Chapter 4.

3.7 Summary

The primary objective of this research is to develop a new enhancement CNN-based model that can perform blur detection and microcalcification contrast enhancement tasks of DBT images. The proposed system will help reduce assessment time and increase microcalcification detection in the diagnosis procedure. This chapter discussed the overall proposed method that was developed by implementing six main methodology stages. Starting with DBT images acquisition and pre-processing, blur image detection using the LbBD algorithm, automated CNN feature extraction, and blur detection, a hybrid features CNNSVM-BF model, CNN-based microcalcifications local contrast enhancement, and performance evaluation.

The first method in detecting blur DBT images involves the Laplacian filter, which is sensitive to kernel size and affected by the input image size. The suitable image size is crucial to get correct variance calculations. Besides, the LbBD algorithm predicting a blurry image based on the threshold value and the selected value will affect the prediction result. Therefore, an automated CNN-based feature extraction and blur detection is a better solution that enables good detection performance with significant accuracy. This study proposed a new hybrid CNNSVM-BF model for blur detection that integrates two feature vectors: one from automated CNN feature extraction and another from a blurry vector formulated by the LbBD algorithm.

Next, the detected blurry images are eliminated, and the non-blurry images are used for further enhancement. A new CNN-based microcalcification local contrast enhancement method was proposed for efficiently enhancing microcalcification in DBT images. The UMVDSR-McCE algorithm was proposed to strengthen microcalcification contrast while preserving the edge information of breast soft tissues and microcalcification. Lastly, to analyses the effect of the proposed enhancement, the Faster-RCNN object detection network was adapted to detect microcalcification on enhanced DBT images. The confidence level of microcalcification detection represents the effectiveness of the enhancements.

Five performance metrics, including accuracy, precision, recall, F1-score, and AUC, were calculated and recorded to evaluate each of the proposed models for blurry DBT image detection. Then, three image quality measurement metrics, MSE, PSNR, and SSIM, were used to measure the enhanced image quality. All the findings of these methodologies are presented and discussed in the next chapter.

CHAPTER 4
RESULT AND DISCUSSION

4.1 Introduction

This chapter presents the experimental results and discussion for the proposed Digital Breast Tomosynthesis (DBT) image enhancement framework. The chapter is structured into four main sections: blur detection, image enhancement, microcalcification detection, and expert evaluation. The first section evaluates the performance of the proposed Laplacian-based Blur Detection (LbBD) algorithm and deep learning-based models in distinguishing between non-blurry and blurry DBT images. Various configurations are tested to determine the most effective approach for accurate and consistent classification.

The second section investigates the effectiveness of the proposed hybrid enhancement approach, which combines a Unsharp Masking Very Deep Super-Resolution (UMVDSR) network with Microcalcification Contrast Enhancement (McCE). This technique is designed to improve the visual quality and structural clarity of DBT images, particularly in regions containing fine calcification details, without introducing excessive noise. The third section focuses on the microcalcification detection stage, analyzing performance for both original non-blurry and VDSR-McCE enhanced non-blurry DBT images across multiple datasets. Quantitative analysis, supported by qualitative visual inspection, is presented to evaluate the improvement in detection confidence and localization accuracy achieved by the enhancement method.

Finally, the expert evaluation section assesses the clinical relevance and perceived quality of the enhanced images by experienced image processing experts and radiologists. This step provides valuable qualitative feedback to complement the quantitative metrics, ensuring that improvements are meaningful in a real diagnostic context.

4.2 Analysis of Blur Detection in DBT Images

This section presents a detailed analysis of blurry image detection in DBT images. The evaluation focuses on the proposed blur detection framework, assessing its

effectiveness through both qualitative assessment of image outputs and quantitative performance metrics. The analysis also considers the impact of accurate blur detection on the downstream microcalcification local contrast enhancement stage, given that the quality of input images directly influences the reliability of subsequent processing.

Performance was evaluated using standard classification metrics: accuracy, precision, recall, and F1-score. In this context, precision denotes the proportion of correctly identified blurry images among all images classified as blurry. At the same time, recall represents the proportion of correctly identified blurry images relative to the total number of accurate blurry images. These two metrics often exhibit a trade-off: increasing sensitivity can improve recall but may reduce precision, whereas stricter classification criteria can yield high precision at the expense of recall. The F1-score, calculated as the harmonic mean of precision and recall, provides a balanced indicator of algorithm performance, rewarding models that maintain both high precision and high recall. A consistently high F1-score, therefore, reflects robust and well-balanced detection capability.

4.2.1 Analysis of Laplacian-based Blur Detection (LbBD) Algorithm

This section presents the results of blurry image detection using the proposed LbBD algorithm. DBT images were selected and annotated as either non-blurry or blurry by a radiologist through visual assessment. The analysis was conducted in two stages: the effect of image resizing on variance calculation and the impact of threshold selection on classification performance.

In the first stage of the analysis, the influence of image resizing on the variance values produced by the Laplacian-based Blur Detection (LbBD) algorithm was systematically investigated. The LbBD algorithm employs a 3×3 Laplacian filter to approximate the second-order spatial derivatives of pixel intensities, thereby highlighting abrupt local intensity changes associated with edges. While this operation is effective for edge detection, its response is highly sensitive to image scale and spatial frequency content. The original DBT images, stored in DICOM format, have pixel dimensions ranging from approximately 1000 to over 2000 pixels per direction, which are substantially larger than the Laplacian kernel. When such high-resolution images are processed directly, the 3×3 filter disproportionately emphasizes high-frequency noise and very fine local variations, which can dominate the variance measure and

obscure the structural edge information relevant for blur discrimination. As a result, variance values computed at the original resolution may not accurately reflect perceived image sharpness.

Resizing the images reduces spatial redundancy and suppresses high-frequency noise while preserving dominant edge structures. As illustrated in Figure 4.1, resizing enhances the relative prominence of meaningful intensity transitions, leading to Laplacian-filtered images with clearer edge patterns and more stable variance estimates. This effect is critical because the variance of the Laplacian response is used as the quantitative indicator of blur in the LbBD framework.

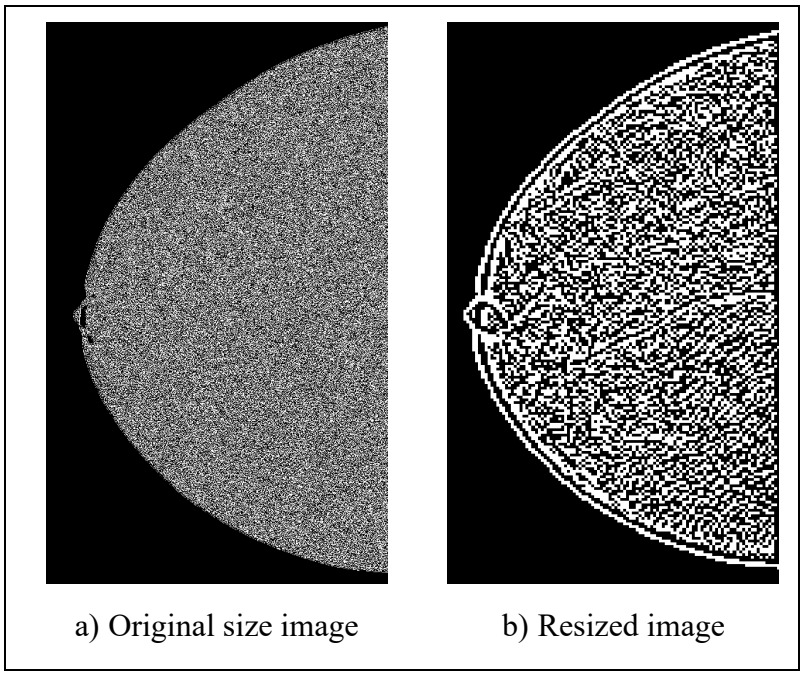

a) Original size image b) Resized image

Figure 4.1 Resizing Effect on Laplacian Filtered Image

The quantitative impact of resizing is summarised in Table 4.1. At aggressive downscaling levels of 25% and 20% of the original image size, the computed variance values showed poor agreement with expert radiologist assessments. Specifically, several non-blurry images (e.g., images 2, 5, 7, 13, and 18) yielded unexpectedly low variance values, while some blurry images exhibited higher variance. These reversals indicate that excessive downsampling removes diagnostically relevant edge information, resulting in unreliable blur characterization. Consequently, these resizing levels produced a high number of classification errors, with nine errors at 25% reduction and six errors at 20%.

When the images were resized to 15% and 10% of their original dimensions, the variance values demonstrated improved consistency with expert evaluations. At these scales, noise suppression and edge preservation were better balanced, allowing the Laplacian variance to more accurately represent perceived image sharpness. Notably, resizing to 15% of the original size yielded the lowest number of classification errors (three errors), outperforming both the 20–25% reductions and the more aggressive 10% reduction, which produced four errors. This indicates that while further downsampling continues to suppress noise, excessive reduction can again diminish essential structural details. Based on these findings, resizing DBT images to 15% of their original dimensions was selected as the optimal preprocessing step for subsequent threshold analysis. This scale provides the best trade-off between noise suppression and edge preservation, leading to variance values that align most closely with radiologist assessments and improving the robustness and reliability of the blur detection process.

Table 4.1
Variance Value for Image Size Reduction by Factors Ranging from 25% to 10%

Image Condition	**Annotation by Radiologist**	**Variance value Possible Threshold range: 150<Th<250**			
		Size 25%	**Size 20%**	**Size 15%**	**Size 10%**
Blurry	1	44.89	57.01	84.37	140.08
	4	32.07	35.43	45.3	71.63
	5	**150.99**	146.1	105.01	119.74
	7	**150.89**	143.66	102.68	114.71
	8	47.38	49.23	60.1	89.71
	9	63.99	75.93	103.28	**167.63**
	12	68.82	89.08	**157.47**	**205.52**
	15	57.54	66.96	91.23	**153.21**
	18	146.01	**155.64**	138.52	**183.22**
	19	127.09	124.28	87.16	86.07
	20	131.24	132.27	99.83	108.52

Image Condition	Annotation by Radiologist	Variance value Possible Threshold range: 150<Th<250			
		Size 25%	**Size 20%**	**Size 15%**	**Size 10%**
Non-blurry	2	**113.77**	159.8	242.79	393.53
	3	**87.77**	**125.94**	200.43	332.43
	6	223.5	260.95	297.65	463.71
	10	**77.7**	**97.95**	**141.33**	241.3
	11	**79.8**	**100.78**	**145.25**	236.62
	13	**124.61**	174.39	259.74	413.65
	14	189.81	256.73	357.14	533.51
	16	**84.84**	**108.82**	158.48	266.79
	17	**105.02**	**135.23**	188.56	291.06
Total Errors		9	6	3	4

Note: Th = threshold

In the second stage, the effect of different threshold values on blur detection performance was investigated. Blurring occurs when light from an object spreads across adjacent pixels, reducing edge contrast in a process often referred to as smearing. The LbBD algorithm quantifies this by convolving the image with the Laplacian operator and calculating the variance, where a lower variance indicates fewer edges and, therefore, greater blurriness. As shown in Table 4.2, three thresholds (150, 200, and 250) were tested on the resized images. The results demonstrated that threshold selection significantly influenced classification outcomes; for instance, image number 3 was classified as non-blurry at Th=150 but as blurry at Th=200 and Th=250. The detailed comparison in Table 4.3 shows that Th=200 achieved the highest accuracy (0.90) with only two errors out of 20 cases, while Th=150 and Th=250 resulted in slightly lower accuracies of 0.85 and 0.80, respectively.

Figure 4.2 presents the confusion matrices for the LbBD algorithm's classification of DBT images as either blurry or non-blurry under three threshold settings: (a) Th=250, (b) Th=200, and (c) Th=150. The rows of each matrix correspond to the actual image condition determined by expert annotation, while the columns represent the algorithm's predicted condition. At Th=250 (Figure 4.2a), the algorithm correctly classified 100% of blurry images but misclassified 74.5% of non-blurry images as blurry, leaving only

25.5% correctly identified as non-blurry. This result shows that a higher threshold maximizes sensitivity to blur but significantly increases false positives. At Th=200 (Figure 4.2b), the algorithm again achieved 100% correct classification of blurry images, while the proportion of non-blurry images correctly identified improved to 62.8%, reducing misclassification to 37.2%. This threshold, therefore, provided the best trade-off between sensitivity (true positive rate for blurry images) and specificity (true positive rate for non-blurry images), consistent with the performance metrics in Table 4.4 showing the highest accuracy (90%).

At Th=150 (Figure 4.2c), the correct classification of non-blurry images remained similar (62.7%), but the recall for blurry images decreased slightly to 90.9%, with 9.1% misclassified as non-blurry. This reduction in sensitivity indicates that lowering the threshold relaxes the blur detection criteria, allowing some blurry images with higher variance values to be incorrectly labeled as non-blurry. Comparing the three configurations, Th=200 provides the optimal trade-off between detecting blurry images and preserving non-blurry image classification accuracy. The Th=250, while excellent at identifying blurry images, tends to over-classify non-blurry images as blurry, leading to unnecessary false positives. Conversely, Th=150 slightly improves non-blurry image classification compared to Th=250 but sacrifices blur detection accuracy. These observations highlight the importance of selecting a threshold that balances both sensitivity and specificity, with Th=200 emerging as the most effective choice for the DBT dataset.

Table 4.2
Sample Result of Blur Detection with LbBD Using Different Threshold Values

No.	DBT Image	Variance	Status (Th = 150)	Status (Th = 200)	Status (Th = 250)
1	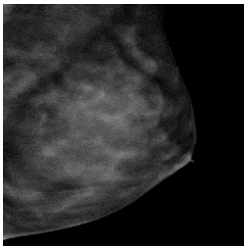	86.07	Blurry	Blurry	Blurry
2	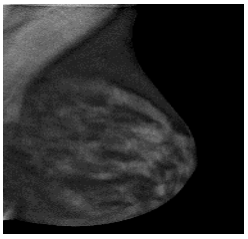	119.74	Blurry	Blurry	Blurry
3	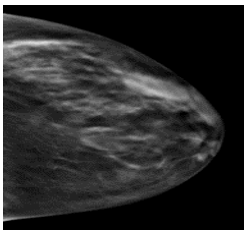	152.08	Non-blurry	Blurry	Blurry
4	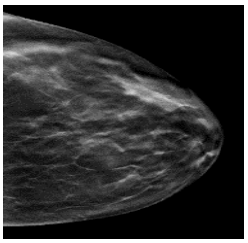	332.43	Non-blurry	Non-blurry	Non-blurry

Note: Th = threshold

Table 4.3
Comparison of Prediction Status for Different Threshold Values for Variance, with Image Reduction Size is 15%

Image No.	Variance	Algorithm Prediction Status			Experts' Annotation Status
		(Th=250)	(Th=200)	(Th=150)	
1	84.37	Blurry	Blurry	Blurry	Blurry
2	242.79	**Blurry**	Non-blurry	Non-blurry	Non-blurry
3	200.43	**Blurry**	Non-blurry	Non-blurry	Non-blurry

Image No.	Variance	Algorithm Prediction Status			Experts' Annotation Status
		(Th=250)	(Th=200)	(Th=150)	
4	45.3	Blurry	Blurry	Blurry	Blurry
5	105.01	Blurry	Blurry	Blurry	Blurry
6	297.65	Non-blurry	Non-blurry	Non-blurry	Non-blurry
7	102.68	Blurry	Blurry	Blurry	Blurry
8	60.1	Blurry	Blurry	Blurry	Blurry
9	103.28	Blurry	Blurry	Blurry	Blurry
10	141.33	**Blurry**	**Blurry**	**Blurry**	Non-blurry
11	145.25	**Blurry**	**Blurry**	**Blurry**	Non-blurry
12	157.47	Blurry	Blurry	**Non-blurry**	Blurry
13	259.74	Non-blurry	Non-blurry	Non-blurry	Non-blurry
14	357.14	Non-blurry	Non-blurry	Non-blurry	Non-blurry
15	91.23	Blurry	Blurry	Blurry	Blurry
16	158.48	Non-blurry	Non-blurry	Non-blurry	Non-blurry
17	188.56	Non-blurry	Non-blurry	Non-blurry	Non-blurry
18	138.52	Blurry	Blurry	Blurry	Blurry
19	87.16	Blurry	Blurry	Blurry	Blurry
20	99.83	Blurry	Blurry	Blurry	Blurry
Total Errors		4	2	3	

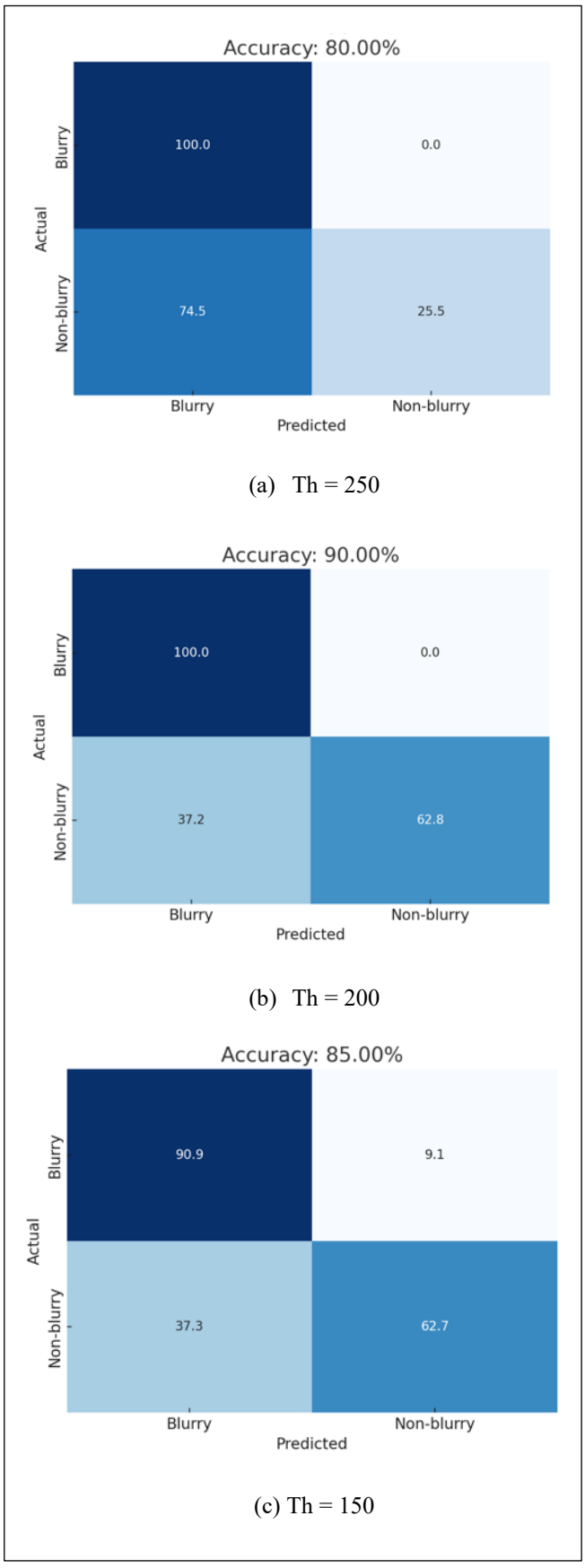

Figure 4.2 Confusion Matrix for LbBD Algorithm Prediction Percentage of Image Condition Status for Three Different Thresholds (a) Th=250, (b) Th=200, and (c) Th=150

Table 4.4
LbBD Algorithm Performance for Three Different Thresholds

Threshold	Accuracy	Precision	Recall	F1-score
250	0.8	0.733	1.0	0.846
200	**0.9**	**0.846**	**1.0**	**0.917**
150	0.85	0.833	0.909	0.869

Misclassifications were most often caused by low-contrast images that generated false blur classifications, as well as blurred images with abrupt changes from high-detail to low-detail regions that were sometimes missed by the algorithm. Since the LbBD method detects singularities affected by blurriness, images with weak edge transitions posed a particular challenge. False detections were particularly associated with small variance differences between non-blurry and blurry categories, especially in images with minimal grey-level intensity variation. Examples of such missed detections are shown in Figure 4.3, which illustrates three cases (images 10, 11, and 12) where low contrast led to incorrect classification.

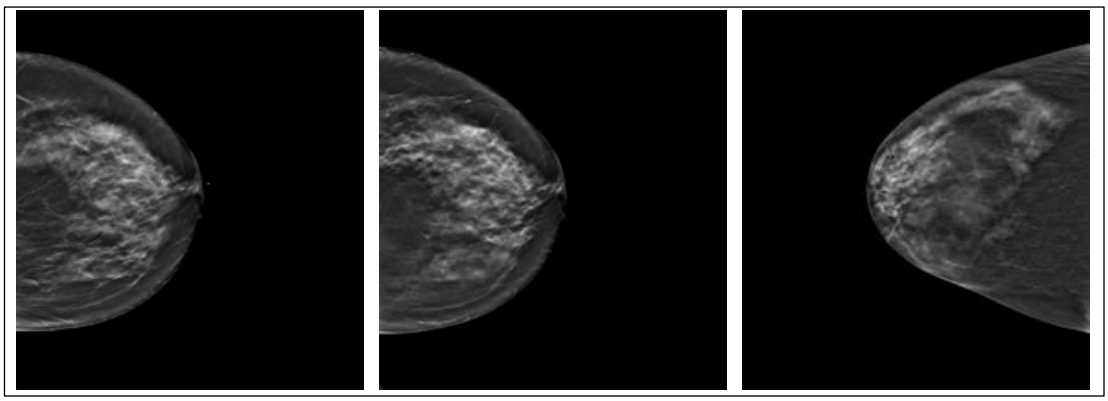

Figure 4.3 Sample Missed Detection by the LbBD Algorithm for Images 10, 11, and 12

In conclusion, the results demonstrate that the LbBD algorithm performs best when applied to images resized to 15% of their original size and when using a threshold of 200. This configuration maximised agreement between algorithm predictions and expert evaluations, achieving high accuracy, precision, and F1-score while minimising both false positives and missed detections. The analysis highlights that accurate blurry image detection in DBT datasets depends critically on appropriate image pre-processing

through resizing and careful threshold tuning, as incorrect parameter selection leads to substantial drops in classification performance.

4.2.2 Analysis of Feature Extraction using CNN Constructed from Scratch

This section analyses the performance of the five proposed BDCNN models constructed from scratch, as described in Section 3.4.2. The aim is to assess how adding convolutional layers influences network performance, particularly in terms of accuracy for blurry image detection in DBT datasets. The choice of the number of convolutional layers and appropriate training settings is critical for achieving high classification accuracy.

Table 4.5 summarises the accuracy, precision, recall, and F1-score for all five models, trained under identical parameters on the same dataset. BDCNN1 already achieves strong performance (accuracy = 0.9299, F1-score = 0.9440). However, the addition of convolutional layers generally improves accuracy and other metrics. The trend reaches its peak with BDCNN4, which achieves the highest accuracy (0.9798) and F1-score (0.9795), reflecting a strong balance between precision (0.9836) and recall (0.9755). Although BDCNN5 incorporates more convolutional layers (seven in total), its accuracy (0.9660) and loss progression indicate a slight performance decline compared to BDCNN4, likely due to increased network complexity, which makes training more challenging and potentially amplifies background noise interference.

Table 4.5
Performance for All BDCNN

Model	Training Parameters	Accuracy	Precision	Recall	F1-score
BDCNN1	Optimizer: SGDM Learning Rate:0.01 Max Epoch: 50	0.9299	0.9390	0.9490	0.9440
BDCNN2		0.9579	0.9290	**1.0000**	0.9632
BDCNN3		0.9486	0.9090	0.9780	0.9422
BDCNN4		**0.9798**	0.9836	0.9755	**0.9795**
BDCNN5		0.9660	**0.9870**	0.9490	0.9676

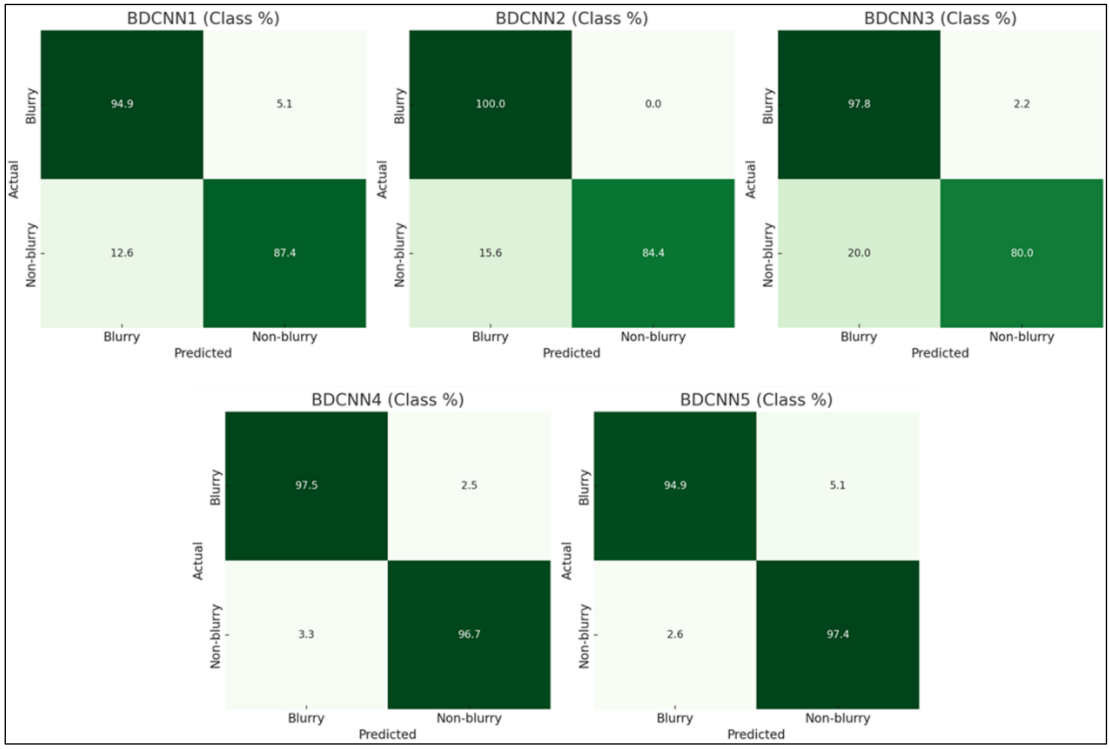

Figure 4.4 Confusion Matrix for Five Models of BDCNN

The performance of the five BDCNN models was further evaluated using class-based percentage confusion matrices in Figure 4.4. The results reveal distinct trade-offs between models. BDCNN2 demonstrated the highest sensitivity to blur, achieving 100% recall for blurry images, meaning that all blurry samples were correctly identified. However, this improvement came at the expense of non-blurry classification, where only approximately 84% of non-blurry images were correctly recognized, leading to a higher false positive rate. In contrast, BDCNN4 delivered the most balanced and robust performance across both classes, correctly classifying about 97.6% of blurry images and 97% of non-blurry images. This balance explains its superior overall accuracy (97.98%), confirming BDCNN4 as the best-performing model for generalizable blur detection. Meanwhile, BDCNN1, BDCNN3, and BDCNN5 performed reasonably well on blurry images (95–98%) but were less consistent on non-blurry classifications, achieving between 87–95% accuracy. Taken together, these findings suggest that while BDCNN2 is optimal when prioritizing sensitivity to blur, BDCNN4 provides the most reliable and generalizable classification across both blurry and non-blurry categories.

This performance trend is also visually supported by Figures 4.5(a) and 4.5(b), which present the accuracy and loss progression, respectively, for each model. In Figure 4.5(a), BDCNN4 not only reaches the highest accuracy but also shows steady

improvement throughout the training epochs. Figure 4.5(b) confirms that BDCNN4 achieves the lowest loss values across all models, indicating effective feature learning and minimal overfitting. In contrast, BDCNN5 shows less consistent accuracy progression and slightly higher loss, reinforcing the finding that increasing layers beyond an optimal depth does not guarantee better results.

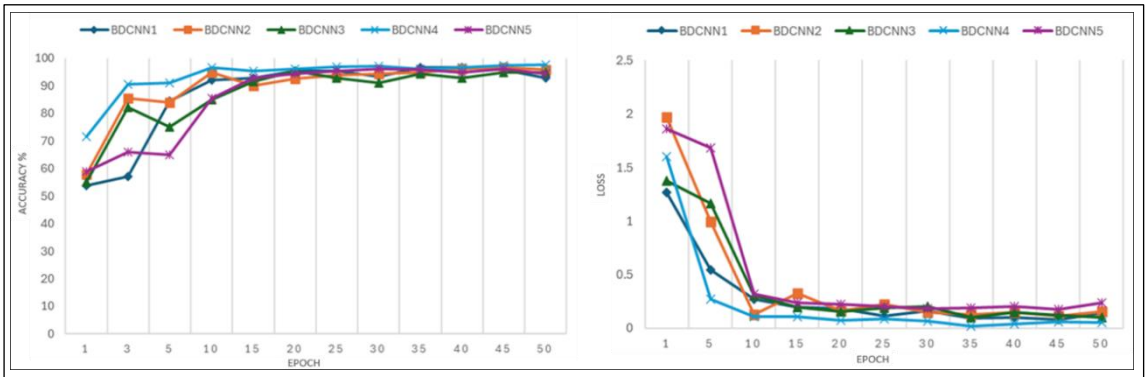

(a)Training Progress (b) Loss Progress

Figure 4.5 Plot of Progress Obtained for All BDCNN

4.2.2.1 Analysis of Deep Learning Optimizer for BDCNN4

To further enhance the performance of the best-performing model (BDCNN4), experiments were conducted with three optimizers: Stochastic Gradient Descent with Momentum (SGDM), Adaptive Moment Estimation (Adam), and Root Mean Square Propagation (RMSProp), each tested at learning rates of 0.001, 0.01, and 0.1.

Table 4.6 presents the results for all combinations. Adam, with a learning rate of 0.001, achieves the best overall performance, with accuracy = 0.9804, precision = 0.9783, recall = 0.9930, and F1-score = 0.9856, outperforming both SGDM and RMSProp. SGDM delivers competitive results at a learning rate of 0.01 (accuracy = 0.9798, F1-score = 0.9795) but shows significant degradation at 0.1 (accuracy = 0.7255). RMSProp consistently underperforms relative to Adam and SGDM, with its best configuration achieving 0.9412 accuracy and 0.9583 F1-score. However, ADAM delivers a significant increase in F1-score. This analysis confirms Adam's superiority in balancing sensitivity and specificity.

Table 4.6
Classification Results of the Proposed Model for Each Optimizer

Optimizer	Learning Rate	Accuracy	Precision	Recall	F1-score
SGDM	0.001	0.9216	0.9167	0.9565	0.9362
	0.01	0.9798	**0.9836**	0.9755	0.9795
	0.1	0.7255	0.7917	0.6333	0.7037
ADAM	0.001	**0.9804**	0.9783	**0.9930**	**0.9856**
	0.01	0.9804	0.9758	0.9910	0.9833
	0.1	0.9216	0.9583	0.8846	0.9200
RMSProp	0.001	0.8824	0.9167	0.9565	0.9362
	0.01	0.9216	0.9583	0.9200	0.9388
	0.1	0.9412	0.9583	0.9583	0.9583

The training behaviour of each optimizer at a learning rate of 0.001 is shown in Figure 4.6. SGDM's curves are smooth, with validation accuracy closely following training accuracy, indicating stable learning without significant overfitting. Adam's curves are the most stable, achieving high accuracy with minimal divergence between training and validation, reflecting efficient convergence. In contrast, RMSProp displays noticeable mid-training fluctuations and less consistent convergence, which may account for its reduced classification performance. Collectively, these results confirm that both network architecture and optimisation strategy critically influence DBT blur detection performance. A moderate depth of convolutional layers, as in BDCNN4, yields optimal results, and the Adam optimizer with a 0.001 learning rate provides the most stable and accurate classification, achieving the highest accuracy, precision, recall, and F1-score across all tested configurations.

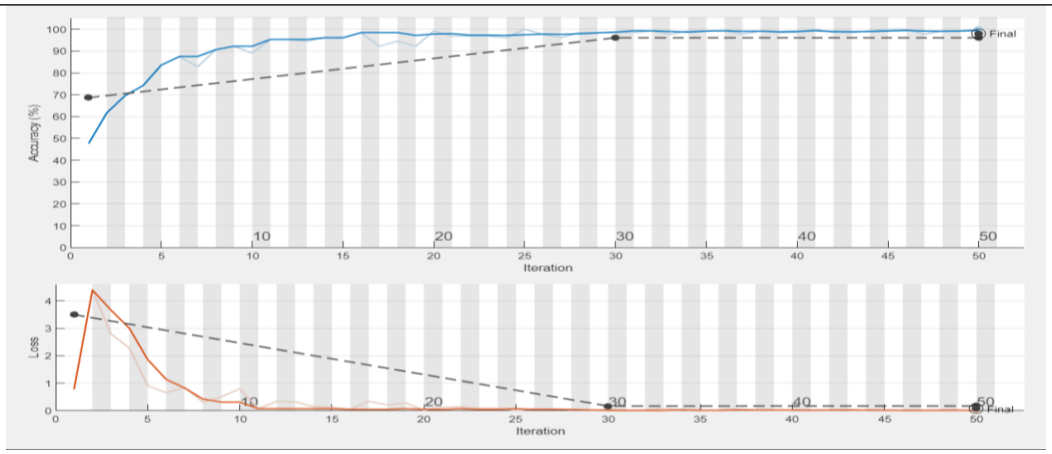

(a) SGDM

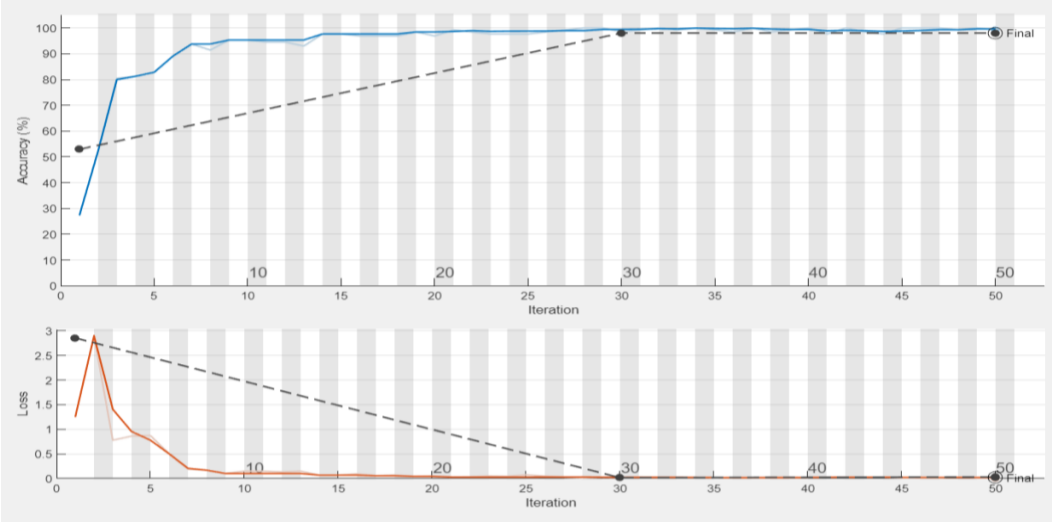

(a) ADAM

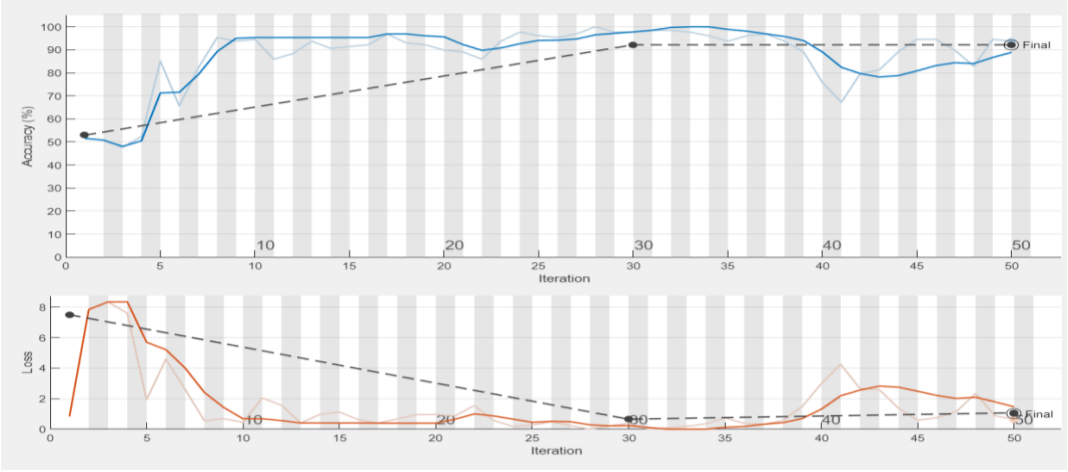

(a) RMSProb

Figure 4.6 Training Progress for Each Optimizer (0.001 Learning Rate)

The experimental results from both the classical LbBD algorithm and the deep learning-based BDCNN architectures demonstrate that accurate blurry image detection in DBT datasets critically depends on optimal parameter selection and model configuration. For the LbBD algorithm, resizing images to 15% of their original dimensions and selecting a threshold of 200 yielded the highest agreement with expert evaluations, achieving 0.9 accuracy while minimizing false detections. In parallel, the deep learning approach showed that increasing convolutional layers improved detection accuracy up to an optimal depth, with BDCNN4 delivering the best overall performance (accuracy = 0.9798, F1-score = 0.9795). Furthermore, the optimization strategy significantly influenced deep learning results, with the Adam optimizer at a 0.001 learning rate achieving the most stable convergence and the highest classification metrics (accuracy = 0.9804, F1-score = 0.9856). These findings collectively indicate that while the LbBD algorithm provides an effective and computationally efficient baseline for blur detection, deep learning models, when optimally designed and trained, offer superior accuracy and robustness, particularly in complex imaging scenarios.

4.2.3 Analysis of Hybrid CNNSVM

The findings in previous sub-section (Section 4.2.1 and 4.2.2) established two key aspects of effective blurry image detection in DBT datasets: first, that optimal pre-processing and threshold tuning enable the classical LbBD algorithm to achieve strong baseline results; and second, that deep learning methods, particularly the BDCNN4 architecture trained with the Adam optimizer at a 0.001 learning rate, outperform traditional approaches by leveraging deeper feature extraction and robust optimisation strategies. Building on these results, this section extends the analysis by investigating performance enhancement through hybrid architectures. Specifically, this next stage examines whether replacing the fully connected (FC) classification stage of CNNs with alternative classifiers, such as SVMs, can further improve detection performance by combining CNN feature extraction strength with SVM's superior generalisation capabilities.

Following the proposed methodology, after pre-processing, the CNN model extracts features through convolutional and pooling layers, passing the resulting activation maps to the fully connected layer for classification. In the hybrid approach, however, the fully connected output is fed to an SVM classifier instead. The SVM

leverages the high-dimensional CNN feature space to train on the structural differences between blurry and non-blurry images, with the classification output determined by margin maximisation rather than empirical risk minimisation, as in FC layers. This experiment aimed to assess whether fusing CNN feature extraction with SVM classification could provide measurable improvements in accuracy over standard CNN-FC architectures.

The BDCNN4 architecture, identified in Section 4.2.2 as the second-best performing CNN from scratch (six convolutional layers), was selected as the feature extractor. Table 4.7 compares the validation accuracy of the standard BDCNN4 with FC classification to the hybrid BDCNN4SVM. The hybrid approach achieved a validation accuracy of 0.9864, F1-score of 0.9868, and AUC of 0.9978, outperforming the CNN-FC configuration (accuracy = 0.9804, F1-score = 0.9856, AUC = 0.9875). The ROC curves in Figure 4.7 clearly illustrate that the hybrid BDCNN4SVM model maintains a curve closer to the ideal value (=1) compared to BDCNN4 alone, demonstrating superior classification separability. This performance gain can be attributed to the SVM's structural risk minimisation, which tends to generalise better on the testing set compared to the FC layer's empirical risk minimisation.

Table 4.7
Comparison of Proposed BDCNN4SVM Accuracy Performance

Model	Training Parameter	Validation Accuracy	Precision	Recall	F1-score	AUC
BDCNN4	Optimizer: ADAM Learning Rate: 0.01 MaxEpoch: 50	0.9804	0.9783	**0.9930**	0.9856	0.9875
BDCNN4SVM		**0.9864**	**1.0**	0.9740	**0.9868**	**0.9978**

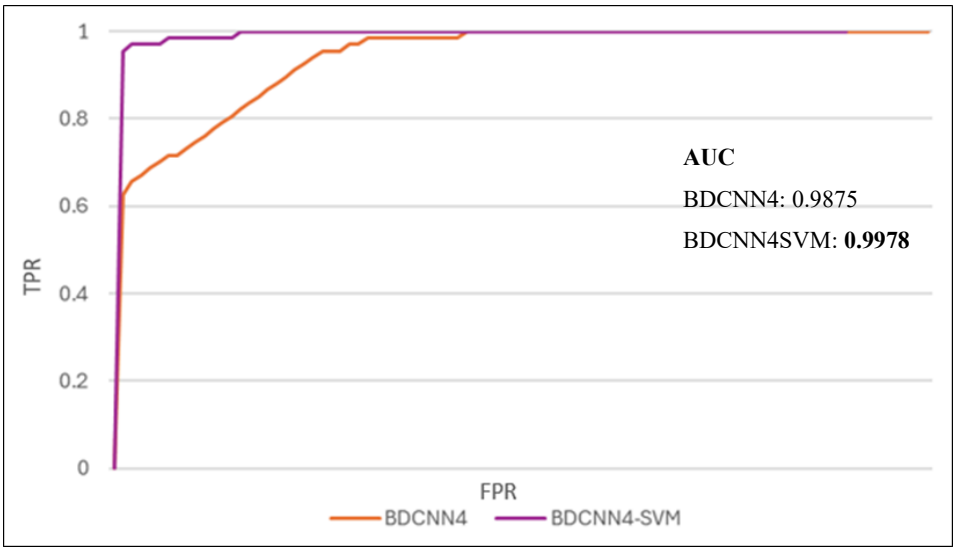

Figure 4.7 ROC Curve of BDCNN4 Vs Combination BDCNN4 with SVM

Despite these improvements, misclassification analysis revealed inherent challenges. As shown in Figure 4.8, certain ambiguous DBT images classified as blurry by the expert but predicted as non-blurry by the system highlight the difficulty in detecting motion blur when it occurs locally or when image variability in normal structures exceeds the variance caused by blurriness. This limitation suggests that while hybrid models can enhance overall accuracy, the effectiveness of feature representation remains critical for borderline cases.

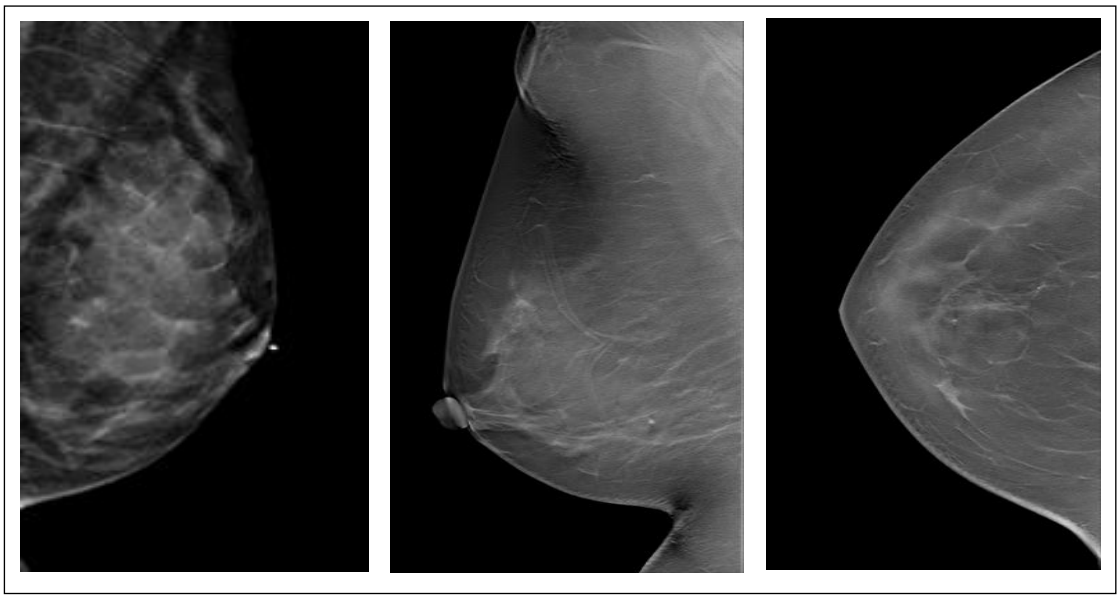

Figure 4.8 Sample Ambiguous DBT Image Considered as Blurry by the Expert and Non-blurry by the System

4.2.3.1 Performance Comparison with Other Classifiers

The BDCNN4SVM configuration was further compared with two alternative classifiers: Decision Tree (DT) and k-Nearest Neighbour (k-NN), to evaluate whether other machine learning methods could benefit similarly from CNN feature extraction. As shown in Table 4.8, all three classifiers achieved acceptable accuracy levels (>0.9500). However, SVM outperformed both DT (accuracy = 0.9730, F1-score = 0.9668) and k-NN (accuracy = 0.9590, F1-score = 0.9508). While DT achieved the highest recall (0.9831), SVM's perfect precision (1.0) combined with strong recall (0.9740) yielded the most balanced classification, minimising false positives, which is particularly important in this study, where misclassifying non-blurry images as blurry could unnecessarily trigger re-acquisition in a clinical workflow. These results reinforce the suitability of SVM as the preferred classifier for hybrid CNN-based blur detection in DBT datasets.

Table 4.8
Performance Comparison of BDCNN4SVM and BDCNN4 with Other Classifiers

Classifier	Accuracy	Precision	Recall	F1-Score
BDCNN4SVM	**0.9864**	**1.0**	0.9740	**0.9868**
BDCNN4DT	0.9730	0.9508	**0.9831**	0.9668
BDCNN4k-NN	0.9590	0.9508	0.9508	0.9508

4.2.3.2 Comparison with the Existing Deep CNN Model

To benchmark the proposed hybrid model against established deep CNN architectures, BDCNN4SVM was compared to five widely used networks: AlexNet, ResNet18, ResNet50, VGG16, and InceptionV3, each coupled with an SVM classifier after their FC layers. All models were trained on the same DBT dataset under identical pre-processing and training conditions, with resized input dimensions adapted to each architecture. As summarised in Table 4.9, the proposed BDCNN4SVM achieved the highest accuracy (0.9864) and AUC (0.9978) while also recording the shortest execution time (3 min 28 sec). The next best performer, ResNet50-SVM, achieved 0.9750 accuracy and 0.9947 AUC but required over 5 minutes for execution. Figure 4.9

shows the ROC curves for all models, with BDCNN4SVM exhibiting a curve closest to the ideal diagonal, indicating superior discriminative capability.

This performance advantage underscores that a tailored CNN architecture such as BDCNN4, combined with an SVM classifier, can not only outperform larger, more complex networks in accuracy and AUC but also do so with lower computational cost and faster convergence. This makes the hybrid BDCNN4SVM a strong candidate for practical deployment in clinical DBT blur detection, where speed, efficiency, and reliability are critical.

Table 4.9
Classification Result Comparison of the Classical Deep CNN Model and the Proposed Model

Architecture	**Training Parameter**	**Accuracy**	**AUC**	**Execution Time**
AlexNet-SVM	Optimizer: ADAM Learning Rate: 0.01 MaxEpoch: 50	0.9580	0.9839	3min 30sec
ResNet18-SVM		0.9583	0.9828	3 min 40 sec
ResNet50-SVM		0.9750	0.9947	5 min 2 sec
VGG16-SVM		0.9420	0.9830	4 min 11sec
InceptionV3-SVM		0.9670	0.9961	6 min 52 sec
BDCNN4SVM		**0.9864**	**0.9978**	**3 min 28 sec**

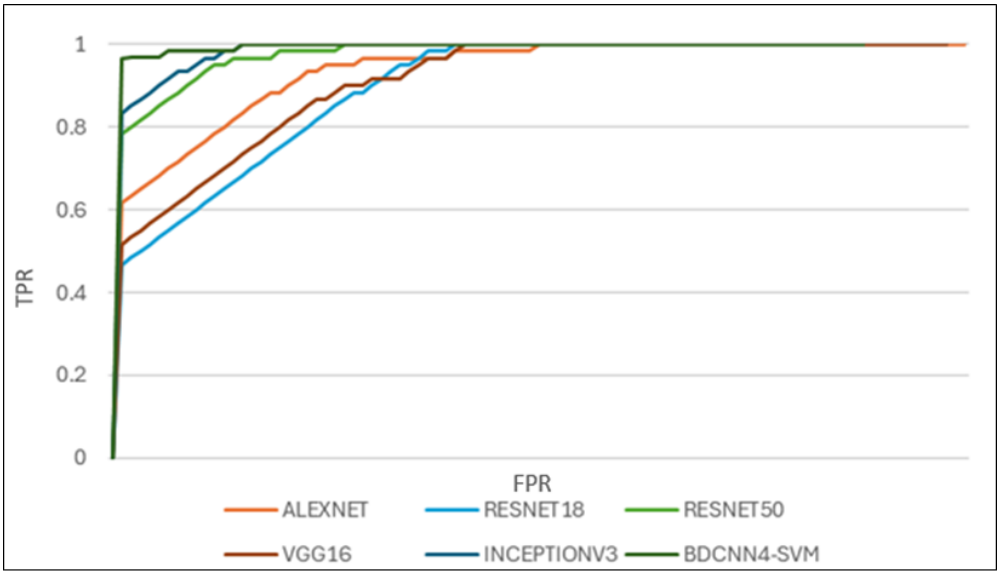

Figure 4.9 Comparison of the ROC Curves for Each CNN

The results of this investigation confirm that integrating SVM classification with CNN feature extraction can provide measurable gains in DBT blur detection performance. By replacing the fully connected layer of the best-performing scratch-built architecture, BDCNN4, with an SVM classifier, the hybrid BDCNN4SVM achieved superior accuracy (0.9864), F1-score (0.9868), and AUC (0.9978) compared to its FC-based counterpart, as well as outperforming other classifiers such as Decision Tree and k-NN. Benchmarking against established deep CNN architectures further demonstrated that the proposed hybrid approach delivers not only the highest accuracy and AUC but also the shortest execution time, highlighting its computational efficiency. Nevertheless, the analysis of misclassified cases revealed that ambiguous local blur patterns and natural structural variability in DBT images remain challenging for all tested models. These findings indicate that hybrid CNNSVM models represent a promising direction for improving clinical blur detection systems, and they provide a strong foundation for the enhancements explored in Section 4.2.3, where further refinements to model architecture and classification strategy are investigated to address the residual limitations observed in this section.

4.2.4 Analysis of Proposed New Hybrid Features CNNSVM Blur Detection Model

Building on the findings from the previous sections, where the LbBD algorithm demonstrated that handcrafted statistical features, particularly variance-based blur features (BF), could effectively discriminate between non-blurry and blurry DBT images, and where the CNNSVM hybrid model achieved superior accuracy by combining deep feature extraction with a robust margin-based classifier, this subsection investigates whether combining these two strengths can further enhance classification performance. The rationale is that while CNN architectures excel at learning high-level, abstract representations from image data, they may not always fully capture the statistical cues identified by classical blur detection methods. Conversely, handcrafted features such as BF provide complementary, structured numerical data that can encode discriminative characteristics, such as edge strength variance, that are not explicitly represented in purely image-based CNN features. By fusing CNN-extracted features from the BDCNN4 architecture with BF features derived from the LbBD method, and applying both FC and SVM classification strategies, the aim is to assess whether this

hybrid feature representation improves DBT blur detection accuracy, precision, recall, and F1-score, beyond what either approach could achieve independently.

In this experiment, four model configurations were compared: BDCNN4 with FC (BDCNN4), BDCNN4 with SVM (BDCNN4SVM), BDCNN4 with hybrid features (BDCNN4-BF), and BDCNN4 with SVM using hybrid features (BDCNN4SVM-BF). The results in Table 4.10 show that, when using only automated CNN features from image data, BDCNN4SVM (accuracy = 0.9864, F1-score = 0.9868) outperforms BDCNN4 (accuracy = 0.9804, F1-score = 0.9856), consistent with the advantage of SVM classification observed in Section 4.2.3. However, when BF features are incorporated into the training process, performance improves across both classification strategies. The BDCNN4-BF model achieves an accuracy of 0.9852 and an F1-score of 0.9780, while the BDCNN4SVM-BF model attains the highest accuracy (0.9921), perfect precision (1.0), high recall (0.9844), and the best F1-score (0.9921).

Table 4.10
Comparison Summary of the Blur Detection Performance Using Different Features and Deep Learning Models

Model	**Feature Type**	**Accuracy**	**Precision**	**Recall**	**F1-score**	**AUC**
BDCNN4	CNN features	0.9804	0.9783	**0.9930**	0.9856	0.9856
BDCNN4SVM	CNN features	0.9864	1.0	0.9740	0.9868	0.9870
BDCNN4-BF	Hybrid features	0.9852	0.9889	0.9674	0.9780	0.9890
BDCNN4SVM-BF	Hybrid features	**0.9921**	**1.0**	0.9844	**0.9921**	**0.9922**

These results indicate that the inclusion of BF features provides additional discriminative power, particularly when coupled with SVM classification. The improvement is especially notable given the high baseline accuracy of BDCNN4SVM, suggesting that the complementary statistical information in BF features enhances decision-making even when deep features are already highly effective. This aligns with the earlier finding from the LbBD algorithm that variance-based measures capture subtle differences between non-blurry and blurry DBT images, which CNNs alone may overlook due to the high similarity in texture, structure, and intensity distribution between the two classes.

Figure 4.10(a) visually reinforces these findings, showing that the BDCNN4SVM-BF model achieves more correct classifications than the other tested models, with its ROC curve lying closest to the top-left corner of the plot, indicating near-ideal classification performance. The highest AUC value was recorded for BDCNN4SVM-BF, closely followed by BDCNN4-BF, confirming that hybrid features enhance the model's ability to distinguish between classes. While the AUC difference between BDCNN4-BF and BDCNN4SVM-BF is small, the improvement in F1-score for BDCNN4SVM-BF demonstrates better balance between precision and recall, making it the superior configuration for DBT blur detection.

Further, the heatmap in Figure 4.10(b) provides a direct visual comparison of Accuracy, Precision, Recall, and F1-score across the four BDCNN4 variants. The results clearly highlight the superior performance of BDCNN4SVM-BF, which achieved consistently high values across all metrics, including perfect precision (100%) and an overall accuracy of 99.21%. In comparison, BDCNN4 displayed the strongest recall (99.30%), reflecting its sensitivity to detecting blurry instances, whereas BDCNN4SVM prioritized precision, reaching a perfect score at the expense of slightly reduced recall (97.40%). The BDCNN4-BF model achieved competitive precision (98.89%) but demonstrated the lowest recall (96.74%), leading to a comparatively weaker F1-score. Overall, the heatmap reinforces that while different models exhibit specific strengths, BDCNN4SVM-BF provides the most balanced and robust performance.

Overall, these results validate the hypothesis that combining deep image features with handcrafted variance-based features leverages the strengths of both methods, producing a hybrid BDCNN4SVM–BF architecture with the highest observed accuracy, AUC, and balanced classification performance in this study. These gains demonstrate that structured numerical features derived from classical image analysis provide complementary information to deep learning representations, enabling more precise discrimination between subtle blur variations in DBT images. The hybrid approach not only surpasses the performance of CNN-FC and CNNSVM models based solely on image data but also reinforces the potential of feature fusion as a strategy for addressing the inherent challenges posed by complex image textures and localised blur.

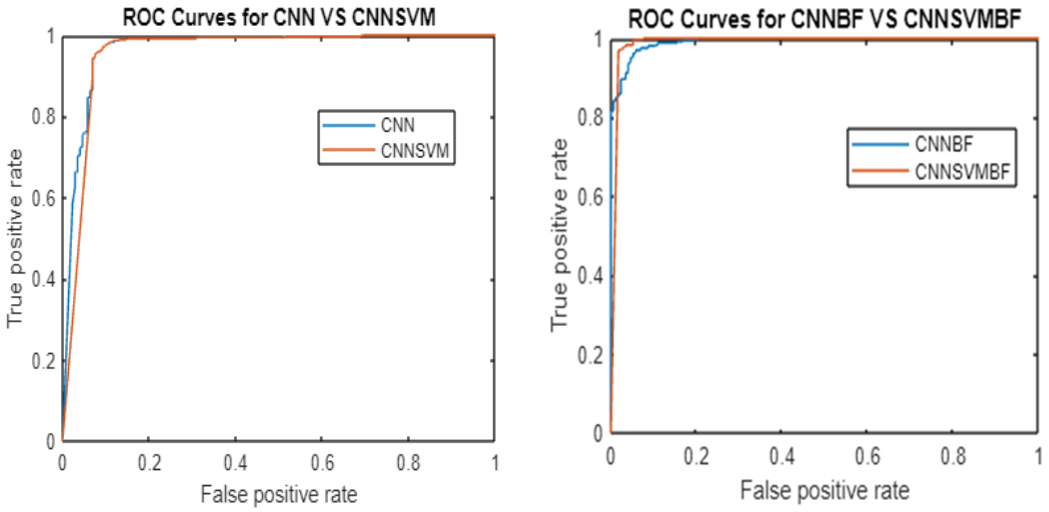

(a) ROC Comparison

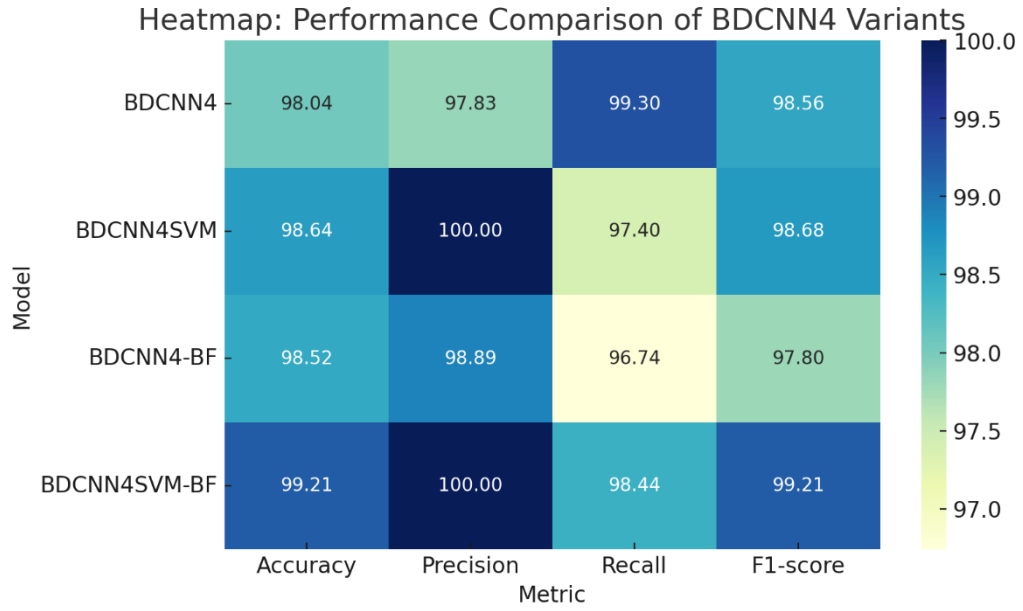

(b) Heatmap Comparison

Figure 4.10 The ROC and Heatmap Comparison of BDCNN4 vs. BDCNN4SVM and BDCNN4-BF vs. BDCNN4SVM-BF Models

4.3 Analysis of Proposed CNN-Based Contrast Enhancement Model for DBT Images

This section focuses exclusively on the non-blurry DBT images identified in the previous classification stage (Sections 4.2–4.2.4). By filtering out blurry cases detected through the LbBD, CNNSVM, and hybrid CNNSVM-BF approaches, the dataset used

here contains only diagnostically acceptable images, ensuring that blur artifacts do not compromise enhancement results. Within this non-blurry dataset, images containing calcifications or microcalcifications were selected for further analysis, as show in Figure 4.11. This stage aims to improve the local contrast of microcalcifications using the proposed UMVDSR-McCE method, thereby addressing Objective 3 of this study. Although visual inspection can demonstrate noticeable changes between original and enhanced images, such subjective evaluations are insufficient for rigorous performance analysis. Therefore, quantitative measures, Peak Signal-to-Noise Ratio (PSNR) and Structural Similarity Index (SSIM) were employed to assess the improvements in clarity, structural preservation, and fidelity.

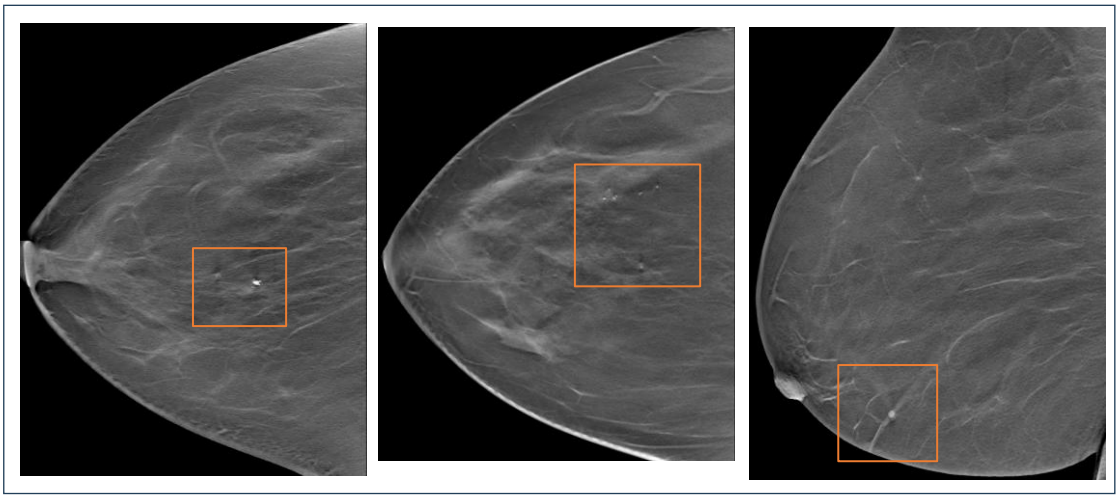

Figure 4.11 Non-Blurry DBT Dataset, Sample Images with Calcification/Microcalcification

The first phase of the evaluation compared the baseline VDSR network and bicubic interpolation (BICUBIC) with their unsharp masking-enhanced counterparts, UMVDSR and UMBICUBIC, for three scalar factors (2, 3, and 4). As reported in Table 4.11, UMVDSR achieved the highest PSNR and SSIM for scalar factor 2, with values of 39.7844 and 0.9695, respectively, followed closely by UMBICUBIC with 39.3856 and 0.9554. For scalar factor 3, UMBICUBIC slightly surpassed UMVDSR in PSNR (34.1489 versus 33.7596), yet UMVDSR retained the highest SSIM of 0.9112, indicating superior structural preservation. For scalar factor 4, UMVDSR once again led in both PSNR (34.1637) and SSIM (0.8966), highlighting its ability to maintain high performance even at greater upscaling levels.

The qualitative comparisons in Figure 4.12 clearly show that UMVDSR produces sharper calcification boundaries than either BICUBIC or VDSR alone while avoiding the exaggerated artifacts that can occur with over-sharpening. The improvement seen in UMVDSR methods is due to the combination of residual learning VDSR with the edge-sharpening effect of UM, which enhances contrast at microcalcification boundaries without significantly increasing noise. The RMSE and loss curves in Figure 4.13 further support this conclusion. The UMVDSR curve converges faster and reaches a lower RMSE than VDSR, indicating that UM pre-processing facilitates more efficient learning and more accurate reconstruction of high-frequency details, which are crucial for microcalcification detection.

Table 4.11
Comparison of PSNR and SSIM

Method	**Metrics (Average)**	**Scalar Factor**		
		2	**3**	**4**
Bicubic	PSNR	35.1035	29.9609	29.4692
	SSIM	0.9516	0.8328	0.793446
VDSR	PSNR	36.4767	29.6948	29.7999
	SSIM	0.9682	0.8446	0.8108
UMBICUBIC	PSNR	39.3856	**34.1489**	33.7857
	SSIM	0.9554	0.9092	0.8885
UMVDSR	PSNR	**39.7844**	33.7596	**34.1637**
	SSIM	**0.9695**	**0.9112**	**0.8966**

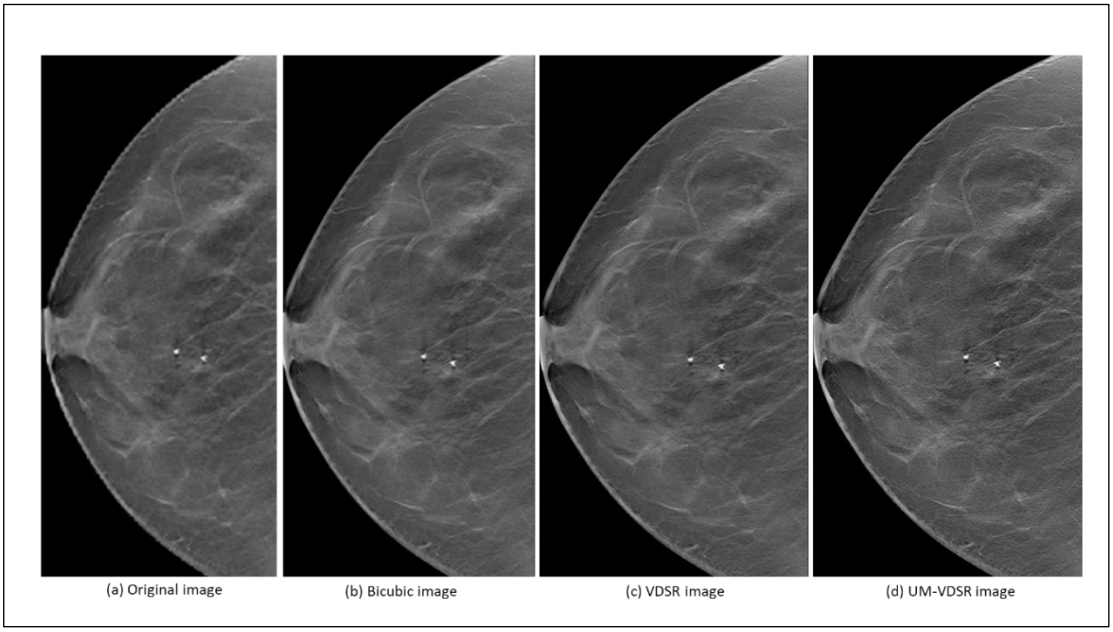

Figure 4.12 (a) Original Image and the Resultant Images After Applying (b) Bicubic, (c) VSDR, and (d) UMVSDR

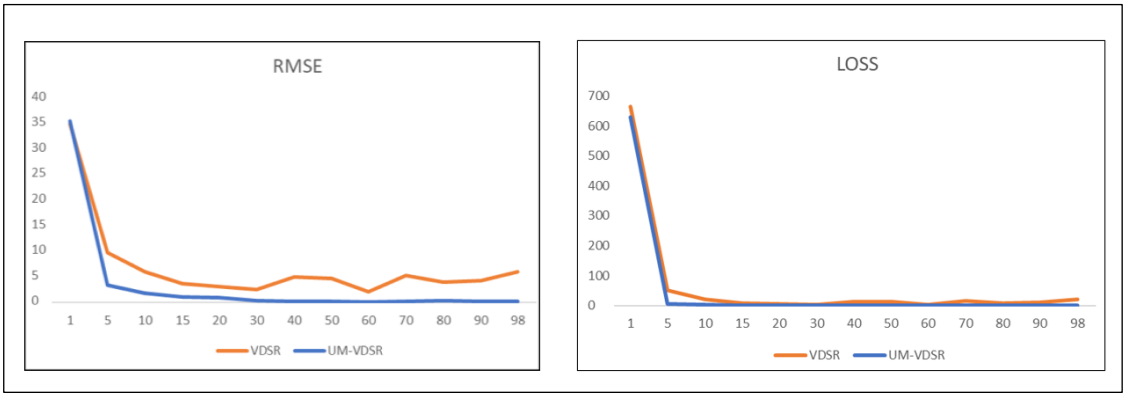

Figure 4.13 RMSE and Loss Performance Curve Comparison Between VDSR and UMVDSR

4.3.1 Analysis of Unsharp Masking Very Deep Super-Resolution - Microcalcification Contrast Enhancement (UMVDSR-McCE)

Although UMVDSR improves detail sharpness, the increase in spatial resolution can also accentuate noise, particularly in homogeneous tissue areas. To mitigate this, the McCE algorithm was applied as a post-processing stage, enhancing contrast selectively in microcalcification regions while suppressing noise in surrounding structures. The side-by-side comparisons in Table 4.12 between original images, UMVDSR outputs, and UMVDSR-McCE outputs for five sample cases (a–e). Visual

inspection reveals that McCE further increases the brightness and visibility of microcalcifications while preserving a natural tissue appearance. The difference is most noticeable in images with faint calcifications, where McCE outputs show clearer, more localised bright spots compared to UMVDSR alone.

Quantitative results in Table 4.13 substantiate these visual observations; for example, in image a, the PSNR increased from 33.555 with UMVDSR to 48.8439 with UMVDSR-McCE, while the SSIM rose from 0.908 to 0.9998. In image d, the PSNR improved from 32.4993 to 42.7417, and the SSIM from 0.8761 to 0.9989. When averaged across all samples, as shown in Table 4.14, UMVDSR-McCE achieved a PSNR of 47.6454 and SSIM of 0.9995, compared to 39.7844 and 0.9695 for UMVDSR, confirming the consistent benefit of the McCE post-processing step. This demonstrates that McCE is particularly effective at enhancing contrast in diagnostically relevant regions while maintaining structural fidelity.

Table 4.12
Comparison of the Original Image and the Resultant Image After Applying UMVDSR and UMVDSR-McCE

Image	Original Image	UMVDSR	UMVDSR-McCE
a	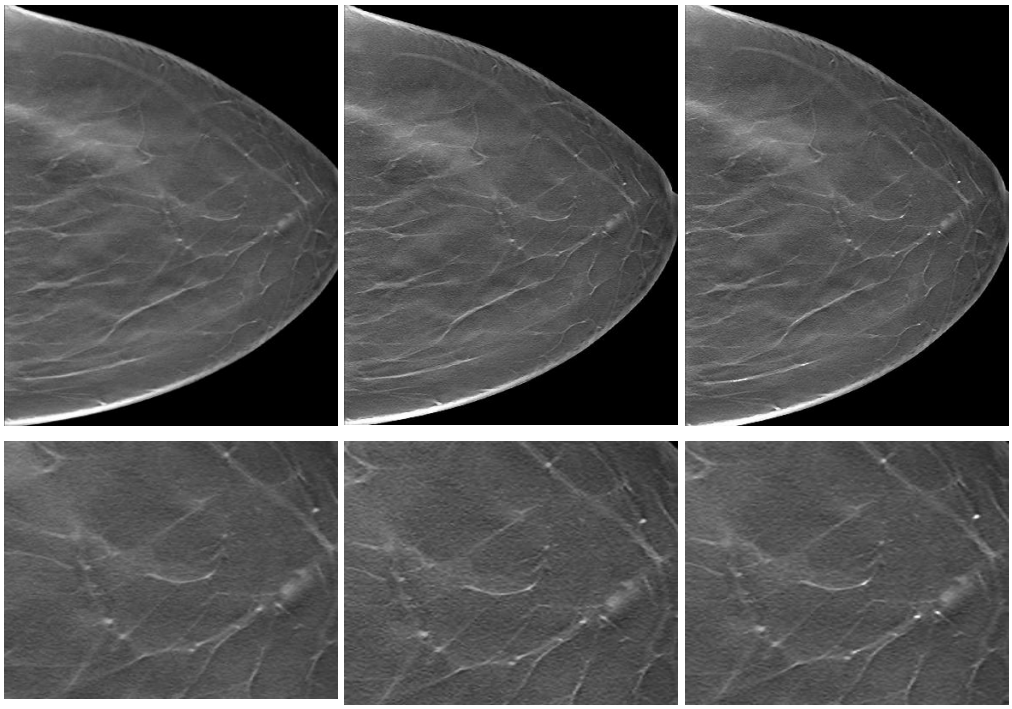		

Image	Original Image	UMVDSR	UMVDSR-McCE
b	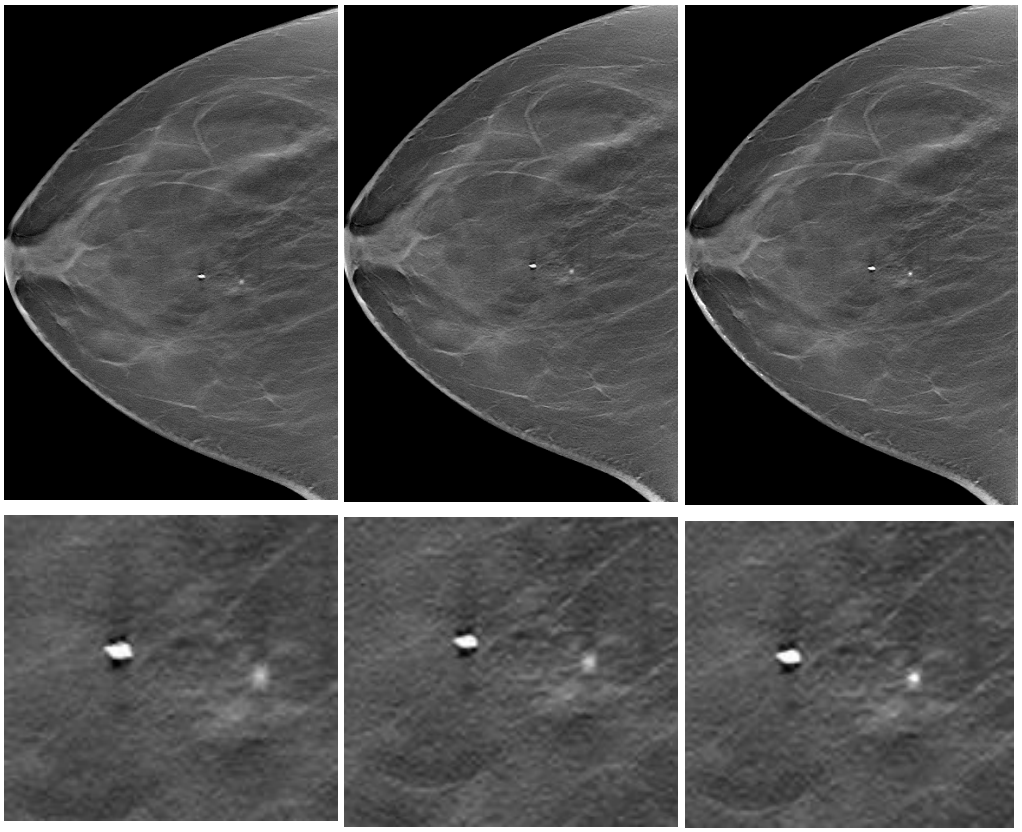		
c	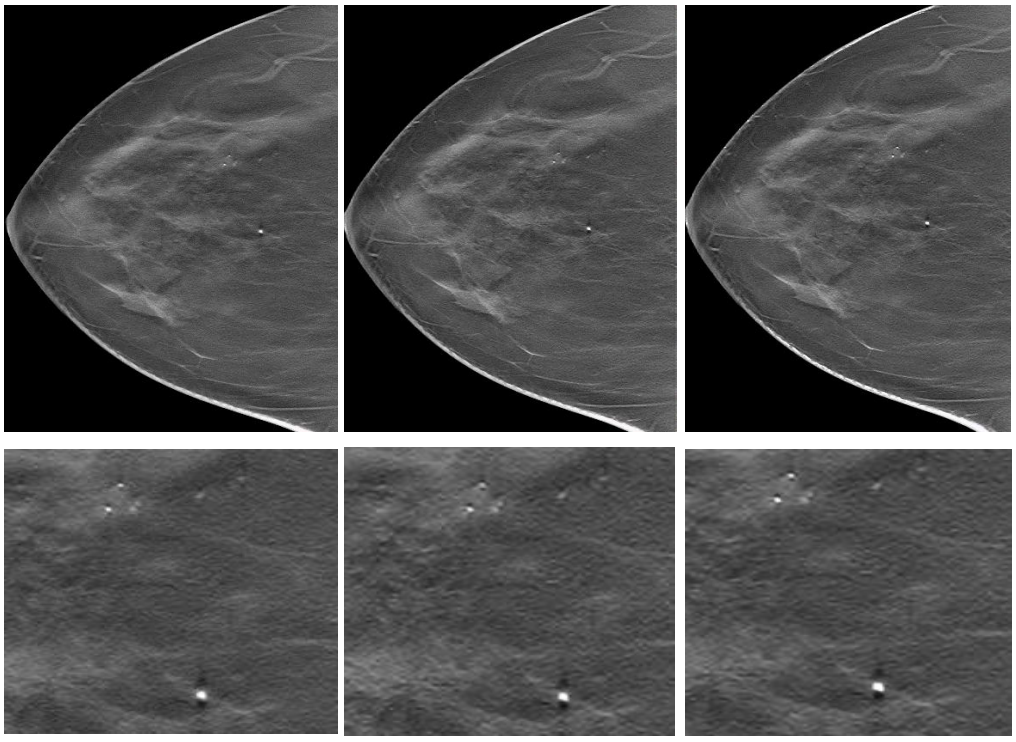		

Image	Original Image	UMVDSR	UMVDSR-McCE
d	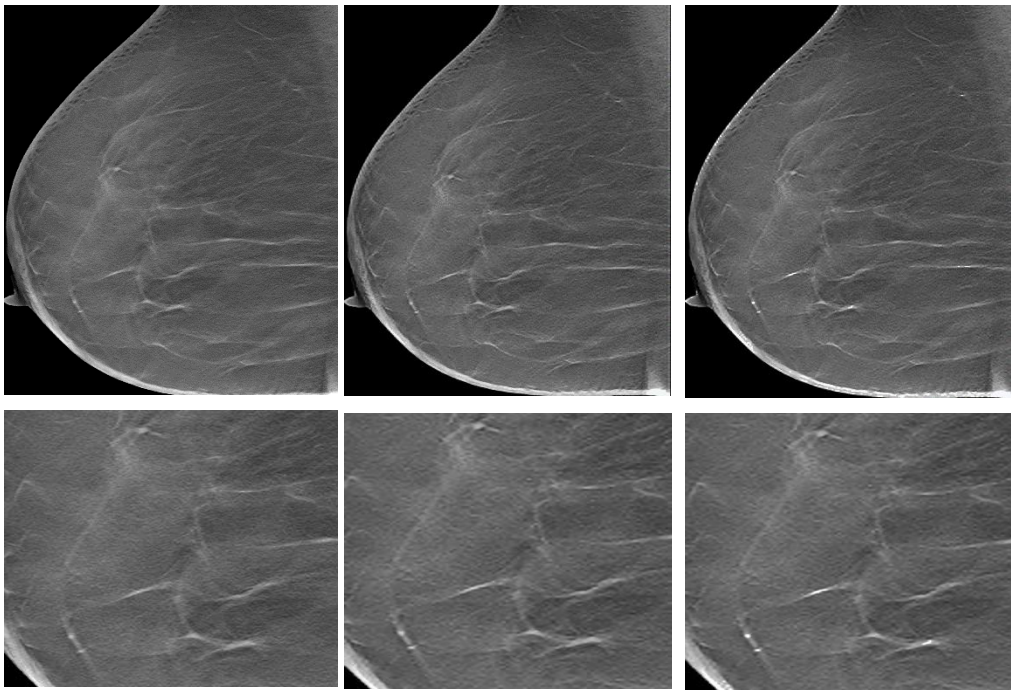		
e	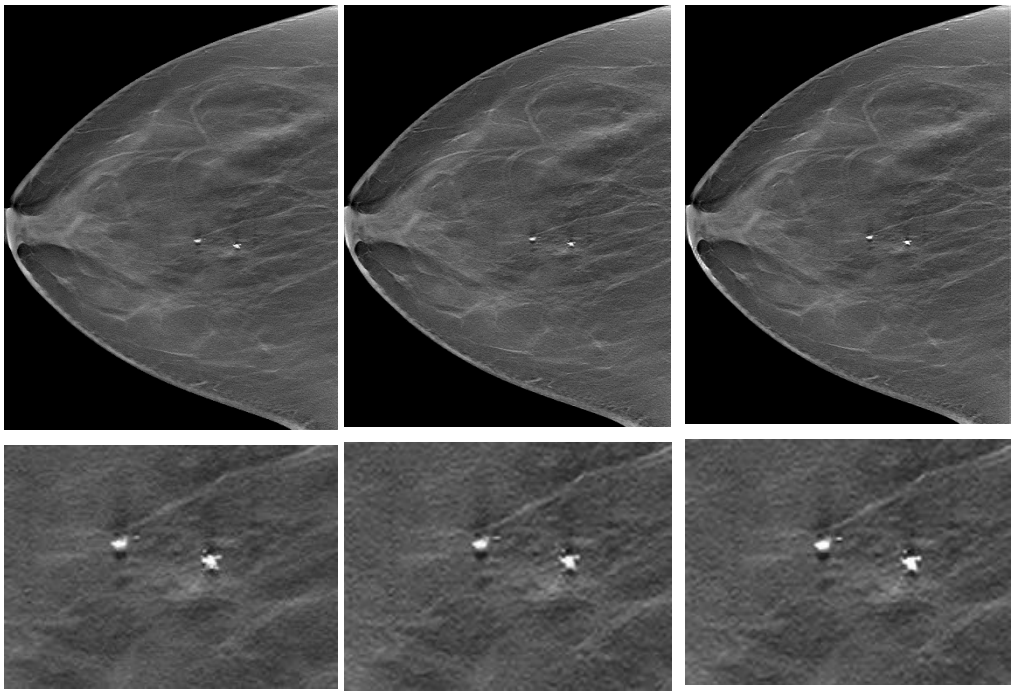		

Table 4.13
PSNR and SSIM Values for a Sample of Test Images

Method	Evaluation Metrics	Image				
		a	b	c	d	e
UMVDSR	PSNR	33.555	34.0977	34.0247	32.4993	34.0806
	SSIM	0.908	0.8915	0.9006	0.8761	0.8909
UMVDSR-McCE	PSNR	**48.8439**	**46.7563**	**42.7596**	**42.7417**	**48.0951**
	SSIM	**0.9998**	**0.9995**	**0.9986**	**0.9989**	**0.9997**

Table 4.14
Average PSNR and SSIM Values

Method	Average	
	PSNR	SSIM
UMVDSR	39.7844	0.9695
UMVDSR-McCE	**47.6454**	**0.9995**

Comparison with Conventional Contrast Enhancement Techniques

The final evaluation compared the proposed UMVDSR-McCE method with three conventional contrast enhancement approaches: contrast stretching, histogram equalization (HE), and contrast-limited adaptive histogram equalization (CLAHE). The qualitative results in Table 4.15 reveal distinct visual differences. HE brightens the entire intensity range uniformly, resulting in images with an artificial, flat appearance that can obscure subtle features. CLAHE performs better than HE by enhancing local contrast, yet it also amplifies both the background and noise, which can distract from diagnostically important structures. Contrast stretching maintains a more natural overall appearance but offers only modest improvement in microcalcification visibility. By comparison, UMVDSR-McCE yields images with markedly improved calcification visibility, sharper boundaries, and preserved anatomical context.

The quantitative analysis in Table 4.16 confirms these qualitative impressions. In image b, for instance, UMVDSR-McCE achieved a PSNR of 46.7563 and SSIM of 0.9995, compared to 14.3228 and 0.8871 for contrast stretching, 5.3821 and 0.2442 for

HE, and 20.9329 and 0.4401 for CLAHE. Across all test images, UMVDSR-McCE consistently recorded the highest PSNR and SSIM values. The average results in Table 4.17 highlight the clear superiority of the proposed method, with 47.6454 PSNR and 0.9995 SSIM, compared to 16.3689 and 0.9116 for contrast stretching, 6.1307 and 0.2790 for HE, and 20.3269 and 0.4618 for CLAHE. These figures confirm that UMVDSR-McCE not only outperforms conventional techniques in enhancing diagnostically relevant features but also preserves the natural visual quality of DBT images, a crucial factor in clinical interpretation.

Table 4.15
Comparison (i) Original Image to Output Images of (ii) Contrast Stretching, (iii) HE, (iv) CLAHE, and (v) UMVDSR-McCE (Proposed) Methods

	Image
a	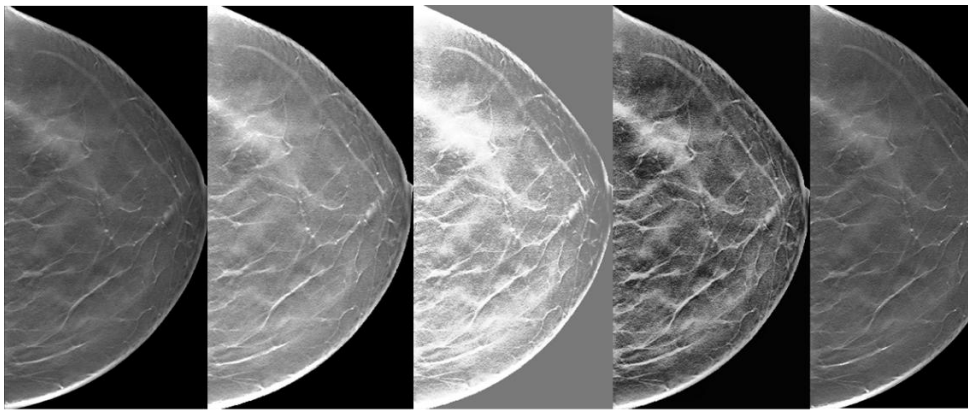
b	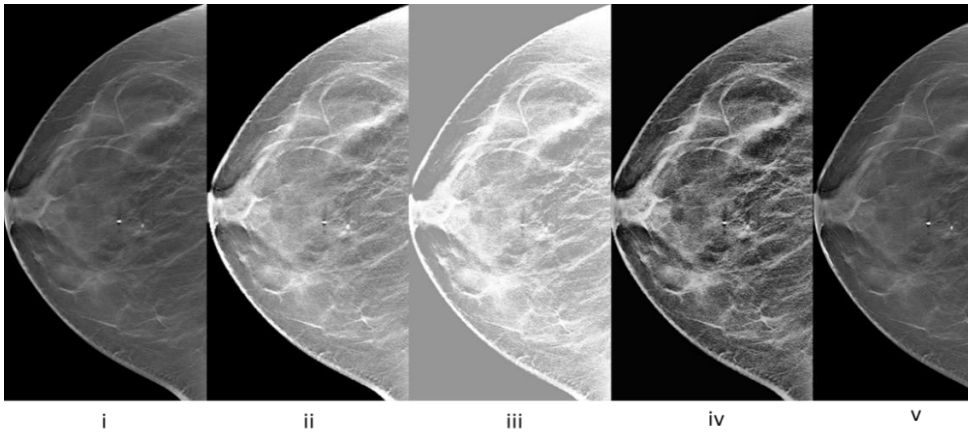

Image	
c	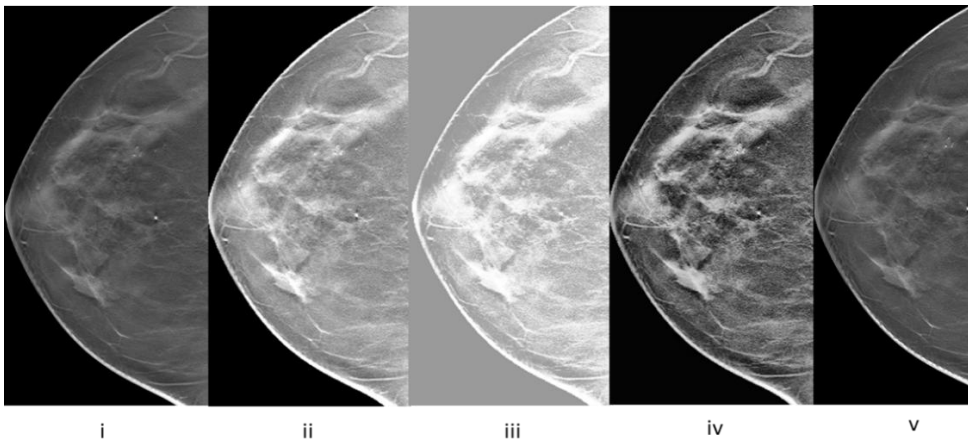 i ii iii iv v
d	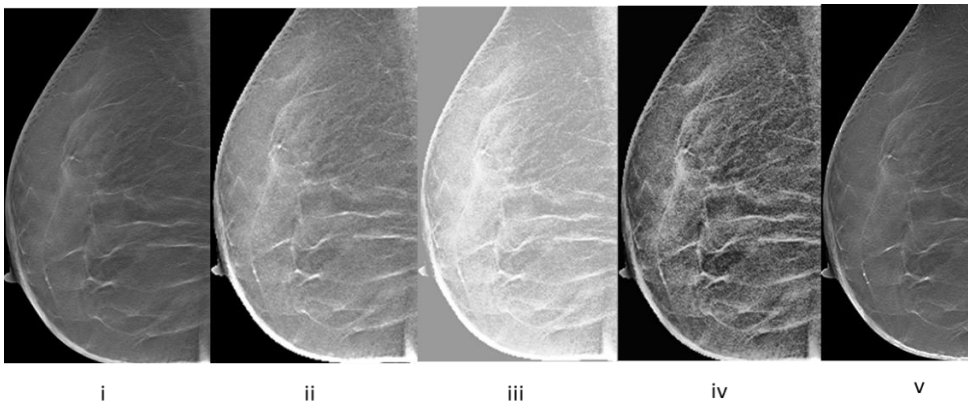 i ii iii iv v
e	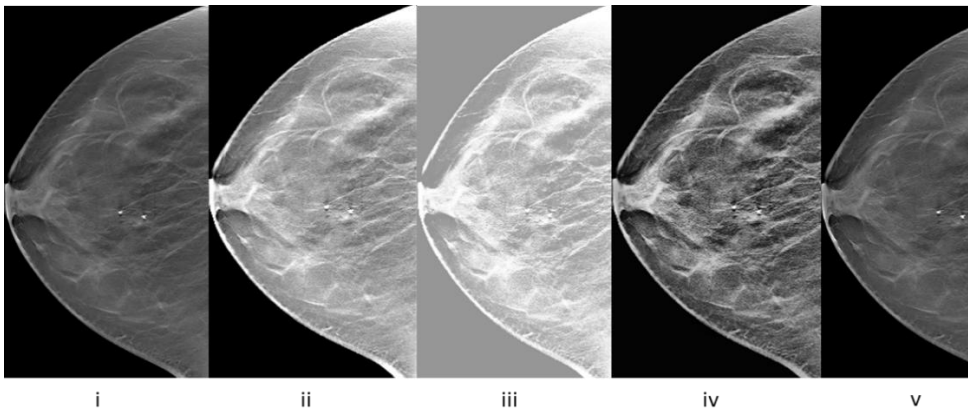 i ii iii iv v

Table 4.16
PSNR and SSIM Values for Each Method of Sample DBT Images

Evaluation Metrics	No	Method	Image				
			a	**b**	**c**	**d**	**e**
PSNR	ii	Contrast Stretching	15.6297	14.3228	14.3639	17.1069	13.7904
	iii	HE	7.2710	5.3821	5.1359	5.4013	5.3794
	iv	CLAHE	21.3161	20.9329	21.2821	23.0134	20.8656
	v	UMVDSR-McCE (Proposed)	**48.8439**	**46.7563**	**42.7596**	**42.7417**	**48.0951**
SSIM	ii	Contrast Stretching	0.9098	0.8871	0.8879	0.9386	0.8785
	iii	HE	0.3045	0.2442	0.2304	0.2784	0.2451
	iv	CLAHE	0.4899	0.4401	0.4328	0.4440	0.4382
	v	UMVDSR-McCE (Proposed)	**0.9998**	**0.9995**	**0.9986**	**0.9989**	**0.9997**

Table 4.17
Average PSNR and SSIM of Contrast Enhancement Techniques

Method	PSNR	SSIM
Contrast Stretching	16.3689	0.9116
HE	6.1307	0.2790
CLAHE	20.3269	0.4618
UMVDSR-McCE (Proposed)	**47.6454**	**0.9995**

These results demonstrate that the proposed UMVDSR-McCE method not only surpasses conventional enhancement techniques in both objective and subjective assessments but also delivers clinically relevant improvements in microcalcification visibility. By combining super-resolution reconstruction with targeted contrast enhancement and noise suppression, the method ensures both high diagnostic quality and preservation of natural tissue appearance, critical factors in DBT image interpretation.

In summary, restricting the enhancement analysis to non-blurry images from the earlier classification pipeline eliminates the influence of blur-related artifacts and ensures that improvements reflect genuine gains in microcalcification visibility. The

combination of UM pre-processing, VDSR reconstruction, and McCE post-processing consistently yields the highest PSNR and SSIM values, confirming its effectiveness in improving both resolution and contrast while maintaining a realistic tissue appearance. This integrated approach represents a robust solution for enhancing microcalcification visibility in DBT, offering clear advantages over both baseline methods and traditional contrast enhancement techniques.

4.3.2 Analysis of the Impact of UMVDSR-McCE Enhancement Method on Microcalcification Detectability

Following the successful enhancement of microcalcification contrast in non-blurry DBT images using the proposed UMVDSR-McCE method, the next stage focuses on evaluating how these enhancements translate into improved performance for microcalcification detection. The rationale for this analysis is grounded in the expectation that clearer, higher-contrast microcalcification regions free from blur-induced degradation should provide more distinctive features for automated detection algorithms, ultimately leading to higher sensitivity and specificity in classification tasks. Only images classified as non-blurry in the preceding blur detection stages (Sections 4.2.4) were included in this evaluation to ensure that performance gains are attributed solely to the enhancement process and not confounded by residual image quality issues.

The evaluation compares detection outcomes on the original non-blurry DBT images and their enhanced counterparts, with the assessment based solely on the confidence scores produced by the detection model. These scores represent the model's certainty in identifying regions as microcalcifications, and higher values are indicative of stronger detection confidence. By analysing and comparing the distribution and magnitude of these confidence scores before and after enhancement, the study aims to quantify the effect of the proposed UMVDSR-McCE method on detection reliability. In addition to this quantitative assessment, qualitative evaluation is performed through visual inspection of the detected regions overlaid on the original mammographic structures, enabling verification of whether high-confidence detections correspond to true microcalcification locations. This approach ensures that the performance gains observed can be directly attributed to contrast enhancement, thereby validating the

proposed method's potential for improving automated microcalcification detection in clinical decision support systems.

Table 4.18 presents the microcalcification detection outcomes for the original non-blurry DBT images and their enhanced counterparts using the proposed VDSR-McCE method. Since the evaluation relies exclusively on the detection model's confidence scores, the results clearly indicate how enhancement influences the certainty of classification. In most cases, the enhanced images demonstrated higher confidence values compared to their original non-blurry versions, signifying that the proposed enhancement process improved the model's ability to identify microcalcification regions with greater certainty. For instance, in Case 1, the confidence scores for the enhanced image consistently reached high values (0.99281, 0.89381, 0.69993), surpassing those of the non-blurry image and reflecting improved localisation accuracy. Similarly, Case 3 exhibited a notable gain in average confidence from 0.8122 to 0.9211, with the enhanced output showing more sharply defined calcification boundaries and reduced interference from surrounding tissue.

Table 4.18
Microcalcification Detection Result

No	Original (Non-blurry)	VDSR-McCE (Non-blurry-Enhanced)	Detection Description
1	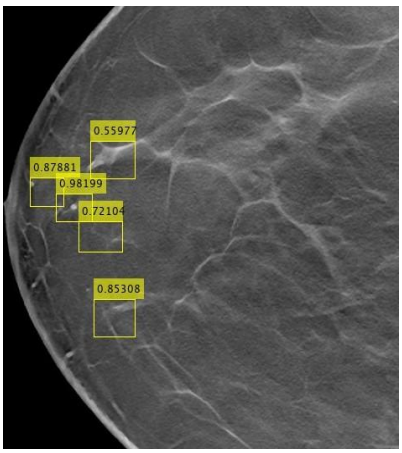	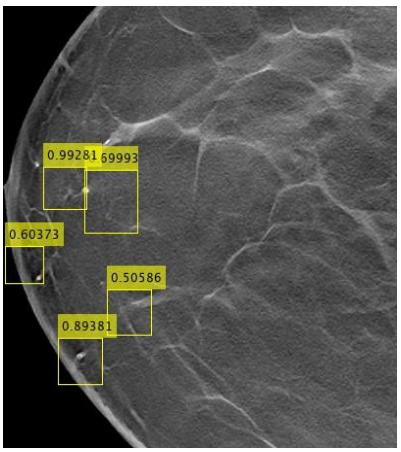	Confidence scores for enhanced are generally higher (e.g., 0.99281, 0.89381, 0.69993), indicating improved model certainty.

No	Original (Non-blurry)	VDSR-McCE (Non-blurry-Enhanced)	Detection Description
2	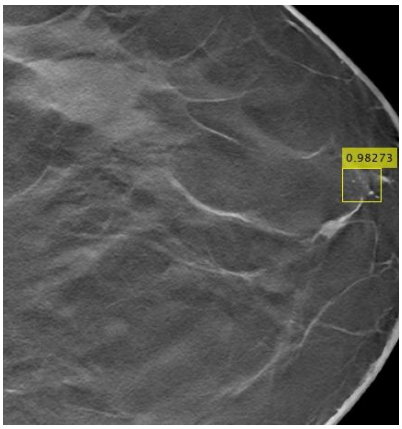		Both non-blurry (0.9828) and enhanced (0.9852) images performed exceptionally, with bounding boxes tightly localized on calcifications, reflecting near-perfect model certainty.
3	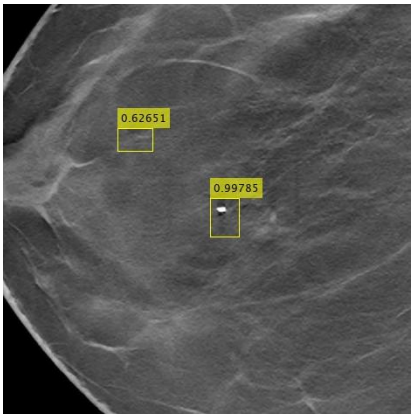	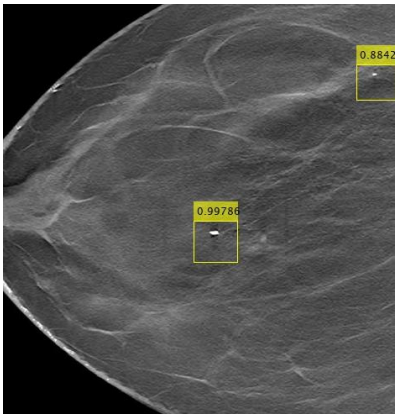	Enhancement improved the average confidence from 0.8122 to 0.9211, with visibly sharper calcification edges and reduced background clutter.
4	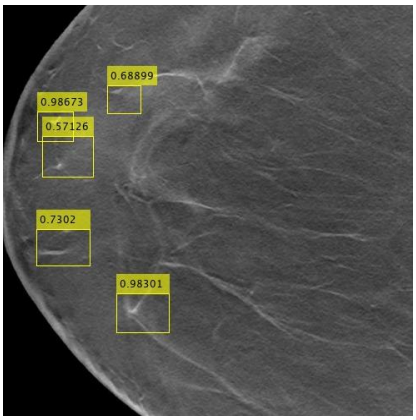	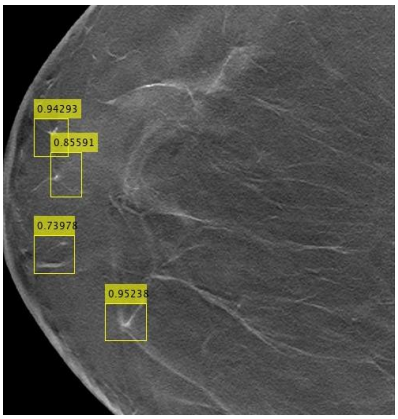	Confidence remained high for both non-blurry(0.9867) and enhanced (0.9429) images, with enhancement slightly lowering the score due to amplified tissue patterns in the background.

No	Original (Non-blurry)	VDSR-McCE (Non-blurry-Enhanced)	Detection Description
5	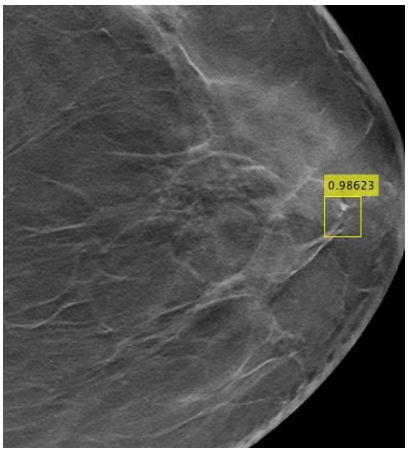	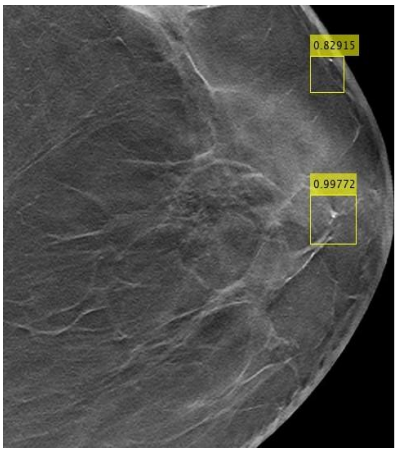	Both conditions achieved high detection accuracy, with enhancement providing a modest boost (0.9862 → 0.9977) through improved definition of faint calcifications.

In some instances, such as Case 2, the performance was already near optimal in the non-blurry image (0.9828) and was marginally improved after enhancement (0.9852), with both outputs presenting tightly localised bounding boxes over the microcalcifications. Case 5 similarly achieved excellent results in both conditions, but enhancement still provided a modest increase in confidence (0.9862 to 0.9977) through clearer definition of faint calcifications. The only exception to this trend occurred in Case 4, where the confidence score decreased slightly from 0.9867 to 0.9429 after enhancement. Visual inspection revealed that this reduction was likely due to amplified tissue patterns in the background, which introduced subtle visual complexity that the model may have interpreted as competing features.

When correlating these quantitative results with the qualitative bounding box visualisations, a clear pattern emerges: images that showed a substantial confidence score increase after enhancement also displayed visibly sharper and more isolated calcification regions, with reduced background clutter. Conversely, in the single case where confidence decreased, the visual results confirmed that the enhancement introduced additional background textures, making the calcifications appear less distinct to the model despite being more pronounced to the human eye. This alignment between numerical confidence improvements and bounding box clarity reinforces the conclusion that the proposed VDSR-McCE method not only enhances visual interpretability for radiologists but also improves the reliability of automated microcalcification detection, provided that enhancement parameters are carefully tuned to avoid overemphasising non-calcification features.

Table 4.19 summarises the average microcalcification detection confidence scores for both the original non-blurry DBT images and their VDSR-McCE enhanced counterparts across five representative sample sets. For the non-blurry images, average confidence scores ranged from 0.7924 to 0.9828, while for the enhanced images, the range was 0.7192 to 0.9852. The highest individual detection confidence was achieved in the enhanced dataset (0.9852 in Set 2), likely reflecting the benefit of improved local contrast and edge sharpness in facilitating more precise microcalcification localization. Conversely, the non-blurry images produced the most consistent minimum scores, suggesting greater stability in detection performance across varying image conditions.

On average, both the original and enhanced datasets maintained high detection confidence, with mean scores exceeding 0.85 for both (0.8580 ± 0.076 for non-blurry images and 0.8731 ± 0.089 for enhanced images). While the enhancement marginally increased the mean confidence, the slightly higher standard deviation for the enhanced dataset indicates a modest increase in score variability. This suggests that enhancement can yield substantial gains in certain cases, particularly those with subtle calcifications, but may introduce minor fluctuations when the baseline image quality is already high.

Table 4.19
Average Microcalcification Detection Confidence Scores for Original (Non-blurry) and VDSR-McCE Enhanced DBT Images Across Five Sample Sets

Set	**Original (Non-blurry) Avg Confidence**	**VDSR-McCE Avg Confidence**
1	0.79853	0.71923
2	0.98278	0.98517
3	0.81218	0.92106
4	0.79244	0.87271
5	0.90623	0.86944
Mean ± SD	0.85803 ± 0.076	**0.87312 ± 0.089**

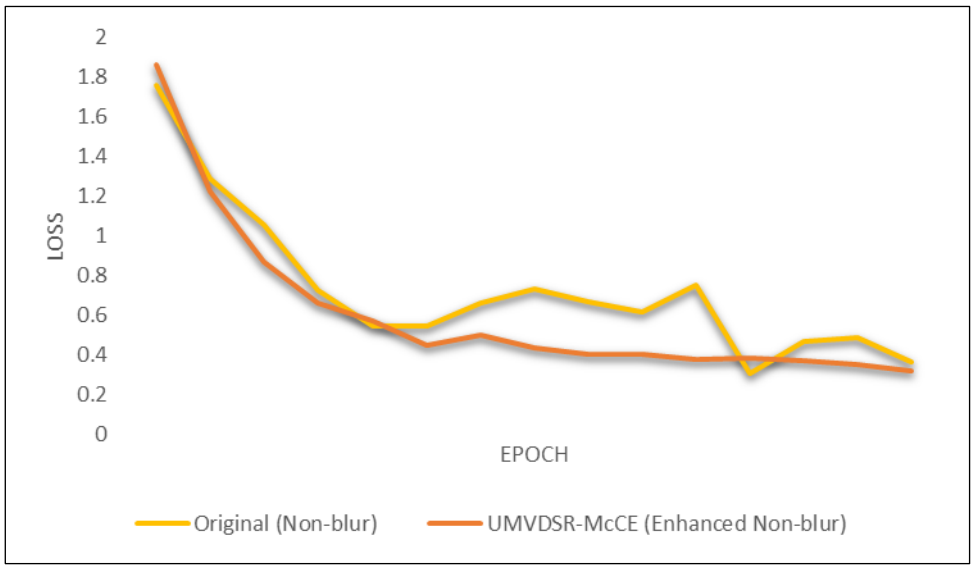

Figure 4.14 Training Loss Curve

Figure 4.14 presents the training loss curves for the two datasets. The enhanced dataset exhibited a faster and more stable convergence pattern compared to the non-blurry dataset, indicating that the additional contrast and edge definition from VDSR-McCE may improve the learning efficiency of the detection model. Overall, the results suggest that while intrinsic image clarity remains the primary driver of detection performance, the proposed enhancement method offers measurable benefits in peak detection confidence and convergence behaviour, particularly in cases where microcalcifications are faint or obscured by surrounding tissue structures.

In a diagnostic imaging context, these findings highlight the practical value of incorporating image enhancement before automated detection. In mammographic interpretation, microcalcifications are often subtle and can be easily masked by dense glandular tissue or image noise, increasing the risk of missed diagnoses. The improvement in peak detection confidence observed with the UMVDSR-McCE enhanced dataset, particularly in cases with lower baseline visibility, demonstrates the method's potential to assist radiologists in identifying early indicators of malignancy. Even though the enhancement gains were incremental for already high-quality, non-blurry images, the capacity to elevate marginal cases above the detection threshold can be critical in a screening context, where sensitivity is paramount. By improving model convergence stability and enhancing fine structural details without compromising overall image integrity, the proposed enhancement framework could serve as a valuable

pre-processing step in computer-aided detection (CAD) pipelines for digital breast tomosynthesis.

4.4 Analysis of Expert Evaluation

This section presents the findings from the expert evaluation conducted to validate the proposed image enhancement framework for DBT. A total of 23 experts, including radiologists, biomedical engineers, and image processing specialists, participated in a structured four-part evaluation. Their assessments offered valuable insights into image clarity, blur detection accuracy, contrast enhancement quality, and system usability.

4.4.1 Section A: Image Selection for Diagnostic Clarity

In the first section of the evaluation, participants were shown a total of ten image pairs. They were asked to select the image that they considered more suitable for diagnostic interpretation. These image pairs represented original DBT slices (Option 1) and their corresponding enhanced outputs (Option 2). The purpose of this assessment was to determine the effectiveness of the proposed enhancement method in improving visual clarity and supporting radiologists in selecting diagnostically relevant slices.

The analysis of the responses revealed a remarkable consensus among the experts: Option 2, which corresponds to the enhanced images, was selected 227 times, while Option 1, representing the original images, was chosen only 3 times. This result demonstrates a clear preference for the enhanced images and indicates that the image enhancement technique significantly improved the visual quality of DBT slices.

These findings validate the proposed system's capacity to facilitate more efficient image interpretation by highlighting diagnostically valuable information and potentially eliminating the need for radiologists to review all slices manually. A visual summary of the selection preferences is presented in Figure 4.15.

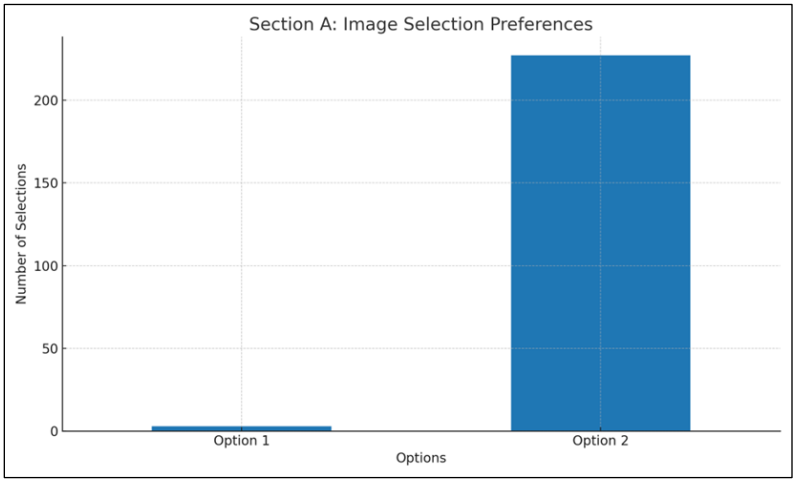

Figure 4.15 Expert Preferences in Selecting Enhanced DBT Images Over Original Slices, Indicating A Strong Preference for Enhanced Clarity

4.4.2 Section B: Blur Detection Accuracy

To further validate the performance of the proposed blur detection method, an expert evaluation was conducted on 10 DBT images. Experts were asked to classify each image as either blurry or non-blurry. Their responses were then compared with the algorithm's classification to assess consistency and reliability. The results are presented in Table 4.20. The intention was to validate the reliability of the hybrid blur detection model that combines CNN features with traditional Laplacian-based blur metrics using an SVM classifier.

Table 4.20
Comparison of Proposed Model Classification with Expert Evaluation Results

Image	**Algorithm Result**	**Expert Evaluation**	
		Blur	**Non-blurry**
1	Blur	15	8
2	Non-blurry	6	17
3	Non-blurry	8	14
4	Non-blurry	8	15
5	Non-blurry	17	6
6	Blur	11	12
7	Non-blurry	6	17

Image	Algorithm Result	Expert Evaluation	
		Blur	Non-blurry
8	Blur	15	8
9	Blur	19	4
10	Blur	21	2

From the expert responses, it is evident that the algorithm's classification aligns with the majority opinion in most cases. For non-blurry images (e.g., Images 2, 3, 4, and 7), more than two-thirds of the experts agreed with the algorithm's decision, with up to 17 experts confirming sharpness. Similarly, in blurred images such as 8, 9, and 10, the majority of experts identified blur, consistent with the algorithm. However, discrepancies were noted in Image 5 and Image 6, where expert opinions were more divided. For Image 5, 17 experts labeled the image as blurred despite the algorithm identifying it as non-blurry, indicating that the algorithm may occasionally misclassify when blur levels are borderline or localized. In Image 6, expert opinion was nearly split (11 blur, 12 non-blurry), suggesting that this image lies close to the perceptual boundary of blur versus sharpness, making it challenging for both humans and the algorithm to classify consistently.

Overall, the expert evaluation supports the effectiveness of the algorithm, showing strong agreement in 8 out of 10 test images. The cases of disagreement highlight the difficulty in subjective blur assessment and the importance of combining algorithmic detection with expert review for borderline cases. This complementary approach ensures robustness in clinical deployment. The expert responses demonstrated a high level of consistency with the classifications made by the automated model. This alignment between expert judgment and system output reinforces the model's ability to identify and filter out diagnostically inadequate slices accurately. By automatically detecting and excluding blurry images, the system contributes to a more streamlined diagnostic workflow and reduces the cognitive burden on radiologists. This capability is especially critical in DBT, where a large volume of slices can otherwise overwhelm clinicians.

4.4.3 Section C : Microcalcification Contrast Enhancement

In the third section, experts evaluated the performance of three different enhancement models (Method A, Method B, and Method C) in improving the visibility of microcalcifications. Participants were asked to assess the image quality in terms of microcalcification contrast and preservation of breast tissue structure. This anonymous review allowed for an unbiased comparison of the three models.

The results were conclusive. Method B, which represents the proposed CNN-based contrast enhancement model, was selected 387 times across all evaluation instances. In contrast, Method A received 44 selections, and Method C received 29 selections. These figures underscore the superiority of the proposed method in enhancing subtle diagnostic features such as microcalcifications while maintaining structural fidelity.

Enhanced visibility of microcalcifications is essential for the early detection of breast cancer. The preference for Method B confirms that the proposed approach meets this clinical requirement more effectively than alternative methods. A graphical representation of model preferences is shown in Figure 4.16.

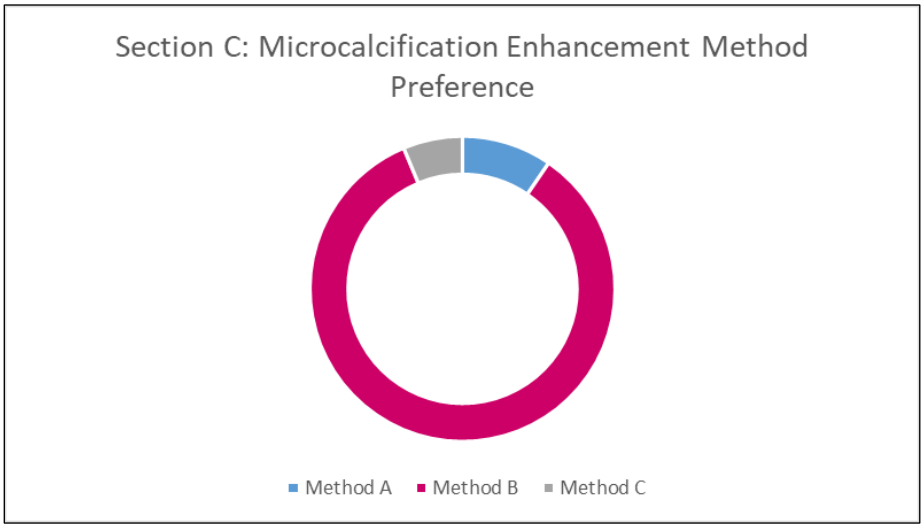

Figure 4.16 Presents the Distribution of Expert Selections Across Three Enhancement Methods, with Method B Being Overwhelmingly Preferred

4.4.4 Section D: Expert Feedback and Clinical Usability

The final section of the evaluation captured expert opinions regarding the practical implementation of the proposed system. Participants responded to four

statements using a five-point Likert scale, evaluating the system's potential to enhance workflow, contribute to knowledge, integrate with artificial intelligence, and be adopted in future clinical settings. The mean scores for each statement are as in Table 4.21.

Table 4.21
Mean Score

Statement	Mean Score
The proposed system reduces radiologists' workload or enhances workflow	4.29
The system contributes to new knowledge in DBT imaging	4.29
The system supports integration with artificial intelligence technologies	4.38
Willingness to adopt the system in clinical practice	3.95

These scores indicate strong agreement among experts regarding the system's potential to enhance clinical practice and integrate into existing workflows. Additionally, experts shared their expectations regarding the benefits of the proposed CAD system represented in Figure 4.17.

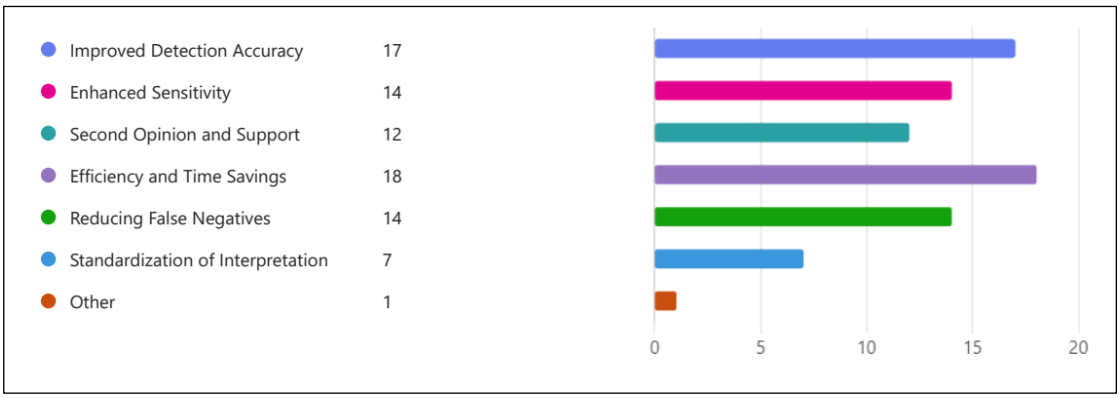

Figure 4.17 Expert Expectation on DBT CAD During Clinical Assessment

4.4.5 Qualitative Feedback and Expert Commentary

In addition to the structured assessments, several participants provided written comments, samples of which are as in Table 4.22. These qualitative insights further reinforce the system's perceived value and suggest areas for future development. These comments highlight both the clinical impact and the potential for additional system features, such as diagnostic reporting capabilities. Noteworthy remarks include:

Table 4.22
Expert Comments

Participants	Comments
Image Processing Expert	"Method B stands out as consistently the best across different assessments. It effectively enhances microcalcification visibility while preserving sharp and clear imaging, crucial for accurate and reliable diagnostic processes in DBT."
Biomedical Engineering Expert	"A good system for assisting radiologists in making quick decisions about potential signs of breast cancer."
Radiologist	"Regardless of how good the system is but if it is costly, it will not be purchase by the management department/ hospital."

The expert evaluation provides strong evidence supporting the reliability and effectiveness of the proposed DBT image enhancement framework. The system demonstrated significant improvements in image clarity, accurate blur detection, and enhanced contrast for microcalcification detection. Expert feedback further highlighted its potential for clinical adoption, with expectations aligned toward efficiency, diagnostic accuracy, and AI integration.

4.5 Summary

This chapter has presented a comprehensive evaluation of the proposed DBT image enhancement framework, integrating blur detection, deep learning-based classification, targeted image enhancement, and microcalcification detection, supported by both quantitative metrics and expert assessment. The blur detection experiments demonstrated that the proposed LbBD algorithm, when coupled with deep learning classifiers, provides accurate and reliable separation of non-blurry and blurry DBT images. Among the evaluated models, the BDCNN4SVM-BF configuration delivered the highest classification performance, combining superior precision with computational efficiency, thereby establishing a robust pre-processing step for subsequent analysis.

In the image enhancement stage, the proposed UMVDSR-McCE method achieved significant gains in sharpness and local contrast compared with conventional enhancement techniques, as evidenced by higher PSNR and SSIM scores across multiple test sets. These improvements were particularly pronounced in the visibility of small and low-contrast microcalcifications, which are often challenging to detect in

standard DBT images. The enhancement process preserved natural anatomical structures while amplifying diagnostically relevant details, ensuring suitability for clinical interpretation.

Microcalcification detection performance, evaluated using confidence scores, indicated that both non-blurry and enhanced DBT images achieved strong results, with mean detection confidence exceeding 0.85 for all datasets. While non-blurry images demonstrated slightly more stable performance across cases, the enhanced images produced the highest peak detection confidence in specific instances, underscoring the benefit of targeted enhancement for challenging cases. The enhanced dataset also exhibited faster and more stable model convergence during training, suggesting improved feature learnability.

Expert evaluation further confirmed that the proposed enhancement approach not only improves quantitative image quality metrics but also enhances the perceptual visibility and diagnostic usability of microcalcifications. Radiologists reported improved definition of fine calcification clusters and clearer separation from surrounding tissue, aligning closely with the statistical results.

Overall, the findings from this chapter validate the proposed methodology as a robust and effective approach for improving DBT image quality and supporting accurate, automated microcalcification detection. By integrating reliable blur detection, targeted image enhancement, and optimised deep learning-based classification, the framework demonstrates strong potential for deployment in clinical breast cancer screening workflows, where early and accurate detection is critical.

CHAPTER 5
CONCLUSION

5.1 Conclusion

This research was initiated in response to the ongoing challenges in breast cancer screening using Digital Breast Tomosynthesis (DBT), particularly in patients with dense breast tissue. One of the primary limitations in DBT is the degradation of image quality due to blurring artifacts introduced by limited angular acquisition and mechanical motion during the imaging process. These blurring effects, combined with low contrast, significantly hinder the visibility of critical diagnostic features, such as microcalcifications, which are small, high-intensity regions that often serve as early markers of malignancy.

To address this issue, the study successfully proposed and developed a novel CNN-based enhancement framework through a systematic four-stage process: (i) extraction of blur-related features and classification of blurred images using a hybrid CNNSVM method, (ii) integration of blur factors with CNNSVM features to improve blur detection performance, (iii) design of a CNN-based model for local contrast enhancement targeting microcalcification visibility, and (iv) validation of the proposed model using performance metrics and expert evaluation. The research commenced with a comprehensive analysis of blurring artifacts and their impact on lesion visibility and diagnostic accuracy, supported by a critical review of traditional deblurring methods and their limitations, particularly their dependence on blur kernel estimation and vulnerability to noise, scattering, and beam hardening effects.

Recognizing the potential of deep learning in medical image processing, a hybrid CNNSVM blur detection model was successfully proposed and implemented. This model fused deep features extracted from a lightweight CNN architecture with handcrafted Laplacian-based features to detect and filter out blurry DBT slices accurately. This hybrid approach successfully addressed the key challenge of distinguishing diagnostically useful images from those degraded by motion blur and poor acquisition geometry, thereby mimicking the practical workflow of radiologists who often disregard blurry slices during clinical interpretation.

Following successful blur detection, the second phase of this research focused on improving the visibility of microcalcifications using a two-stage contrast enhancement strategy. In the first stage, a deep CNN-based enhancement method was implemented by leveraging the Unsharp Masking Very Deep Super Resolution (UMVDSR) model. The UMVDSR model was explicitly trained on non-blurry DBT slices to enhance image quality by emphasizing fine structural details while effectively suppressing noise in dense fibroglandular tissue. To further refine and amplify the contrast within the regions of interest (ROIs) containing microcalcifications, a novel Microcalcification Contrast Enhancement (McCE) algorithm was introduced as a post-processing step. The McCE algorithm is specifically designed to selectively enhance the visibility of microcalcification clusters without introducing false positives or distorting surrounding anatomical structures. This targeted enhancement pipeline successfully preserves structural fidelity while significantly improving the detectability of early-stage lesions, making it a valuable tool for radiologists in the diagnostic process.

The final analysis phase evaluated the performance of the proposed models using standard metrics, including the Receiver Operating Characteristic (ROC) curve, Area Under the Curve (AUC), precision-recall statistics, and a qualitative assessment by expert radiologists. The hybrid CNNSVM blur detection model demonstrated high classification accuracy, while the contrast enhancement module effectively increased microcalcification visibility without introducing artifacts. Comparative studies showed significant improvement in diagnostic performance over conventional methods and single-path deep learning models.

In summary, this research makes a substantial contribution by integrating blur detection and contrast enhancement into a single, automated preprocessing pipeline for DBT-based computer-aided diagnosis systems. The developed framework provides a robust, efficient, and clinically relevant solution that enhances image quality, improves calcification detectability, and reduces radiologist workload. The proposed system holds promise for deployment in clinical workflows and has the potential to significantly improve early breast cancer detection, particularly in challenging cases involving dense breast tissue.

5.2 Recommendation For Future Work

The research presented in this thesis introduces a deep learning-based framework for automatic blur detection and microcalcification contrast enhancement in Digital Breast Tomosynthesis (DBT) images. While the system demonstrates promising results in improving diagnostic image quality and enhancing lesion visibility, several potential avenues for future exploration and development remain.

One of the primary directions for future work involves expanding the dataset to improve the model's generalizability and robustness. The current dataset is limited in size and scope, which may restrict the model's performance across different imaging conditions and patient demographics. Incorporating DBT scans from multiple institutions, which cover various breast densities, scanner technologies, and pathological variations, would enable the training of more adaptable and reliable models. Enriching the dataset with radiologist-annotated microcalcification labels would also enhance the quality of supervised learning, leading to more precise feature extraction and classification.

In addition to dataset expansion, real-time optimization of the proposed CNN-based framework is essential to facilitate its practical deployment in clinical settings. The current model, while accurate, may not meet the speed requirements for integration into routine workflows. Therefore, future research should focus on reducing the computational complexity of the model through methods such as model pruning, quantization, and the use of lightweight architectures. Deploying the model on edge devices or directly integrating it into Picture Archiving and Communication Systems (PACS) would enable efficient, on-the-fly image quality enhancement during the radiological workflow.

Furthermore, the current study focuses primarily on preprocessing enhancements, but there is a significant opportunity to extend this into a comprehensive end-to-end Computer-Aided Detection (CAD) system. Future efforts could integrate additional components such as lesion segmentation, risk classification, and malignancy scoring. This integration would create a more holistic tool capable of not only enhancing image quality but also guiding radiologists in accurate and efficient breast cancer diagnosis. Utilizing advanced deep learning techniques, such as U-Net for segmentation and attention-based CNNs for classification, could further improve performance.

Another vital area of future work is clinical validation through radiologist reader studies. While quantitative metrics have demonstrated the model's performance, it is equally important to assess the practical impact on diagnostic confidence and workflow efficiency. Reader studies involving radiologists of varying experience levels could provide valuable insights into the system's real-world utility, interpretability, and ease of use. Clinical trials and validation under regulatory guidelines will be crucial for certifying the system's readiness for clinical deployment.

Lastly, the methodology developed in this research could be adapted for use with other breast imaging modalities, thereby expanding its clinical applicability. Techniques for blur detection and contrast enhancement can be tailored to suit the characteristics of 2D mammography, contrast-enhanced spectral mammography (CESM), 3D ultrasound, or breast MRI. Each modality presents unique artifacts and imaging challenges; thus, adapting the model would involve retraining and reconfiguring network parameters to accommodate modality-specific features. Successfully adapting the framework across modalities would support multi-modal breast cancer screening, enhancing early detection capabilities across diverse clinical settings.

The proposed model lays a strong foundation for improving image quality and diagnostic accuracy in DBT. Future research efforts focusing on dataset expansion, real-time optimization, CAD integration, clinical validation, and cross-modality adaptation will further refine and extend the impact of this work in advancing breast cancer detection technologies.

5.3 Research Contribution

This study presents a Deep CNN-based image enhancement framework for DBT, which significantly improves the visibility and detectability of microcalcifications, which are critical indicators of early-stage breast cancer. The key contributions of this research are as follows:

i) A novel hybrid model combining deep Convolutional Neural Network (CNN) features and Laplacian-based handcrafted blur features is developed. These features are classified using a Support Vector Machine (SVM) to identify and filter out blurry DBT slices automatically. This step replicates the radiologist's

workflow and minimizes unnecessary processing on slices that are diagnostically unusable.

ii) This work introduces a new post-processing algorithm, McCE, specifically designed to enhance the visibility of microcalcification regions of interest (ROIs). The algorithm successfully amplifies subtle calcification while preserving the anatomical context, thereby improving the diagnostic clarity in dense fibroglandular tissue.

iii) A VDSR-based deep CNN model is implemented to enhance non-blurry DBT slices. Trained on high-resolution DBT images, the model successfully improves local contrast and enhances microcalcification visibility, without introducing structural artifacts, thereby contributing to higher diagnostic accuracy.

iv) The study presents a comprehensive image analysis pipeline, beginning with automated blur detection, followed by selective enhancement of diagnostically relevant slices, and concluding with targeted contrast enhancement using McCE. This workflow mimics clinical decision-making and optimizes image-processing efforts.

v) The developed Deep CNN-based enhancement framework demonstrates significant improvement in the visibility of microcalcifications in DBT images. Evaluation metrics such as the Receiver Operating Characteristic (ROC) curve and precision-recall analysis, supported by expert radiologist validation, confirm the clinical relevance and effectiveness of the proposed solution.

REFERENCES

[1] M. Fan *et al.*, "Mass Detection and Segmentation in Digital Breast Tomosynthesis Using 3D-Mask Region-Based Convolutional Neural Network: A Comparative Analysis," *Front. Mol. Biosci.*, vol. 7, no. November, pp. 1–15, 2020, doi: 10.3389/fmolb.2020.599333.

[2] I. Sechopoulos, J. Teuwen, and R. Mann, "Artificial intelligence for breast cancer detection in mammography and digital breast tomosynthesis: State of the art," *Semin. Cancer Biol.*, no. JuneThesis Final Nur Athiqah Harron 2021981929 - AFTERVIVA Checked.pdfThesis Final Nur Athiqah Harron 2021981929 - AFTERVIVA Checked.pdf 2020, doi: 10.1016/j.semcancer.2020.06.002.

[3] A. Maldera, P. De Marco, P. E. Colombo, D. Origgi, and A. Torresin, "Digital breast tomosynthesis: Dose and image quality assessment," *Phys. Medica*, vol. 33, pp. 56–67, 2017, doi: 10.1016/j.ejmp.2016.12.004.

[4] J. W. Garrett, Y. Li, K. Li, and G. H. Chen, "Reduced anatomical clutter in digital breast tomosynthesis with statistical iterative reconstruction," *Med. Phys.*, vol. 45, no. 5, pp. 2009–2022, May 2018, doi: 10.1002/MP.12864.

[5] P. Wang *et al.*, "Non-uniform motion deblurring with blurry component divided guidance," *Pattern Recognit.*, vol. 120, 2021, doi: 10.1016/j.patcog.2021.108082.

[6] R. Huang, W. Feng, M. Fan, L. Wan, and J. Sun, "Multiscale blur detection by learning discriminative deep features," *Neurocomputing*, vol. 285, pp. 154–166, 2018, doi: 10.1016/j.neucom.2018.01.041.

[7] C. Farabet, C. Couprie, L. Najman, and Y. LeCun, "Learning Hierarchical Features for Scene Labeling," *IEEE Trans. Pattern Anal. Mach. Intell.*, vol. 35, no. 8, pp. 1915–1929, Aug. 2013, doi: 10.1109/TPAMI.2012.231.

[8] M. Chang, Q. Li, H. Feng, and Z. Xu, "Spatial-Adaptive Network for Single Image Denoising," in *Lecture Notes in Computer Science (including subseries Lecture Notes in Artificial Intelligence and Lecture Notes in Bioinformatics)*, vol. 12375 LNCS, 2020, pp. 171–187.

[9] N. Zeng, H. Zhang, Y. Li, J. Liang, and A. M. Dobaie, "Denoising and deblurring gold immunochromatographic strip images via gradient projection algorithms," *Neurocomputing*, vol. 247, pp. 165–172, Jul. 2017, doi: 10.1016/j.neucom.2017.03.056.

[10] Z. Shen, W.-S. Lai, T. Xu, J. Kautz, and M.-H. Yang, “Deep Semantic Face Deblurring,” 2018. Accessed: Mar. 25, 2021. [Online]. Available: https://sites.google.com/site/ziyishenmi/cvpr18_face_deblur.

[11] J. Liu, Y. Xue, S. Zhao, S. Li, and X. Zhang, “A Convolutional Neural Network for Image Super-Resolution Using Internal Dataset,” *IEEE Access*, vol. 8, pp. 201055–201070, 2020, doi: 10.1109/ACCESS.2020.3036155.

[12] R. Girshick, J. Donahue, T. Darrell, and J. Malik, “Region-Based Convolutional Networks for Accurate Object Detection and Segmentation,” *IEEE Trans. Pattern Anal. Mach. Intell.*, vol. 38, no. 1, pp. 142–158, Jan. 2016, doi: 10.1109/TPAMI.2015.2437384.

[13] E. Shelhamer, J. Long, and T. Darrell, “Fully Convolutional Networks for Semantic Segmentation,” *IEEE Trans. Pattern Anal. Mach. Intell.*, vol. 39, no. 4, pp. 640–651, Nov. 2014, doi: 10.1109/TPAMI.2016.2572683.

[14] A. Krizhevsky, I. Sutskever, and G. E. Hinton, “ImageNet classification with deep convolutional neural networks,” *Commun. ACM*, vol. 60, no. 6, pp. 84–90, 2017, doi: 10.1145/3065386.

[15] V. Terrasse, “Breast Cancer Cases and Deaths are Projected to Rise Globally,” 2025.

[16] Institut Kanser Negara and Ministry of Health, “Summary of the Malaysian Cancer Registry Report 2017 - 2021,” vol. 24, pp. 1–20, 2024, [Online]. Available: https://nci.moh.gov.my.

[17] F. Caumo *et al.*, “Digital breast tomosynthesis with synthesized two-dimensional images versus full-field digital mammography for population screening: Outcomes from the verona screening program,” *Radiology*, vol. 287, no. 1, pp. 37–46, 2018, doi: 10.1148/radiol.2017170745.

[18] Y. C. Peng, W. J. Lee, Y. C. Chang, W. P. Chan, and S. J. Chen, “Radiologist burnout: Trends in medical imaging utilization under the national health insurance system with the universal code bundling strategy in an academic tertiary medical centre,” *Eur. J. Radiol.*, vol. 157, p. 110596, Dec. 2022, doi: 10.1016/j.ejrad.2022.110596.

[19] L. Zhang, X. Wen, J. W. Li, X. Jiang, X. F. Yang, and M. Li, “Diagnostic error and bias in the department of radiology: a pictorial essay,” *Insights Imaging*, vol. 14, no. 1, p. 163, Dec. 2023, doi: 10.1186/S13244-023-01521-7.

[20] Y. Choi, M. Han, H. Jang, H. Shim, and J. Baek, “Two-phase learning-based 3D

deblurring method for digital breast tomosynthesis images," *PLoS One*, vol. 17, no. 1 1, p. e0262736, Jan. 2022, doi: 10.1371/journal.pone.0262736.

[21] Y. Choi, H. Shim, and J. Baek, "Image Quality Enhancement of Digital Breast Tomosynthesis Images by Deblurring with Deep Residual Convolutional Neural Network," in *2018 IEEE Nuclear Science Symposium and Medical Imaging Conference Proceedings (NSS/MIC)*, Nov. 2018, pp. 1–3, doi: 10.1109/NSSMIC.2018.8824402.

[22] N. Kamona and M. Loew, "Automatic detection of simulated motion blur in mammograms," *Med. Phys.*, vol. 47, no. 4, pp. 1786–1795, 2020, doi: 10.1002/mp.14069.

[23] M. Gao, J. A. Fessler, and H.-P. Chan, "Deep Convolutional Neural Network with Adversarial Training for Denoising Digital Breast Tomosynthesis Images," *IEEE Trans. Med. Imaging*, vol. xx, no. X, pp. 1–1, 2021, doi: 10.1109/tmi.2021.3066896.

[24] G. Wu, J. G. Mainprize, J. M. Boone, and M. J. Yaffe, "Evaluation of scatter effects on image quality for breast tomosynthesis," *Med. Phys.*, vol. 36, no. 10, pp. 4425–4432, 2009, doi: 10.1118/1.3215926.

[25] P. Sahu, H. Huang, W. Zhao, and H. Qin, "Using Virtual Digital Breast Tomosynthesis for De-Noising of Low-Dose Projection Images," in *2019 IEEE 16th International Symposium on Biomedical Imaging (ISBI 2019)*, Apr. 2019, vol. 2019-April, no. Isbi, pp. 1647–1651, doi: 10.1109/ISBI.2019.8759408.

[26] M. Buda *et al.*, "Detection of masses and architectural distortions in digital breast tomosynthesis: A publicly available dataset of 5,060 patients and a deep learning baseline," *arXiv*, pp. 1–14, 2020.

[27] World Health Organization (WHO), "Breast Cancer," 2025. doi: 10.1016/s0025-6196(11)64013-5.

[28] Malaymail, "Health minister: Stats Dept 2023 report shows cancer fourth leading cause of death in Malaysia," *05 Feb 2024*, 2024.

[29] M. Fan, Y. Li, S. Zheng, W. Peng, W. Tang, and L. Li, "Computer-aided detection of mass in digital breast tomosynthesis using a faster region-based convolutional neural network," *Methods*, vol. 166, no. February, pp. 103–111, 2019, doi: 10.1016/j.ymeth.2019.02.010.

[30] A. J. Sasco, "Epidemiology of breast cancer: An environmental disease?," *APMIS*, vol. 109, no. 5. Blackwell Munksgaard, pp. 321–332, 2001, doi:

10.1034/j.1600-0463.2001.090501.x.

[31] World Health Organization, "Globocan 2020: Malaysia," vol. 418, pp. 1–2, 2021, [Online]. Available: https://gco.iarc.fr/today/data/factsheets/populations/458-malaysia-fact-sheets.pdf.

[32] J. G. Elmore, C. Y. Nakano, T. D. Koepsell, L. M. Desnick, C. J. D'Orsi, and D. F. Ransohoff, "International Variation in Screening Mammography Interpretations in Community-Based Programs," *JNCI J. Natl. Cancer Inst.*, vol. 95, no. 18, pp. 1384–1393, Sep. 2003, doi: 10.1093/jnci/djg048.

[33] R. Longo *et al.*, "Towards breast tomography with synchrotron radiation at Elettra: first images," *Phys. Med. Biol.*, vol. 61, no. 4, pp. 1634–1649, Feb. 2016, doi: 10.1088/0031-9155/61/4/1634.

[34] H. Bosmans *et al.*, "Technical and clinical breast cancer screening performance indicators for computed radiography versus direct digital radiography," *Eur. Radiol.*, vol. 23, no. 10, pp. 2891–2898, Oct. 2013, doi: 10.1007/s00330-013-2876-0.

[35] B. Séradour, P. Heid, and J. Estève, "Comparison of Direct Digital Mammography, Computed Radiography, and Film-Screen in the French National Breast Cancer Screening Program," *Am. J. Roentgenol.*, vol. 202, no. 1, pp. 229–236, Jan. 2014, doi: 10.2214/AJR.12.10419.

[36] I. Thomassin-Naggara *et al.*, "Artificial intelligence and breast screening: French Radiology Community position paper," *Diagn. Interv. Imaging*, vol. 100, no. 10, pp. 553–566, 2019, doi: 10.1016/j.diii.2019.08.005.

[37] T. M. Kolb, J. Lichy, and J. H. Newhouse, "Comparison of the Performance of Screening Mammography, Physical Examination, and Breast US and Evaluation of Factors that Influence Them: An Analysis of 27,825 Patient Evaluations," *Radiology*, vol. 225, no. 1, pp. 165–175, Oct. 2002, doi: 10.1148/radiol.2251011667.

[38] M. T. Mandelson *et al.*, "Breast density as a predictor of mammographic detection: Comparison of interval- and screen-detected cancers," *J. Natl. Cancer Inst.*, vol. 92, no. 13, pp. 1081–1087, 2000, doi: 10.1093/jnci/92.13.1081.

[39] K. C. Siang and C. K. M. John, "A review of lung cancer research in Malaysia," *Medical Journal of Malaysia*, vol. 71. pp. 70–78, 2016.

[40] J. H. Sumkin *et al.*, "Optimal Reference Mammography: A Comparison of

Mammograms Obtained 1 and 2 Years Before the Present Examination," *Am. J. Roentgenol.*, vol. 180, no. 2, pp. 343–346, Feb. 2003, doi: 10.2214/ajr.180.2.1800343.

[41] M. Gelig Thurfjell, B. Vitak, E. Azavedo, G. Svane, and E. Thurfjell, "Effect on Sensitivity and Specificity of Mammography Screening With or Without Comparison of Old Mammograms," *Acta radiol.*, vol. 41, no. 1, pp. 52–56, Jan. 2000, doi: 10.1034/j.1600-0455.2000.041001052.x.

[42] A. A. J. Roelofs *et al.*, "Importance of Comparison of Current and Prior Mammograms in Breast Cancer Screening," *Radiology*, vol. 242, no. 1, pp. 70–77, Jan. 2007, doi: 10.1148/radiol.2421050684.

[43] C. Varela, N. Karssemeijer, J. H. C. L. Hendriks, and R. Holland, "Use of Prior Mammograms In the Classification of Benign and Malignant Masses," *Eur. J. Radiol.*, vol. 56, no. 2, pp. 248–255, Nov. 2005, doi: 10.1016/j.ejrad.2005.04.007.

[44] M. A. Helvie, "Digital Mammography Imaging: Breast Tomosynthesis and Advanced Applications," *Radiologic Clinics of North America*, vol. 48, no. 5. Radiol Clin North Am, pp. 917–929, Sep. 2010, doi: 10.1016/j.rcl.2010.06.009.

[45] H. C. R. de Oliveira *et al.*, "A Cross-Cutting Approach for Tracking Architectural Distortion Loci on Digital Breast Tomosynthesis Slices," *Biomed. Signal Process. Control*, vol. 50, pp. 92–102, Apr. 2019, doi: 10.1016/j.bspc.2019.01.001.

[46] A. Rodriguez-Ruiz *et al.*, "New Reconstruction Algorithm for Digital Breast Tomosynthesis: Better Image Quality for Humans and Computers," *Acta radiol.*, vol. 59, no. 9, pp. 1051–1059, 2018, doi: 10.1177/0284185117748487.

[47] S. M. Friedewald *et al.*, "Breast Cancer Screening Using Tomosynthesis in Combination With Digital Mammography," *JAMA Netw. Open*, vol. 311, no. 24, p. 2499, Jun. 2014, doi: 10.1001/jama.2014.6095.

[48] E. A. Rafferty *et al.*, "Assessing Radiologist Performance Using Combined Digital Mammography and Breast Tomosynthesis Compared with Digital Mammography Alone: Results of a Multicenter, Multireader Trial," *Radiology*, vol. 266, no. 1, pp. 104–113, Jan. 2013, doi: 10.1148/radiol.12120674.

[49] H. N. Şendur *et al.*, "Accuracy in Tumor Size Measurements: Comparison of Digital Mammography, Digital Breast Tomosynthesis and Synthetic Mammography," *Clin. Imaging*, vol. 69, no. July 2020, pp. 115–119, Jan. 2021,

doi: 10.1016/j.clinimag.2020.07.004.

[50] P. Skaane *et al.*, “Comparison of Digital Mammography Alone and Digital Mammography Plus Tomosynthesis in a Population-based Screening Program,” *Radiology*, vol. 267, no. 1, pp. 47–56, Apr. 2013, doi: 10.1148/radiol.12121373.

[51] American College of Radiology - ACR, “BI-RADS® ACR Breast Imaging Reporting and Data System.,” *American College of Radiology - ACR*, 2016. https://www.acr.org/Clinical-Resources/Clinical-Tools-and-Reference/Reporting-and-Data-Systems/BI-RADS (accessed Jan. 26, 2026).

[52] D. Bernardi *et al.*, “Breast Cancer Screening with Tomosynthesis (3D Mammography) with Acquired or Synthetic 2D Mammography Compared with 2D Mammography Alone (STORM-2): A Population-Based Prospective Study,” *Lancet Oncol.*, vol. 17, no. 8, pp. 1105–1113, Aug. 2016, doi: 10.1016/S1470-2045(16)30101-2.

[53] M. Gao, J. A. Fessler, and H.-P. Chan, “X-Ray Source Motion Blur Modelling and Deblurring with Generative Diffusion for Digital Breast Tomosynthesis,” *Phys. Med. Biol.*, vol. 69, no. 11, p. 115003, Jun. 2024, doi: 10.1088/1361-6560/ad40f8.

[54] N. Tirada *et al.*, “Digital Breast Tomosynthesis: Physics, Artifacts, and Quality Control Considerations,” *RadioGraphics*, vol. 39, no. 2, pp. 413–426, Mar. 2019, doi: 10.1148/rg.2019180046.

[55] A. Tagliafico and N. Houssami, “Digital Breast Tomosynthesis Might Not Be the Optimal Modality for Detecting Microcalcification,” *Radiology*, vol. 275, no. 2, pp. 618–619, May 2015, doi: 10.1148/radiol.2015142752.

[56] S. Kulkarni, V. Freitas, and D. Muradali, “Digital Breast Tomosynthesis: Potential Benefits in Routine Clinical Practice,” *Canadian Association of Radiologists Journal*, vol. 73, no. 1. SAGE Publications Inc., pp. 107–120, Feb. 01, 2022, doi: 10.1177/08465371211025229.

[57] D. Gur *et al.*, “Dose Reduction in Digital Breast Tomosynthesis (DBT) Screening using Synthetically Reconstructed Projection Images. An Observer Performance Study.,” *Acad. Radiol.*, vol. 19, no. 2, pp. 166–171, Feb. 2012, doi: 10.1016/j.acra.2011.10.003.

[58] M. L. Zuley *et al.*, “Digital breast tomosynthesis versus supplemental diagnostic mammographic views for evaluation of noncalcified breast lesions,” *Radiology*, vol. 266, no. 1, pp. 89–95, Jan. 2013, doi: 10.1148/radiol.12120552.

[59] I. Sechopoulos, *A review of breast tomosynthesis. Part I. The image acquisition process*, vol. 40, no. 1. John Wiley and Sons Ltd, 2013.

[60] Z. Wang *et al.*, "Breast Cancer Detection Using Extreme Learning Machine Based on Feature Fusion With CNN Deep Features," *IEEE Access*, vol. 7, pp. 105146–105158, 2019, doi: 10.1109/ACCESS.2019.2892795.

[61] D. Bernardi *et al.*, "Effect of Integrating 3D-Mammography (Digital Breast Tomosynthesis) with 2D-Mammography on Radiologists' True-Positive and False-Positive Detection in a Population Breast Screening Trial," *Eur. J. Cancer*, vol. 50, no. 7, pp. 1232–1238, May 2014, doi: 10.1016/j.ejca.2014.02.004.

[62] J. Wang, X. Yang, H. Cai, W. Tan, C. Jin, and L. Li, "Discrimination of Breast Cancer with Microcalcifications on Mammography by Deep Learning," *Sci. Rep.*, vol. 6, no. 1, p. 27327, Jun. 2016, doi: 10.1038/srep27327.

[63] K. J. Geras *et al.*, "High-Resolution Breast Cancer Screening with Multi-View Deep Convolutional Neural Networks," Mar. 2017, Accessed: May 13, 2025. [Online]. Available: https://arxiv.org/pdf/1703.07047.

[64] H. E. H. H. Kim *et al.*, "Changes in cancer detection and false-positive recall in mammography using artificial intelligence: a retrospective, multireader study," *Lancet Digit. Heal.*, vol. 2, no. 3, pp. e138–e148, Mar. 2020, doi: 10.1016/S2589-7500(20)30003-0.

[65] B. Xiao *et al.*, "Classification Of Microcalcification Clusters In Digital Breast Tomosynthesis Using Ensemble Convolutional Neural Network," *Biomed. Eng. Online*, vol. 20, no. 1, 2021, doi: 10.1186/s12938-021-00908-1.

[66] M. S. Hossain, "Microcalcification Segmentation Using Modified U-net Segmentation Network from Mammogram Images," *J. King Saud Univ. - Comput. Inf. Sci.*, vol. 34, no. 2, pp. 86–94, Feb. 2022, doi: 10.1016/j.jksuci.2019.10.014.

[67] N. Wu *et al.*, "Deep Neural Networks Improve Radiologists' Performance in Breast Cancer Screening," *IEEE Trans. Med. Imaging*, vol. 39, no. 4, pp. 1184–1194, Apr. 2020, doi: 10.1109/TMI.2019.2945514.

[68] C. Wu, Y. Wo, G. Han, Z. Wu, and J. Liang, "Non-uniform image blind deblurring by twostage fully convolution network," *IET Image Process.*, vol. 14, no. 11, pp. 2588–2596, Sep. 2020, doi: 10.1049/iet-ipr.2018.5716.

[69] K. Kim *et al.*, "A blind-deblurring method based on a compressed-sensing scheme in digital breast tomosynthesis," *Opt. Lasers Eng.*, vol. 110, no. January,

pp. 228–235, 2018, doi: 10.1016/j.optlaseng.2018.06.011.

[70] R. Ricciardi *et al.*, "Physica Medica A deep learning classifier for digital breast tomosynthesis," *Phys. Medica*, vol. 83, no. February, pp. 184–193, 2021, doi: 10.1016/j.ejmp.2021.03.021.

[71] Y. Zhang, X. Wang, H. Blanton, G. Liang, X. Xing, and N. Jacobs, "2D Convolutional Neural Networks for 3D Digital Breast Tomosynthesis Classification," *arXiv*, pp. 1013–1017, 2020.

[72] K. Mendel, H. Li, D. Sheth, and M. Giger, "Transfer Learning From Convolutional Neural Networks for Computer-Aided Diagnosis: A Comparison of Digital Breast Tomosynthesis and Full-Field Digital Mammography," *Acad. Radiol.*, vol. 26, no. 6, pp. 735–743, Jun. 2019, doi: 10.1016/j.acra.2018.06.019.

[73] M. Yousefi, A. Krzyżak, and C. Y. Suen, "Mass detection in digital breast tomosynthesis data using convolutional neural networks and multiple instance learning," *Comput. Biol. Med.*, vol. 96, no. February, pp. 283–293, 2018, doi: 10.1016/j.compbiomed.2018.04.004.

[74] J. Y. Yeh and S. Chan, "CNN-based CAD for breast cancer classification in digital breast tomosynthesis," in *ACM International Conference Proceeding Series*, 2018, pp. 26–30, doi: 10.1145/3282286.3282305.

[75] R. K. Samala, H.-P. Chan, L. M. Hadjiiski, M. A. Helvie, C. Richter, and K. Cha, "Evolutionary Pruning of Transfer Learned Deep Convolutional Neural Network for Breast Cancer Diagnosis in Digital Breast Tomosynthesis," *Physiol. Behav.*, vol. 176, no. 5, pp. 139–148, 2018, doi: 10.1088/1361-6560/aabb5b.Evolutionary.

[76] D. H. Kim, S. T. Kim, and Y. M. Ro, "Latent Feature Representation with 3-D Multi-View Deep Convolutional Neural Network for Bilateral Analysis in Digital Breast Tomosynthesis," in *2016 IEEE International Conference on Acoustics, Speech and Signal Processing (ICASSP)*, Mar. 2016, vol. 2016-May, pp. 927–931, doi: 10.1109/ICASSP.2016.7471811.

[77] J. Zheng *et al.*, "3D Context-Aware Convolutional Neural Network for False Positive Reduction in Clustered Microcalcifications Detection," *IEEE J. Biomed. Heal. Informatics*, vol. 25, no. 3, pp. 764–773, Mar. 2021, doi: 10.1109/JBHI.2020.3003316.

[78] W. Lotter *et al.*, "Robust breast cancer detection in mammography and digital breast tomosynthesis using an annotation-efficient deep learning approach," *Nat.*

Med., vol. 27, no. 2, pp. 244–249, Feb. 2021, doi: 10.1038/s41591-020-01174-9.

[79] J. Teuwen *et al.*, "Deep Learning Reconstruction of Digital Breast Tomosynthesis Images for Accurate Breast Density and Patient-Specific Radiation Dose Estimation," *Med. Image Anal.*, vol. 71, p. 102061, Jul. 2021, doi: 10.1016/j.media.2021.102061.

[80] and M. P. E. Aditya Jonnalagadda, Miguel A. Lago, Bruno Barufaldi, Predrag R. Bakic, Craig K. Abbey, Andrew D. Maidment, "Evaluation of Convolutional Neural Networks for Search in 1/f 2.8 Filtered Noise and Digital Breast Tomosynthesis Phantoms," *Physiol. Behav.*, vol. 176, no. 1, pp. 139–148, 2020, doi: 10.1117/12.2549362.

[81] T. Su *et al.*, "DIR-DBTnet: Deep iterative reconstruction network for three-dimensional digital breast tomosynthesis imaging," *Med. Phys.*, vol. 48, no. 5, pp. 2289–2300, May 2021, doi: 10.1002/mp.14779.

[82] J. L. Pech-Pacheco, G. Cristöbal, J. Chamorro-Martínez, and J. Fernândez-Valdivia, "Diatom autofocusing in brightfield microscopy: A comparative study," in *Proceedings - International Conference on Pattern Recognition*, 2000, vol. 15, no. 3, pp. 314–317, doi: 10.1109/icpr.2000.903548.

[83] H. Tong, M. Li, H. Zhang, and C. Zhang, "Blur detection for digital images using wavelet transform," *2004 IEEE Int. Conf. Multimed. Expo*, vol. 1, pp. 17–20, 2004, doi: 10.1109/icme.2004.1394114.

[84] R. Wang, W. Li, and L. Zhang, "Blur image identification with ensemble convolution neural networks," *Signal Processing*, vol. 155, pp. 73–82, Feb. 2019, doi: 10.1016/j.sigpro.2018.09.027.

[85] O. Kupyn, V. Budzan, M. Mykhailych, D. Mishkin, and J. Matas, "DeblurGAN: Blind Motion Deblurring Using Conditional Adversarial Networks," in *2018 IEEE/CVF Conference on Computer Vision and Pattern Recognition*, Jun. 2018, pp. 8183–8192, doi: 10.1109/CVPR.2018.00854.

[86] A. Karaali, N. Harte, and C. R. Jung, "Deep Multi-Scale Feature Learning for Defocus Blur Estimation," *IEEE Trans. Image Process.*, vol. 31, pp. 1097–1106, 2022, doi: 10.1109/TIP.2021.3139243.

[87] S. Nowakowska *et al.*, "Technical Feasibility of Automated Blur Detection in Digital Mammography using Convolutional Neural Network," *Eur. Radiol. Exp.*, vol. 8, no. 1, p. 129, Nov. 2024, doi: 10.1186/s41747-024-00527-0.

[88] M. Muhammad Danyal, S. Shah Khan, R. Shah Khan, S. Jan, and N. ur Rahman,

"Enhancing Multi-Modality Medical Imaging: A Novel Approach with Laplacian Filter + Discrete Fourier Transform Pre-Processing and Stationary Wavelet Transform Fusion," *J. Intell. Med. Healthc.*, vol. 2, pp. 35–53, 2024, doi: 10.32604/jimh.2024.051340.

[89] M. Zhu, L. Yu, Z. Wang, Z. Ke, and C. Zhi, "Review: A Survey on Objective Evaluation of Image Sharpness," *Appl. Sci.*, vol. 13, no. 4, pp. 1–20, 2023, doi: 10.3390/app13042652.

[90] Q. Lu and D. Liu, "Research on Edge Detection of Medical Image Based on Wavelet Transform and Fuzzy Algorithm," in *2021 International Wireless Communications and Mobile Computing (IWCMC)*, Jun. 2021, pp. 1025–1029, doi: 10.1109/IWCMC51323.2021.9498955.

[91] R. V. Sonawane and P. K. Sujatha, "CPBD Metric for Blur Detection of a No Reference Image & It ' s Removal," pp. 15515–15521, 2016, doi: 10.15680/IJIRSET.2016.0508153.

[92] A. Shen, H. Dong, K. Wang, Y. Kong, J. Wu, and H. Shu, "Automatic Extraction of Blur Regions on a Single Image Based on Semantic Segmentation," *IEEE Access*, vol. 8, pp. 44867–44878, 2020, doi: 10.1109/ACCESS.2020.2978084.

[93] C. Tang, X. Zhu, X. Liu, L. Wang, and A. Zomaya, "Defusionnet: Defocus blur detection via recurrently fusing and refining multi-scale deep features," *Proc. IEEE Comput. Soc. Conf. Comput. Vis. Pattern Recognit.*, vol. 2019-June, pp. 2695–2704, 2019, doi: 10.1109/CVPR.2019.00281.

[94] R. Huang, H. Lu, Y. Xing, and W. Fan, "Multi-scale Convolutional Feature Approximation for Defocus Blur Detection," *Proc. 2023 26th Int. Conf. Comput. Support. Coop. Work Des. CSCWD 2023*, pp. 1172–1177, 2023, doi: 10.1109/CSCWD57460.2023.10152667.

[95] W. Zhao, B. Zheng, Q. Lin, and H. Lu, "Enhancing diversity of defocus blur detectors via cross-ensemble network," *Proc. IEEE Comput. Soc. Conf. Comput. Vis. Pattern Recognit.*, vol. 2019-June, pp. 8897–8905, 2019, doi: 10.1109/CVPR.2019.00911.

[96] W. Zhao, X. Hou, Y. He, and H. Lu, "Defocus Blur Detection via Boosting Diversity of Deep Ensemble Networks," *IEEE Trans. Image Process.*, vol. 30, pp. 5426–5438, 2021, doi: 10.1109/TIP.2021.3084101.

[97] F. Zhao, H. Lu, W. Zhao, and L. Yao, "Image-Scale-Symmetric Cooperative Network for Defocus Blur Detection," *IEEE Trans. Circuits Syst. Video*

Technol., vol. 32, no. 5, pp. 2719–2731, May 2022, doi: 10.1109/TCSVT.2021.3095347.

[98] C. Tang *et al.*, "DeFusionNET: Defocus Blur Detection via Recurrently Fusing and Refining Discriminative Multi-Scale Deep Features," *IEEE Trans. Pattern Anal. Mach. Intell.*, vol. 44, no. 2, Feb. 2022, doi: 10.1109/TPAMI.2020.3014629.

[99] Z. Jiang, X. Xu, L. Zhang, C. Zhang, C. S. Foo, and C. Zhu, "MA-GANet: A Multi-Attention Generative Adversarial Network for Defocus Blur Detection," *IEEE Trans. Image Process.*, vol. 31, pp. 3494–3508, 2022, doi: 10.1109/TIP.2022.3171424.

[100] J. Park, Y. W. Tai, D. Cho, and I. S. Kweon, "A unified approach of multi-scale deep and hand-crafted features for defocus estimation," *Proc. - 30th IEEE Conf. Comput. Vis. Pattern Recognition, CVPR 2017*, vol. 2017-Janua, pp. 2760–2769, 2017, doi: 10.1109/CVPR.2017.295.

[101] K. Zeng, Y. Wang, J. Mao, J. Liu, W. Peng, and N. Chen, "A Local Metric for Defocus Blur Detection Based on CNN Feature Learning," *IEEE Trans. Image Process.*, vol. 28, no. 5, pp. 2107–2115, Nov. 2018, doi: 10.1109/tip.2018.2881830.

[102] B. Kim, H. Son, S. J. Park, S. Cho, and S. Lee, "Defocus and Motion Blur Detection with Deep Contextual Features," *Comput. Graph. Forum*, vol. 37, no. 7, pp. 277–288, Oct. 2018, doi: 10.1111/cgf.13567.

[103] X. Wang, X. Liang, S. Li, and J. Zheng, "Efficient image blur detection via hierarchical edge guidance and region complementation," *Complex Intell. Syst.*, 2023, doi: 10.1007/s40747-023-01093-5.

[104] T. Szandala, "Convolutional Neural Network for Blur Image Detection as an Alternative for Laplacian Method," *2020 IEEE Symp. Ser. Comput. Intell. SSCI 2020*, pp. 2901–2904, 2020, doi: 10.1109/SSCI47803.2020.9308594.

[105] W. Samek, A. Binder, G. Montavon, S. Lapuschkin, and K. R. Müller, "Evaluating The Visualization Of What A Deep Neural Network Has Learned," *IEEE Trans. Neural Networks Learn. Syst.*, vol. 28, no. 11, pp. 2660–2673, 2017, doi: 10.1109/TNNLS.2016.2599820.

[106] M. Versaci, F. C. Morabito, and G. Angiulli, "Adaptive Image Contrast Enhancement by Computing Distances into a 4-Dimensional Fuzzy Unit Hypercube," *IEEE Access*, vol. 5, pp. 26922–26931, Nov. 2017, doi:

10.1109/ACCESS.2017.2776349.

[107] M. Veluchamy and B. Subramani, “Fuzzy Dissimilarity Color Histogram Equalization For Contrast Enhancement And Color Correction,” *Appl. Soft Comput. J.*, vol. 89, p. 106077, Apr. 2020, doi: 10.1016/j.asoc.2020.106077.

[108] M. Shakeri, M. H. Dezfoulian, H. Khotanlou, A. H. Barati, and Y. Masoumi, “Image Contrast Enhancement Using Fuzzy Clustering With Adaptive Cluster Parameter And Sub-Histogram Equalization,” *Digit. Signal Process.*, vol. 62, pp. 224–237, Mar. 2017, doi: 10.1016/J.DSP.2016.10.013.

[109] T. Zhang *et al.*, “A Feature Fusion Method with Guided Training for Classification Tasks,” *Comput. Intell. Neurosci.*, vol. 2021, 2021.

[110] M. O. Khairandish, M. Sharma, V. Jain, J. M. Chatterjee, and N. Z. Jhanjhi, “A Hybrid CNN-SVM Threshold Segmentation Approach for Tumor Detection and Classification of MRI Brain Images,” *Irbm*, vol. 43, no. 4, pp. 290–299, 2022, doi: 10.1016/j.irbm.2021.06.003.

[111] N. Houssami and P. Skaane, “Overview of the evidence on digital breast tomosynthesis in breast cancer detection,” *The Breast*, vol. 22, no. 2, pp. 101–108, Apr. 2013, doi: 10.1016/J.BREAST.2013.01.017.

[112] D. Bernardi *et al.*, “Effect of implementing digital breast tomosynthesis (DBT) instead of mammography on population screening outcomes including interval cancer rates: Results of the Trento DBT pilot evaluation,” *Breast*, vol. 50, pp. 135–140, 2020, doi: 10.1016/j.breast.2019.09.012.

[113] Y. S. Leong, K. Hasikin, K. W. Lai, N. Mohd Zain, and M. M. Azizan, “Microcalcification Discrimination in Mammography Using Deep Convolutional Neural Network: Towards Rapid and Early Breast Cancer Diagnosis,” *Front. Public Heal.*, vol. 10, p. 875305, Apr. 2022, doi: 10.3389/fpubh.2022.875305.

[114] A. K. Mohideen and K. Thangavel, “Contrast enhancement of digital mammograms using a novel walking ant histogram equalisation,” *Int. J. Comput. Vis. Robot.*, vol. 5, no. 2, pp. 181–201, Jan. 2015, doi: 10.1504/IJCVR.2015.068796.

[115] E. D. Pisano *et al.*, “Contrast Limited Adaptive Histogram Equalization Image Processing To Improve The Detection Of Simulated Spiculations In Dense Mammograms,” *J. Digit. Imaging*, vol. 11, no. 4, pp. 193–200, 1998, doi: 10.1007/BF03178082.

[116] H. Avcı and J. Karakaya, “A Novel Medical Image Enhancement Algorithm for Breast Cancer Detection on Mammography Images Using Machine Learning,” *Diagnostics*, vol. 13, no. 3, p. 348, Feb. 2023, doi: 10.3390/diagnostics13030348.

[117] K. K. Kavitha and A. Kangaiammal, “Contrast Enhancement of Digital Mammograms Based on High Contrast-Limited Adaptive Histogram Equalisation,” in *EAI/Springer Innovations in Communication and Computing*, vol. Part F274, Springer Science and Business Media Deutschland GmbH, 2023, pp. 279–287.

[118] N. Singh, J. Marak, P. Joshi, and D. K. Singh, “Morphological and Distribution Pattern of Calcifications on Full Field Digital Mammography versus Digital Breast Tomosynthesis and Comparison of Diagnostic Abilities of the Two Modalities: A Retrospective Study,” *J. Clin. DIAGNOSTIC Res.*, 2023, doi: 10.7860/jcdr/2023/55632.17675.

[119] M. Sghaier, E. Chouzenoux, J. C. Pesquet, and S. Muller, “A Novel Task-Based reconstruction approach for digital breast tomosynthesis,” *Med. Image Anal.*, vol. 77, Apr. 2022, doi: 10.1016/j.media.2021.102341.

[120] J. Wang *et al.*, “CAPNet: Context attention pyramid network for computer-aided detection of microcalcification clusters in digital breast tomosynthesis,” *Comput. Methods Programs Biomed.*, vol. 242, p. 107831, Dec. 2023, doi: 10.1016/j.cmpb.2023.107831.

[121] J. Ouyang, S. Liu, H. Peng, H. Garg, and D. N. H. Thanh, “LEA U-Net: a U-Net-based deep learning framework with local feature enhancement and attention for retinal vessel segmentation,” *Complex Intell. Syst.*, vol. 9, no. 6, pp. 6753–6766, Dec. 2023, doi: 10.1007/s40747-023-01095-3.

[122] Z. Lian and H. Wang, “An image deblurring method using improved U-Net model based on multilayer fusion and attention mechanism,” *Sci. Rep.*, vol. 13, no. 1, p. 21402, Dec. 2023, doi: 10.1038/s41598-023-47768-4.

[123] Y. Jiménez-Gaona, D. Carrión-Figueroa, V. Lakshminarayanan, and M. José Rodríguez-Álvarez, “Gan-based data augmentation to improve breast ultrasound and mammography mass classification,” *Biomed. Signal Process. Control*, vol. 94, p. 106255, Aug. 2024, doi: 10.1016/j.bspc.2024.106255.

[124] H. P. Chan *et al.*, “Deep learning denoising of digital breast tomosynthesis: Observer performance study of the effect on detection of microcalcifications in breast phantom images,” *Med. Phys.*, vol. 50, no. 10, pp. 6177–6189, Oct. 2023,

doi: 10.1002/mp.16439.

[125] T. Gomi, H. Hara, Y. Watanabe, and S. Mizukami, “Improved digital chest tomosynthesis image quality by use of a projection-based dual-energy virtual monochromatic convolutional neural network with super resolution,” *PLoS One*, vol. 15, no. 12, December, pp. 1–24, 2020, doi: 10.1371/journal.pone.0244745.

[126] M. Buda *et al.*, “A Data Set and Deep Learning Algorithm for the Detection of Masses and Architectural Distortions in Digital Breast Tomosynthesis Images,” *JAMA Netw. Open*, vol. 4, no. 8, p. e2119100, Aug. 2021, doi: 10.1001/jamanetworkopen.2021.19100.

[127] Y. Brima and M. Atemkeng, “Saliency-driven explainable deep learning in medical imaging: bridging visual explainability and statistical quantitative analysis,” *BioData Min.*, vol. 17, no. 1, p. 18, Jun. 2024, doi: 10.1186/s13040-024-00370-4.

[128] V. R. Joseph, “Optimal ratio for data splitting,” *Stat. Anal. Data Min.*, vol. 15, no. 4, pp. 531–538, Aug. 2022, doi: 10.1002/sam.11583.

[129] R. Bansal, G. Raj, and T. Choudhury, “Blur image detection using Laplacian operator and Open-CV,” in *2016 International Conference System Modelling & Advancement in Research Trends (SMART)*, 2016, pp. 63–67, doi: 10.1109/SYSMART.2016.7894491.

[130] G. T. Shrivakshan and C. Chandrasekar, “A Comparison of various Edge Detection Techniques used in Image Processing,” *Int. J. Comput. Sci. Issues*, vol. 9, no. 5, pp. 269–276, 2012, Accessed: Nov. 16, 2021. [Online]. Available: www.IJCSI.org.

[131] C. Szegedy *et al.*, “Going deeper with convolutions,” in *Proceedings of the IEEE Computer Society Conference on Computer Vision and Pattern Recognition*, Oct. 2015, vol. 07-12-June, pp. 1–9, doi: 10.1109/CVPR.2015.7298594.

[132] K. He, X. Zhang, S. Ren, and J. Sun, “Deep residual learning for image recognition,” in *Proceedings of the IEEE Computer Society Conference on Computer Vision and Pattern Recognition*, 2016, vol. 2016-Decem, pp. 770–778, doi: 10.1109/CVPR.2016.90.

[133] K. Simonyan and A. Zisserman, “Very deep convolutional networks for large-scale image recognition,” Sep. 2015, Accessed: Jan. 11, 2022. [Online]. Available: https://arxiv.org/abs/1409.1556v6.

[134] A. G. Howard *et al.*, “MobileNets: Efficient Convolutional Neural Networks for

Mobile Vision Applications," Apr. 2017, Accessed: Aug. 19, 2025. [Online]. Available: https://arxiv.org/pdf/1704.04861.

[135] M. Sandler, A. Howard, M. Zhu, A. Zhmoginov, and L. C. Chen, "MobileNetV2: Inverted Residuals and Linear Bottlenecks," *Proc. IEEE Comput. Soc. Conf. Comput. Vis. Pattern Recognit.*, pp. 4510–4520, Dec. 2018, doi: 10.1109/CVPR.2018.00474.

[136] M. A. Islam, M. Kowal, S. Jia, K. G. Derpanis, and N. D. B. Bruce, "Position, Padding and Predictions: A Deeper Look at Position Information in CNNs," *Int. J. Comput. Vis.*, vol. 132, no. 9, pp. 3889–3910, Jan. 2021, doi: 10.1007/s11263-024-02069-9.

[137] S. Ioffe and C. Szegedy, "Batch Normalization: Accelerating Deep Network Training By Reducing Internal Covariate Shift," in *32nd International Conference on Machine Learning, ICML 2015*, Feb. 2015, vol. 1, pp. 448–456, Accessed: May 23, 2023. [Online]. Available: https://arxiv.org/abs/1502.03167v3.

[138] V. Nair and G. E. Hinton, "Rectified linear units improve Restricted Boltzmann machines," *ICML 2010 - Proceedings, 27th Int. Conf. Mach. Learn.*, no. 3, pp. 807–814, 2010.

[139] Y. Liu, Y. Gao, and W. Yin, "An Improved Analysis of Stochastic Gradient Descent with Momentum," *Adv. Neural Inf. Process. Syst.*, vol. 2020-December, Jul. 2020, Accessed: Aug. 19, 2025. [Online]. Available: https://arxiv.org/pdf/2007.07989.

[140] J. Fu, B. Wang, H. Zhang, Z. Zhang, W. Chen, and N. Zheng, "When and Why Momentum Accelerates SGD:An Empirical Study," Jun. 2023, Accessed: Aug. 19, 2025. [Online]. Available: https://arxiv.org/pdf/2306.09000.

[141] K. Tang, W. Liu, Y. Zhang, and X. Chen, "Acceleration Of Stochastic Gradient Descent With Momentum By Averaging: Finite-Sample Rates And Asymptotic Normality," May 2023, Accessed: Aug. 19, 2025. [Online]. Available: https://arxiv.org/pdf/2305.17665.

[142] D. P. Kingma and J. L. Ba, "Adam: A Method For Stochastic Optimization," *3rd Int. Conf. Learn. Represent. ICLR 2015 - Conf. Track Proc.*, pp. 1–15, Dec. 2015, Accessed: May 23, 2023. [Online]. Available: https://arxiv.org/abs/1412.6980v9.

[143] V. N. Vapnik, "An overview of statistical learning theory," *IEEE Transactions*

on Neural Networks, vol. 10, no. 5. pp. 988–999, 1999, doi: 10.1109/72.788640.

[144] C. A. Santos and D. Welfer, "A Novel Hybrid SVM-CNN Method for Extracting Characteristics and Classifying Cattle Branding," *Lat. Am. J. Comput.*, vol. VI, no. 1, pp. 9–16, 2019, [Online]. Available: https://lajc.epn.edu.ec/index.php/LAJC/article/view/157.

[145] D.-X. X. Xue, R. Zhang, H. Feng, Y.-L. L. Wang, • Hui Feng, and Y.-L. L. Wang, "CNN-SVM for Microvascular Morphological Type Recognition with Data Augmentation," *J. Med. Biol. Eng.*, vol. 36, no. 6, pp. 755–764, 2016, doi: 10.1007/s40846-016-0182-4.

[146] M. Piergentili, D. Zefiro, F. Ielo, F. Foppiano, and P. Boccacci, "256. Synthesized 2D image reconstruction from Digital Breast Tomosynthesis (DBT)," *Phys. Medica*, vol. 56, no. August, p. 220, 2018, doi: 10.1016/j.ejmp.2018.04.267.

[147] C. Szegedy, V. Vanhoucke, S. Ioffe, J. Shlens, and Z. Wojna, "Rethinking the Inception Architecture for Computer Vision," in *Proceedings of the IEEE Computer Society Conference on Computer Vision and Pattern Recognition*, 2016, vol. 2016-Decem, pp. 2818–2826, doi: 10.1109/CVPR.2016.308.

[148] J. Kim, J. K. Lee, and K. M. Lee, "Accurate Image Super-Resolution Using Very Deep Convolutional Networks," in *2016 IEEE Conference on Computer Vision and Pattern Recognition (CVPR)*, Jun. 2016, vol. 2016-Decem, pp. 1646–1654, doi: 10.1109/CVPR.2016.182.

[149] H. T. Mustafa, J. Yang, and M. Zareapoor, "Multi-scale convolutional neural network for multi-focus image fusion," *Image Vis. Comput.*, vol. 85, pp. 26–35, May 2019, doi: 10.1016/j.imavis.2019.03.001.

[150] S. S. Khan, M. Khan, Y. Alharbi, U. Haider, K. Ullah, and S. Haider, "Hybrid Sharpening Transformation Approach for Multifocus Image Fusion Using Medical and Nonmedical Images," *J. Healthc. Eng.*, vol. 2021, no. 1, p. 7000991, Jan. 2021, doi: 10.1155/2021/7000991.

[151] B. Kurt, V. V. Nabiyev, and K. Turhan, "Comparison of Enhancement Methods for Mammograms with Performance Measures," *Stud. Health Technol. Inform.*, vol. 205, pp. 486–490, 2014, doi: 10.3233/978-1-61499-432-9-486.

[152] K. Munadi, K. Muchtar, N. Maulina, and B. Pradhan, "Image Enhancement for Tuberculosis Detection Using Deep Learning," *IEEE Access*, vol. 8, pp. 217897–217907, 2020, doi: 10.1109/ACCESS.2020.3041867.

[153] P. Teare, M. Fishman, O. Benzaquen, E. Toledano, and E. Elnekave, “Malignancy Detection on Mammography Using Dual Deep Convolutional Neural Networks and Genetically Discovered False Color Input Enhancement,” *J. Digit. Imaging*, vol. 30, no. 4, pp. 499–505, 2017, doi: 10.1007/s10278-017-9993-2.

[154] Erwin and D. R. Ningsih, “Improving Retinal Image Quality Using the Contrast Stretching, Histogram Equalization, and CLAHE Methods with Median Filters,” *Int. J. Image, Graph. Signal Process.*, vol. 12, no. 2, pp. 30–41, Apr. 2020, doi: 10.5815/ijigsp.2020.02.04.

APPENDICES

APPENDIX 1

Ethical Approval and Ethical Extension Approval

Jawatankuasa Etika
Penyelidikan Manusia USM (JEPeM)

Human Research Ethics Committee USM (HREC)

Universiti Sains Malaysia
Kampus Kesihatan
16150 Kubang Kerian, Kelantan, Malaysia.
Tel. : +609 - 767 3000/2354/2362
Fax. : + 609 - 767 2351
Email : jepem@usm.my
Laman Web : www.jepem.kk.usm.my
www.usm.my

13th December 2021

Assoc. Prof. Ir. Ts. Dr. Siti Noraini Sulaiman
School of Electrical Engineering
Universiti Teknologi Mara Cawangan Pulau Pinang
Kampus Permatang Pauh
13500 Permatang Pauh, Pulau Pinang

JEPeM Code : USM/JEPeM/21090622
Protocol Title : A New Cascaded Convolutional Neural Network Model for Deblurring and Contrast Enhancement of Extremely Dense Breast Tissue in Digital Breast Tomosynthesis Images

Dear Dr. Siti Noraini,

We wish to inform you that your study protocol has been reviewed and is hereby granted approval for implementation by the Jawatankuasa Etika Penyelidikan Manusia Universiti Sains Malaysia (JEPeM-USM). Your study has been assigned study protocol code **USM/JEPeM/21090622,** which should be used for all communications to JEPeM-USM in relation to this study. This ethical approval is valid from **13th December 2021** until **12th December 2022.**

Study Site: Advanced Medical and Dental Institute, Kepala Batas (Pulau Pinang) and Universiti Teknologi MARA (Pulau Pinang)

The following researchers are also involved in this study:

1. Ir. Dr. Iza Sazanita Isa
2. Dr. Muhammad Khusairi Osman
3. Dr. Noor Khairiah A. Karim
4. Mdm. Nur Athiqah Harron
5. Mr. Mohd Ikmal Fitri Maruzuki

The following document has been approved for use in the study:

1. Research Proposal

In addition to the abovementioned document, the following document was included in the review on which this approval is based:

1. Data Collection Sheet

While the study is in progress, we request that you submit to us the following documents:

1. Application for renewal of ethical approval 60 days before the expiration date of this approval through submission of **JEPeM-USM FORM 3(B) 2019: Continuing Review Application Form.**
2. Any changes in the protocol, especially those that may adversely affect the safety of the participants during the conduct of the trial including changes in personnel, must be submitted or reported using **JEPeM-USM FORM 3(A) 2019: Study Protocol Amendment Submission Form.**
3. Revisions in the informed consent form using the **JEPeM-USM FORM 3(A) 2019: Study Protocol Amendment Submission Form.**

JEPeM
JAWATANKUASA ETIKA PENYELIDIKAN MANUSIA

4. Reports of adverse events including from other study sites (national, international) using the **JEPeM-USM FORM 3(G) 2019: Adverse Events Report.**
5. Notice of early termination of the study and reasons for such using **JEPeM-USM FORM 3(E) 2019.**
6. Any event which may have ethical significance.
7. Any information which is needed by the JEPeM-USM to do ongoing review.
8. Notice of time of completion of the study using **JEPeM-USM FORM 3(C) 2019: Final Report Form.**

Please note that forms may be downloaded from the JEPeM-USM website:
www.jepem.kk.usm.my

JEPeM-USM is in compliance with the Declaration of Helsinki, International Conference on Harmonization (ICH) Guidelines, Good Clinical Practice (GCP) Standards, Council for International Organizations of Medical Sciences (CIOMS) Guidelines, World Health Organization (WHO) Standards and Operational Guidance for Ethics Review of Health-Related Research and Surveying and Evaluating Ethical Review Practices, EC/IRB Standard Operating Procedures (SOPs), and Local Regulations and Standards in Ethical Review.

Thank you.

"WAWASAN KEMAKMURAN BERSAMA 2030"

"BERKHIDMAT UNTUK NEGARA"

Sincerely,

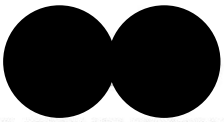

ASSOC. PROF. DR. KHAIRIAH @ SALWA MOKHTAR
Deputy Chairperson
Jawatankuasa Etika Penyelidikan (Manusia) JEPeM
Universiti Sains Malaysia

Jawatankuasa Etika
Penyelidikan Manusia USM (JEPeM)

Human Research Ethics Committee USM (HREC)

Universiti Sains Malaysia
Kampus Kesihatan
16150 Kubang Kerian, Kelantan, Malaysia.
Tel. : +609 - 767 3000/2354/2362
Fax. : + 609 - 767 2351
Email : jepem@usm.my
Laman Web : www.jepem.kk.usm.my
www.usm.my

22nd December 2023

Assoc. Prof. Ir. Ts. Dr. Siti Noraini Sulaiman
School of Electrical Engineering
Universiti Teknologi Mara Cawangan Pulau Pinang
Kampus Permatang Pauh
13500 Permatang Pauh, Pulau Pinang

JEPeM USM Code: USM/JEPeM/21090622
Study Protocol Title: A New Cascaded Convolutional Neural Network Model for Deblurring and Contrast Enhancement of Extremely Dense Breast Tissue in Digital Breast Tomosynthesis Images

Dear Assoc. Prof. Ir. Ts. Dr. Siti Noraini,

We wish to inform you that the Jawatankuasa Etika Penyelidikan Manusia, Universiti Sains Malaysia (JEPeM-USM) acknowledged receipt of the Continuing Review Application dated 13th December 2023.

Upon review of JEPeM-USM Form 3(B) 2021: Continuing Review Application Form, the committee **AGREED** for the **EXTENSION OF APPROVAL (commencing from 5th February 2024 to 4th February 2025)**. The document is included in the protocol file.

Thank you for your continuing compliance with the requirements of JEPeM-USM.

"MALAYSIA MADANI"

"BERKHIDMAT UNTUK NEGARA"

Sincerely,

[redacted]

ASSOC. PROF. DR. HASLINA HAROON
Deputy Chairperson
Jawatankuasa Etika Penyelidikan (Manusia), JEPeM
Universiti Sains Malaysia

c.c Secretary
Jawatankuasa Etika Penyelidikan (Manusia), JEPeM
Universiti Sains Malaysia

APPENDIX 2

Flowchart for Applying JEPeM USM Ethical Approval

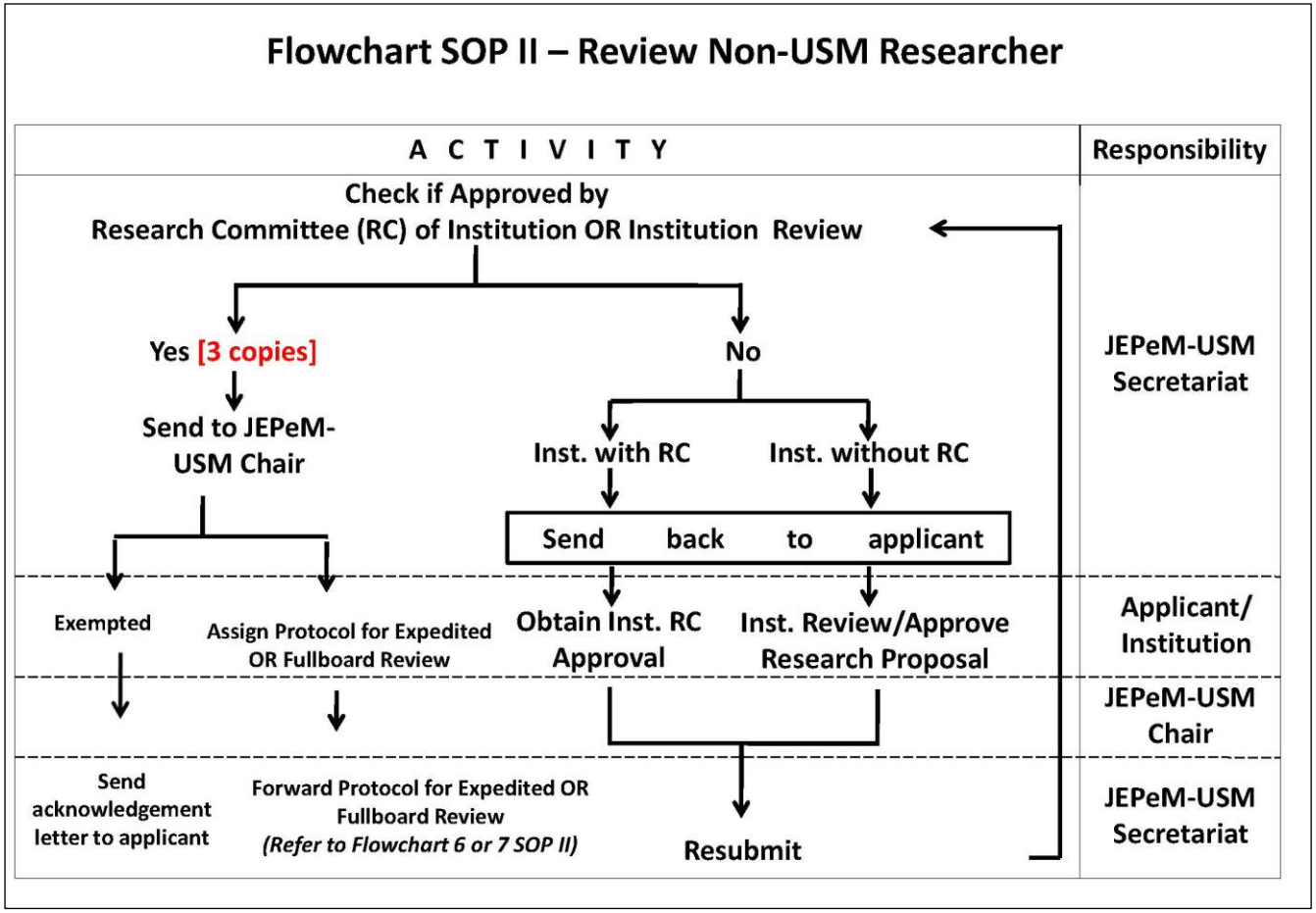

APPENDIX 3

Expert Evaluation Form for Enhancement of Digital Breast Tomosynthesis Images Using CNN

Expert Evaluation Form for Enhancement of Digital Breast Tomosynthesis Images Using CNN

Assalamualaikum and Hello, Prof./Dr./Sir/Madam,

My name is Nur Athiqah Harron, and I am a PhD student in Electrical Engineering at Universiti Teknologi MARA (UiTM), Permatang Pauh Campus. I am reaching out to seek your valuable assistance as a medical imaging expert, radiologist, or image processing specialist in responding to the Expert Evaluation Form for Digital Breast Tomosynthesis (DBT) Image Enhancement Systems.

This Expert Evaluation Form analyzes expert/manual/visual clinical diagnosis evaluation of enhanced DBT images based on radiologist/expert selection. Your responses will be used to assess the image enhancement model developed in this study. The evaluation form consists of:

1. Assessor Demographic Information.
2. Three Evaluation Sections (A, B, and C) – Each section contains 10 to 20 images for assessment.
3. Section D – Specific to radiologists/medical experts, providing opinions on the proposed Computer-Aided Diagnosis (CAD) system.

Your feedback is highly valuable for advancing research in CAD-based breast cancer screening, helping to refine techniques for DBT image enhancement. We truly appreciate your time and effort in completing this evaluation.

📌 Important Notes:
✅ Please take your time to carefully evaluate each image within the given timeframe.
✅ Your responses will remain strictly private and confidential and will only be used for research purposes.
✅ Kindly refrain from discussing your assessment with other radiologists to maintain the integrity of individual evaluations.

We sincerely appreciate your expertise and feedback and thank you for your time and valuable contribution to this study. 🙏

Best regards,
Nur Athiqah Harron
PhD Candidate,
Universiti Teknologi MARA (UiTM)

Assessor Demographic Information

1

Name

2

Email *

3

Occupation *

- ◯ Radiologist
- ◯ Medical Dr.
- ◯ Biomedical Engineering Expert
- ◯ Image Processing Expert
- ◯ Radiographer

4

Year of Expertise *

Section A : Evaluation of Image Selection in Digital Breast Tomosynthesis (DBT)

DBT produces a series of cross-sectional images over a range of angles known as projection images in limited angular range, which produces image blurring in the reconstructed images. The unwanted artefacts can severely shroud the cancer region, especially in extremely dense fibroglandular breast tissue. These issues degrade diagnostic accuracy. Conventionally, DBT images are scanned slice by slice, which brings a huge workload to radiologists. Marking abnormalities on DBT slices requires experienced radiologists to review each frame from the DBT z-Stacks and identify tumor locations, which is extremely time-consuming considering the number of slices per DBT scanning [15].

This section aims to evaluate expert preferences in image selection to determine which images are most suitable for further cancer diagnosis. Expert feedback will help refine the research objective of detecting and eliminating blurred DBT slices that are unnecessary for diagnosis, thereby reducing the data volume and improving efficiency.

Each question in this section presents two slices from the same DBT volume. One image is considered more suitable than the other for cancer diagnosis. Please select the image that, based on your visual assessment, is clearer and more useful for further diagnosis.

5

1. Choose the better image based on your preferences for further diagnosis. *

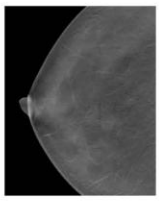

◯ Option 1

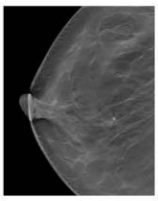

◯ Option 2

6

2. Choose the better image based on your preferences. *

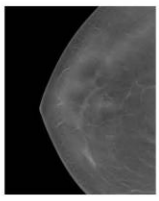

◯ Option 1

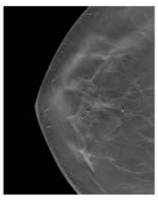

◯ Option 2

7

3. Choose the better image based on your preferences. *

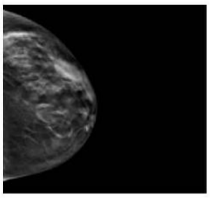

◯ Option 1

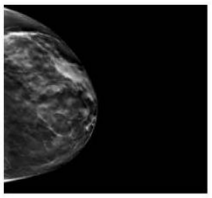

◯ Option 2

8

4. Choose the better image based on your preferences. *

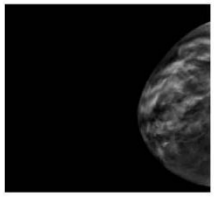

◯ Option 1

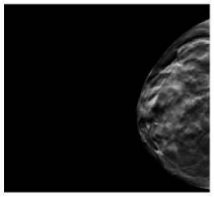

◯ Option 2

9

5. Choose the better image based on your preferences. *

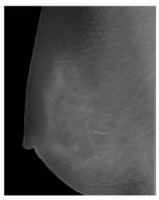

◯ Option 1

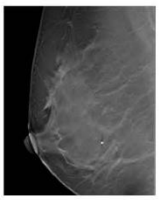

◯ Option 2

10

6. Choose the better image based on your preferences. *

◯ Option 1

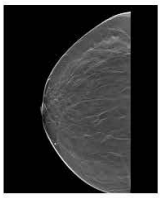

◯ Option 2

11

7. Choose the better image based on your preferences. *

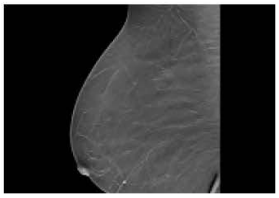

◯ Option 1

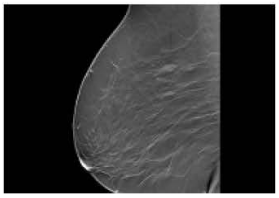

◯ Option 2

12

8. Choose the better image based on your preferences. *

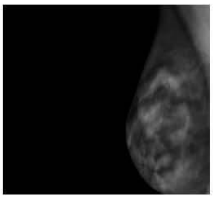

◯ Option 1

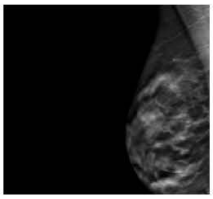

◯ Option 2

13

9. Choose the better image based on your preferences. *

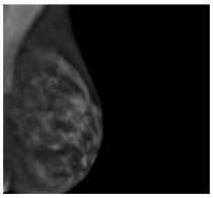

◯ Option 1

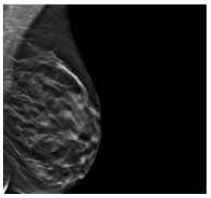

◯ Option 2

14

10. Choose the better image based on your preferences. *

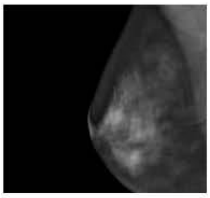

◯ Option 1

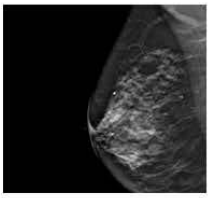

◯ Option 2

Section B : Blur Detection in Digital Breast Tomosynthesis (DBT)

In clinical diagnosis, radiologists typically ignore blurred slices and focus directly on clear, non-blurred images. Therefore, blur detection should be a crucial preprocessing step before image restoration. By utilizing various blur detection algorithms, the quality of an image can be assessed to determine whether it is blurry or sharp.

This research follows a structured methodology to address blurring artifacts in DBT. A significant feature extraction approach for blur detection has been developed using a hybrid Support Vector Machine-Convolutional Neural Network (SVM-CNN) model. The proposed enhancement integrates two feature vectors—one extracted from CNN features and another from a Laplacian-based Blur Detection algorithm—to improve blur classification accuracy.

This section evaluates the effectiveness of the proposed blur detection method. Based on visual interpretation, experts are required to assess whether the provided images are blurry or sharp.

15

1.

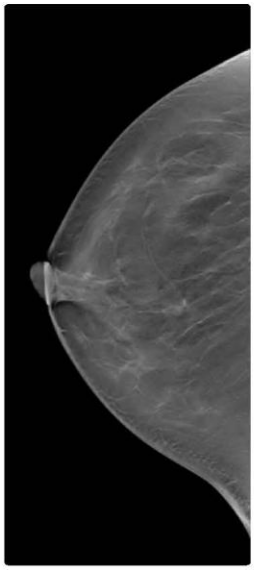

- ◯ Blur image
- ◯ Sharp image

16

2.

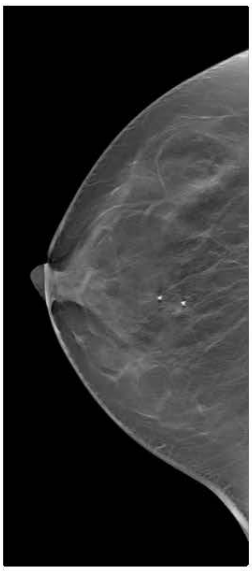

- ◯ Blur image
- ◯ Sharp image

17

3.

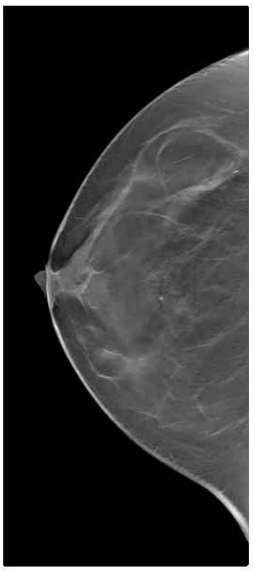

- ◯ Blur image
- ◯ Sharp image

18

4.

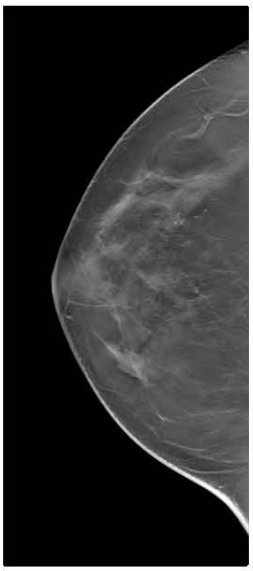

- ◯ Blur image
- ◯ Sharp image

19

5.

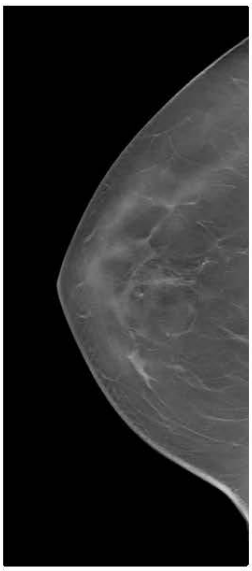

- ◯ Blur image
- ◯ Sharp image

20

6.

- ◯ Blur image
- ◯ Sharp image

21

7.

- ◯ Blur image
- ◯ Sharp image

22

8.

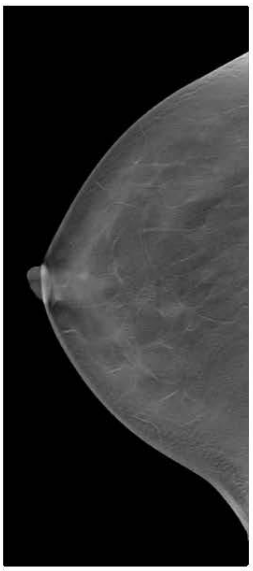

- ◯ Blur image
- ◯ Sharp image

23

9.

- ◯ Blur image
- ◯ Sharp image

24

10.

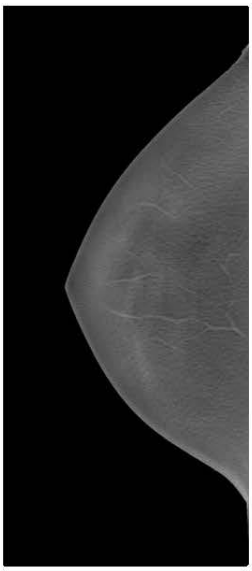

- ◯ Blur image
- ◯ Sharp image

Section C : Evaluation of Microcalcification Detection and Enhancement

Detecting microcalcifications, reconstructing clusters, and classifying them as malignant or benign are crucial for early breast cancer detection. To improve this process, a novel Deep CNN-based method has been proposed to enhance local contrast, increasing the visibility of microcalcifications and improving detection accuracy.

To ensure a fair comparison between the conventional method and the proposed approach, this section adopts a blind review concept. Experts will assess and compare original DBT images with the enhanced output images. The evaluation focuses on overall DBT image enhancement, including general image improvement and microcalcification contrast enhancement (point of interest enhancement).

Experts are invited to provide their assessments based on visual interpretation to determine the most effective enhancement method for DBT images.

25

1. Please choose the model that produces the best quality of enhanced microcalcification contrast on the DBT image while maintaining the breast tissue structure and background.

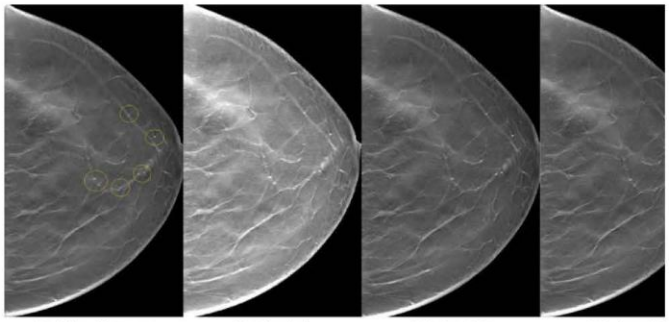

Original Image Method A Method B Method C

- ◯ Method A
- ◯ Method B
- ◯ Method C

26

2. Please choose the model that produces the best quality of enhanced microcalcification contrast on the DBT image while maintaining the breast tissue structure and background.

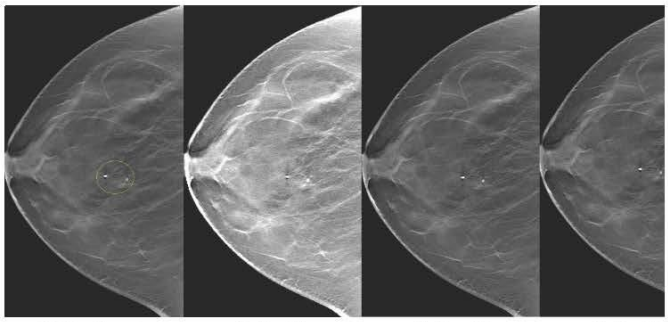

- ◯ Method A
- ◯ Method B
- ◯ Method C

27

3. Please choose the model that produces the best quality of enhanced microcalcification contrast on the DBT image while maintaining the breast tissue structure and background.

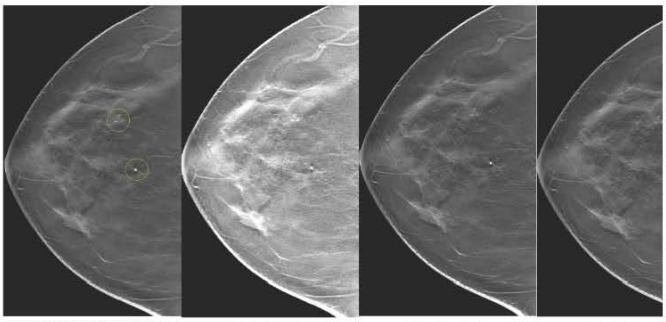

- ◯ Method A
- ◯ Method B
- ◯ Method C

28

4. Please choose the model that produces the best quality of enhanced microcalcification contrast on the DBT image while maintaining the breast tissue structure and background.

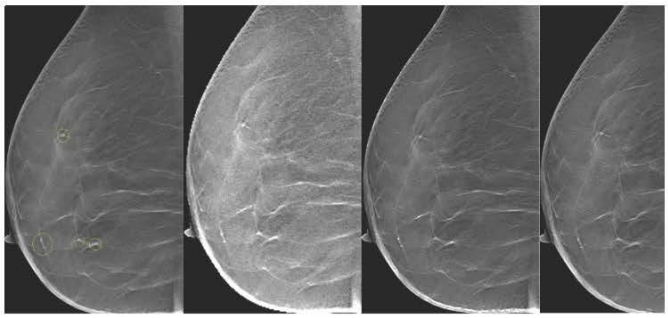

- ◯ Method A
- ◯ Method B
- ◯ Method C

29

5. Please choose the model that produces the best quality of enhanced microcalcification contrast on the DBT image while maintaining the breast tissue structure and background.

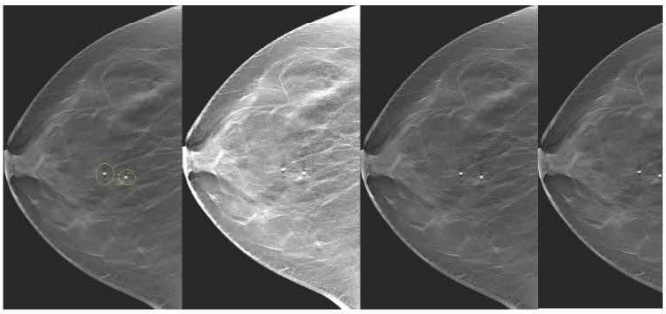

- ◯ Method A
- ◯ Method B
- ◯ Method C

30

6. Please choose the model that produces the best quality of enhanced microcalcification contrast on the DBT image while maintaining the breast tissue structure and background.

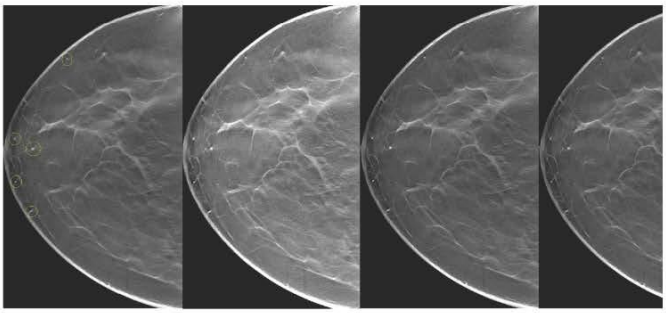

- ◯ Method A
- ◯ Method B
- ◯ Method C

31

7. Please choose the model that produces the best quality of enhanced microcalcification contrast on the DBT image while maintaining the breast tissue structure and background.

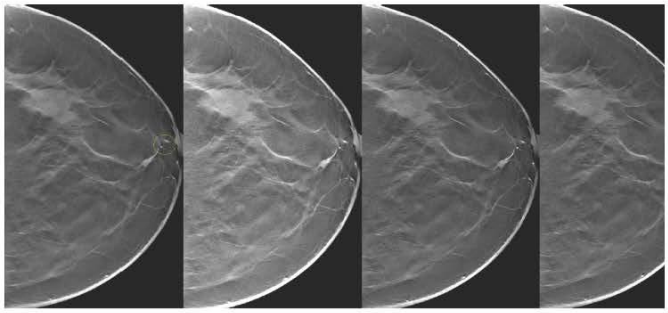

- ◯ Method A
- ◯ Method B
- ◯ Method C

32

8. Please choose the model that produces the best quality of enhanced microcalcification contrast on the DBT image while maintaining the breast tissue structure and background.

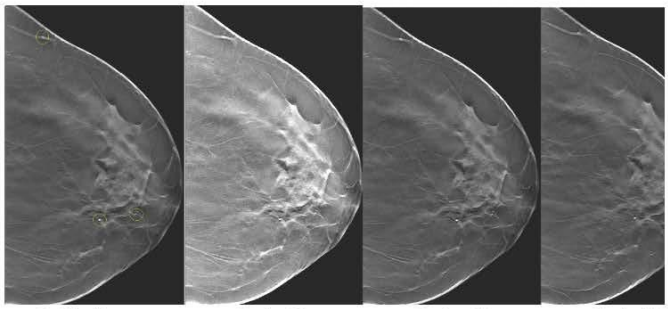

- ◯ Method A
- ◯ Method B
- ◯ Method C

33

9. Please choose the model that produces the best quality of enhanced microcalcification contrast on the DBT image while maintaining the breast tissue structure and background.

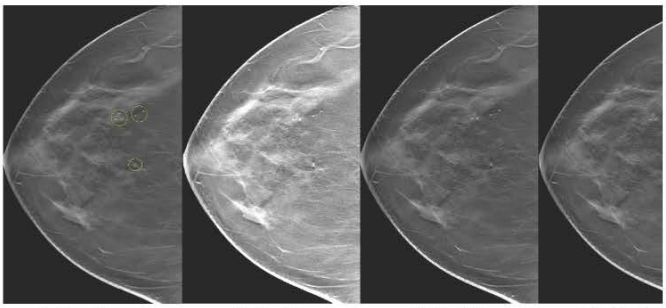

Original Image Method A Method B Method C

- ◯ Method A
- ◯ Method B
- ◯ Method C

34

10. Please choose the model that produces the best quality of enhanced microcalcification contrast on the DBT image while maintaining the breast tissue structure and background.

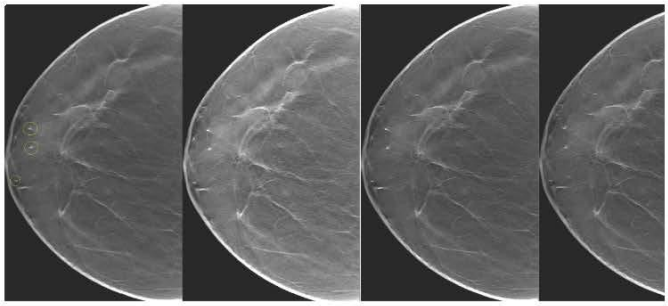

- ◯ Method A
- ◯ Method B
- ◯ Method C

35

11. Please choose the model that produces the best quality of enhanced microcalcification contrast on the DBT image while maintaining the breast tissue structure and background.

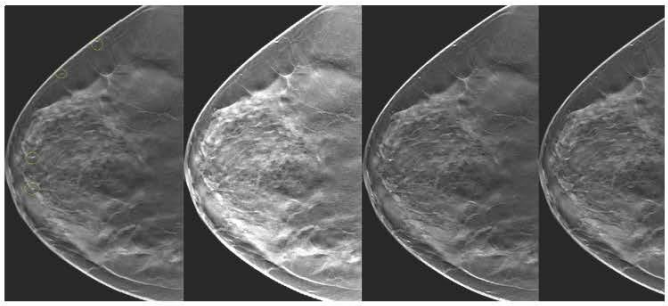

- ◯ Method A
- ◯ Method B
- ◯ Method C

36

12. Please choose the model that produces the best quality of enhanced microcalcification contrast on the DBT image while maintaining the breast tissue structure and background.

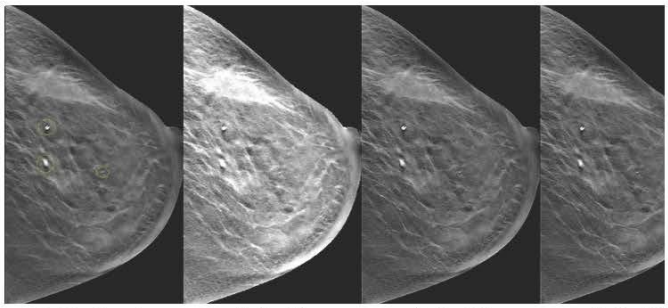

Original Image Method A Method B Method C

- ◯ Method A
- ◯ Method B
- ◯ Method C

37

13. Please choose the model that produces the best quality of enhanced microcalcification contrast on the DBT image while maintaining the breast tissue structure and background.

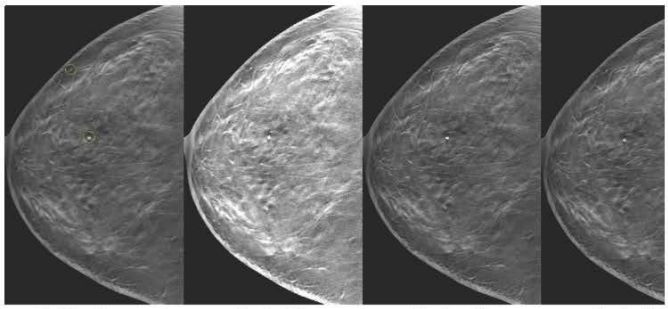

- ◯ Method A
- ◯ Method B
- ◯ Method C

38

14. Please choose the model that produces the best quality of enhanced microcalcification contrast on the DBT image while maintaining the breast tissue structure and background.

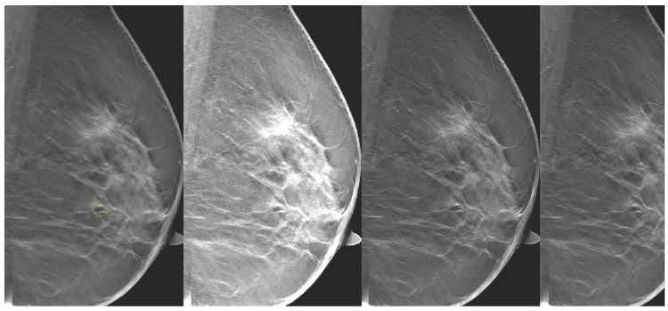

- ◯ Method A
- ◯ Method B
- ◯ Method C

39

15. Please choose the model that produces the best quality of enhanced microcalcification contrast on the DBT image while maintaining the breast tissue structure and background.

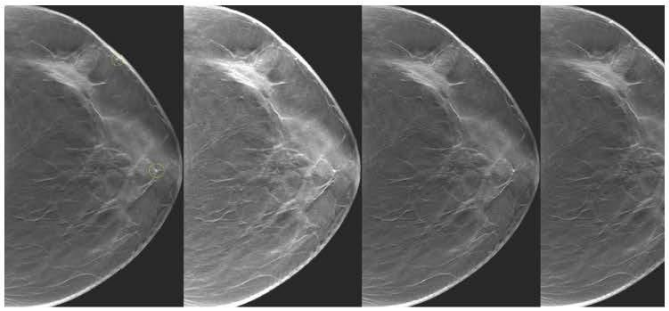

- ◯ Method A
- ◯ Method B
- ◯ Method C

40

16. Please choose the model that produces the best quality of enhanced microcalcification contrast on the DBT image while maintaining the breast tissue structure and background.

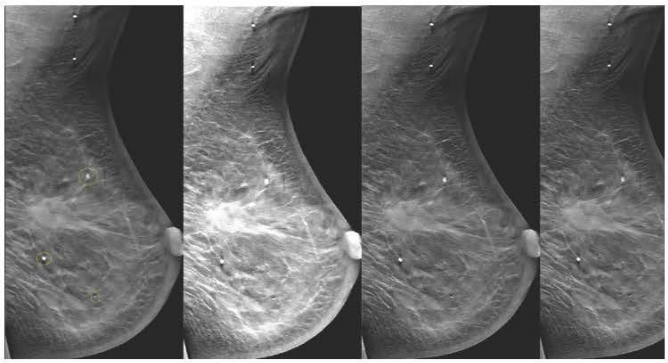

- ◯ Method A
- ◯ Method B
- ◯ Method C

41

17. Please choose the model that produces the best quality of enhanced microcalcification contrast on the DBT image while maintaining the breast tissue structure and background.

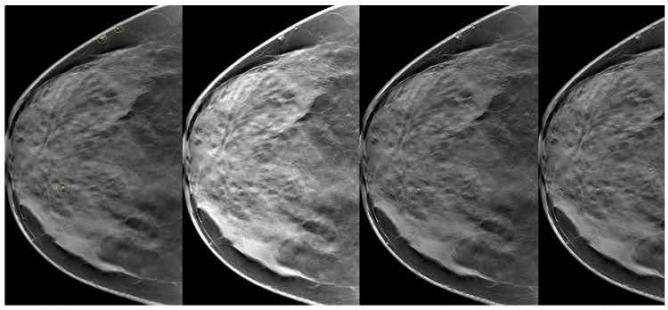

Original Image Method A Method B Method C

- ◯ Method A
- ◯ Method B
- ◯ Method C

42

18. Please choose the model that produces the best quality of enhanced microcalcification contrast on the DBT image while maintaining the breast tissue structure and background.

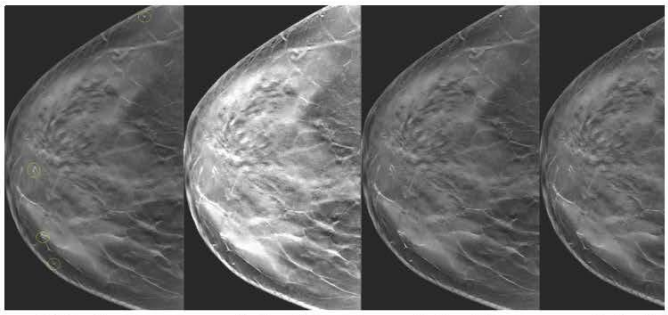

- ◯ Method A
- ◯ Method B
- ◯ Method C

43

19. Please choose the model that produces the best quality of enhanced microcalcification contrast on the DBT image while maintaining the breast tissue structure and background.

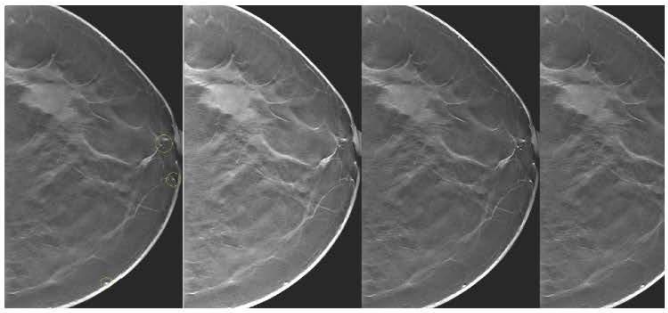

- ◯ Method A
- ◯ Method B
- ◯ Method C

44

20. Please choose the model that produces the best quality of enhanced microcalcification contrast on the DBT image while maintaining the breast tissue structure and background.

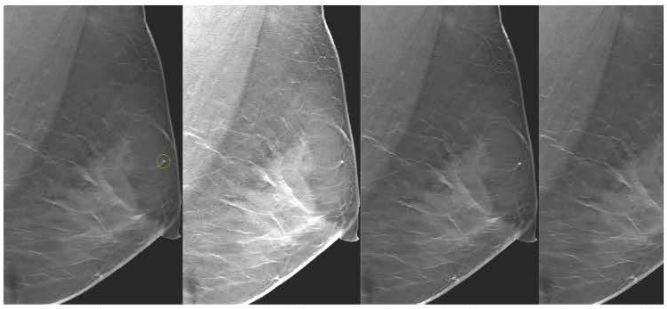

- ◯ Method A
- ◯ Method B
- ◯ Method C

Section D : Evaluation of the Proposed DBT Enhancement Pipeline

(Radiologist/Medical Expert ONLY)

45

Refer to the attached flow diagram below of the proposed DBT enhancement pipeline for breast cancer detection. The blue arrows show the flow of automated processing step for the proposed DBT enhancement, and the orange arrows show the flow of manual processing practice by human expert. Based on the flow comparison, please rate the following question based on your satisfaction levels (1= Strongly Disagree, 2= Disagree, 3= Neutral, 4= Agree, 5= Strongly Agree)

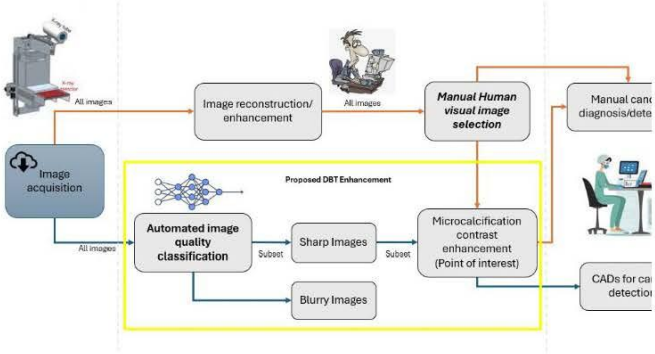

	1	2	3	4	5
The proposed process outcome will reduce radiologists' workload or enhance current workflow.	○	○	○	○	○
This proposed process outcome will contribute to the new knowledge findings on DBT.	○	○	○	○	○
The proposed process outcome will induce collaboration with current artificial intelligence technology.	○	○	○	○	○
I will use this system in the future	○	○	○	○	○

46

What are your expectations when/if using DBT CAD during your clinical assessment?

- [ ] Improved Detection Accuracy
- [ ] Enhanced Sensitivity
- [ ] Second Opinion and Support
- [ ] Efficiency and Time Savings
- [ ] Reducing False Negatives
- [ ] Standardization of Interpretation
- [ ] Other

47

Please provide additional comments/suggestions: *

APPENDIX 4

Results Summary Expert Evaluation Form for Enhancement of Digital Breast Tomosynthesis Images Using CNN

8/7/25, 4:59 PM Expert Evaluation Form for Enhancement of Digital Breast Tomosynthesis Images Using CNN

Responses Overview Closed

Responses 23

Average Time 209:11

Duration 150 Days

1. Name

23 Responses

Latest Responses
"marlina tanty ramli hamid"
"MSMK"
"SITI AISHAH"
...

4 respondents (17%) answered Dr for this question.

Jegdiswary krishinan Slamet Riyadi Norafida Bahari
Kamarul SITI AISHAH BINTI Dr BIN Mohd
binti Hasikin Aqmariah
Fadzilah Siti Nurul Ahmad
Razali Noor ramli hamid SAMSUL SETUMIN Kanafiah

2. Email

23 Responses

Latest Responses
"marlina352@uitm.edu.my"
"shukry2300@gmail.com"
"aishahmaulana@unisza.edu.my"
...

3. Occupation

Radiologist	9
Medical Dr.	1
Biomedical Engineering Expert	3
Image Processing Expert	10
Radiographer	0

https://forms.office.com/Pages/DesignPageV2.aspx?origin=NeoPortalPage&subpage=design&id=4rDLzeqfVE-GcGcnB3l62j5tamJUPptAizT1j4p... 1/13

4. Year of Expertise

23
Responses

Latest Responses
"20"
"13 years"
"13 years"
...

6 respondents (26%) answered years for this question.

22 2 years 8 12 10 13 30 15 20

5. 1. Choose the better image based on your preferences for further diagnosis.

6. 2. Choose the better image based on your preferences.

7. 3. Choose the better image based on your preferences.

8. 4. Choose the better image based on your preferences.

Option 1	1
Option 2	22

9. 5. Choose the better image based on your preferences.

Option 1	0
Option 2	23

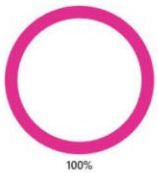

10. 6. Choose the better image based on your preferences.

Option 1	2
Option 2	21

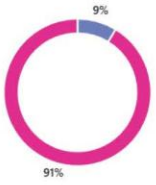

11. 7. Choose the better image based on your preferences.

Option 1	0
Option 2	23

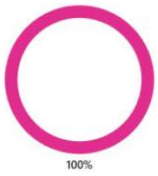

12. 8. Choose the better image based on your preferences.

Option 1	0
Option 2	23

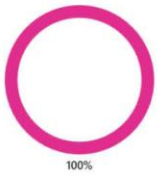

13. 9. Choose the better image based on your preferences.

Option 1	0
Option 2	23

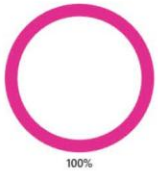

14. 10. Choose the better image based on your preferences.

Option 1	0
Option 2	23

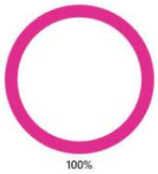

15. 1.

Blur image	15
Sharp image	8

16. 2.

17. 3.

18. 4.

19. 5.

20. 6.

21. 7.

22. 8.

23. 9.

24. 10.

25. 1. Please choose the model that produces the best quality of enhanced microcalcification contrast on the DBT image while maintaining t he breast tissue structure and background.

26. 2. Please choose the model that produces the best quality of enhanced microcalcification contrast on the DBT image while maintaining t he breast tissue structure and background.

27. 3. Please choose the model that produces the best quality of enhanced microcalcification contrast on the DBT image while maintaining t he breast tissue structure and background.

28. 4. Please choose the model that produces the best quality of enhanced microcalcification contrast on the DBT image while maintaining t he breast tissue structure and background.

29. 5. Please choose the model that produces the best quality of enhanced microcalcification contrast on the DBT image while maintaining t he breast tissue structure and background.

30. 6. Please choose the model that produces the best quality of enhanced microcalcification contrast on the DBT image while maintaining t he breast tissue structure and background.

31. 7. Please choose the model that produces the best quality of enhanced microcalcification contrast on the DBT image while maintaining t he breast tissue structure and background.

32. 8. Please choose the model that produces the best quality of enhanced microcalcification contrast on the DBT image while maintaining t he breast tissue structure and background.

33. 9. Please choose the model that produces the best quality of enhanced microcalcification contrast on the DBT image while maintaining t he breast tissue structure and background.

34. 10. Please choose the model that produces the best quality of enhanced microcalcification contrast on the DBT image while maintaining the breast tissue structure and background.

35. 11. Please choose the model that produces the best quality of enhanced microcalcification contrast on the DBT image while maintaining the breast tissue structure and background.

36. 12. Please choose the model that produces the best quality of enhanced microcalcification contrast on the DBT image while maintaining the breast tissue structure and background.

37. 13. Please choose the model that produces the best quality of enhanced microcalcification contrast on the DBT image while maintaining the breast tissue structure and background.

38. 14. Please choose the model that produces the best quality of enhanced microcalcification contrast on the DBT image while maintaining the breast tissue structure and background.

39. 15. Please choose the model that produces the best quality of enhanced microcalcification contrast on the DBT image while maintaining the breast tissue structure and background.

40. 16. Please choose the model that produces the best quality of enhanced microcalcification contrast on the DBT image while maintaining the breast tissue structure and background.

41. 17. Please choose the model that produces the best quality of enhanced microcalcification contrast on the DBT image while maintaining the breast tissue structure and background.

42. 18. Please choose the model that produces the best quality of enhanced microcalcification contrast on the DBT image while maintaining the breast tissue structure and background.

43. 19. Please choose the model that produces the best quality of enhanced microcalcification contrast on the DBT image while maintaining the breast tissue structure and background.

44. 20. Please choose the model that produces the best quality of enhanced microcalcification contrast on the DBT image while maintaining the breast tissue structure and background.

45. Refer to the attached flow diagram below of the proposed DBT enhancement pipeline for breast cancer detection. The blue arrows show the flow of automated processing step for the proposed DBT enhancement, and the orange arrows show the flow of manual processing practice by human expert. Based on the flow comparison, please rate the following question based on your satisfaction levels (1= Strongly Disagree, 2= Disagree, 3= Neutral, 4= Agree, 5= Strongly Agree)

46. What are your expectations when/if using DBT CAD during your clinical assessment?

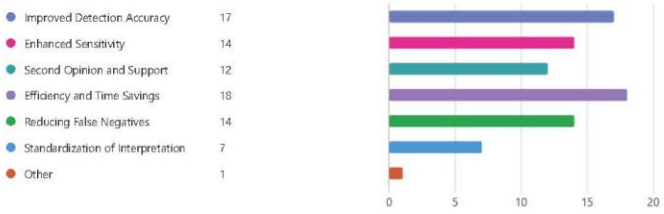

47. Please provide additional comments/suggestions:

23
Responses

Latest Responses
"NA"
"try enhancing/aid lymph node detection"
"NO COMMENT"
...

6 respondents (26%) answered image for this question.

AUTHOR'S PROFILE

Nur Athiqah Harron obtained her Bachelor of Electrical Engineering (Computer) from Universiti Teknologi Malaysia in 2007 and MSc in Electronic System Design Engineering from Universiti Sains Malaysia in 2011. She is currently a senior lecturer at Universiti Teknologi MARA (UiTM), Permatang Pauh campus, Pulau Pinang. She is attached to the Department of Computer in Electrical Engineering Studies. She began her PhD at UiTM in March 2021. Her research interests include computer applications, Internet of Things (IoT), artificial intelligence, biomedical engineering, and image processing.

LIST OF PUBLICATIONS:

Grant

Title: A New Cascaded Convolutional Neural Network Model for Deblurring and Contrast Enhancement of Extremely Dense Breast Tissue in Digital Breast Tomosynthesis Images.
Code/Amount: FRGS/1/2021/TK0/UITM/02/19 - RM 90,500.
From: Fundamental Research Grant (FRGS), Ministry of Higher Education, Malaysia.
Nur Athiqah Harron, Iza Sazanita Isa, Siti Noraini Sulaiman, Mohd Ikmal Fitri Maruzuki, Noor Khairiah A. Karim, and Yessi Jusman.
Duration: 6 September 2021 – 7 August 2023 (Completed)

Refereed Journal

1. **Nur Athiqah Harron**, Siti Noraini Sulaiman, Muhammad Khusairi Osman, Iza Sazanita Isa, Noor Khairiah A. Karim, and Mohd Ikmal Fitri Maruzuki. "Deep Learning Approach for Blur Detection of Digital Breast Tomosynthesis Images", Journal of Electrical and Electronics Systems Research. DOI: https://doi.org/10.24191/jeesr.v21i1.006. **MyCite Indexed, Status: Published.**

2. **Nur Athiqah Harron**, Siti Noraini Sulaiman, Muhammad Khusairi Osman, Noor Khairiah A. Karim, and Iza Sazanita Isa. "Laplacian-based Blur Detection Algorithm for Digital Breast Tomosynthesis Images in Improving Breast Cancer Detection", The Journal of Health and Translational Medicine. Special Issue: Jummec 2023: 1. DOI: https://doi.org/10.22452/jummec.sp2023no1.15. **Scopus Indexed, Status: Published.**

3. Syafiqah Aqilah Saifudin, Siti Noraini Sulaiman, Muhammad Khusairi Osman, Noor Khairiah A. Karim, Iza Sazanita Isa, **Nur Athiqah Harron**. "Adaptive fuzzy weighted median filter for microcalcifications detection in digital breast tomosynthesis images", Indonesian Journal of Electrical Engineering and Computer Science. Vol. 34, No. 1, April 2024, pp. 197~209. **Scopus Indexed, Status: Published.**

Book Chapter

Nur Athiqah Harron, Siti Noraini Sulaiman, Muhammad Khusairi Osman, Noor Khairiah A. Karim, and Iza Sazanita Isa. "CNN-SVM with data augmentation for robust blur detection of digital breast tomosynthesis images", for Intelligent Multimedia Signal Processing for Smart Ecosystems: Springer Book Chapter (2023). **Scopus Indexed, Status: Published.**

Proceedings

1. **Nur Athiqah Harron**, Nadzmi Faridzuan Osman, Siti Noraini Sulaiman, Noor Khairiah A. Karim, Ahmad Puad Ismail, and Zainal Hisham Che Soh. "An Image Denoising Model using Deep Learning for Digital Breast Tomosynthesis Images", in 2022 IEEE 13th Control and System Graduate Research Colloquium (ICSGRC), 23 July 2022. **Scopus Indexed, Status: Published.**

2. Siti Noraini Sulaiman, Muhammad Hanzalah Normazli, **Nur Athiqah Harron**, Noor Khairiah A. Karim, Khairul Azman Ahmad, and Zainal Hisham Che Soh. "A Convolutional Neural Network Model for Image Enhancement of Extremely Dense Breast Tissue in Digital Breast Tomosynthesis Images", in 2022 IEEE 12th International Conference on Control System, Computing and Engineering (ICCSCE), 21–22 October 2022. **Scopus Indexed, Status: Published.**

3. **Nur Athiqah Harron**, Siti Noraini Sulaiman, Muhammad Khusairi Osman, Noor Khairiah A. Karim, Iza Sazanita Isa, and Yessi Jusman. "Deep Learning Optimizer Evaluation in Blur Detection of Digital Breast Tomosynthesis Image using CNN Constructed from Scratch", in 2023 International Conference on Artificial Intelligence Robotics, Signal and Image Processing (AIRoSIP), 9-10 August 2023. **Scopus Indexed, Status: Published.**

4. **Nur Athiqah Harron**, Siti Noraini Sulaiman, Muhammad Afiq Iqmal Mohammad Nizam, Noor Khairiah A. Karim, Adi Izahar Che Ani, and Syafiqah Aqilah Saifudin. "Microcalcification Detection for Digital Breast Tomosynthesis Images Using Faster-RCNN", in 2024 IEEE 14th International Conference on Control System, Computing and Engineering (ICCSCE), 23–24 Aug 2024. **Scopus Indexed, Status: Published.**

Copyright/Patent

1. Enhancement of Extremely Dense Breast Tissue Digital Breast Tomosynthesis Images based on Deep Convolutional Neural Network Approach.
   - No. LY2022P05098, (2022). Intellectual Property Corporation Malaysia (MyIPO).

2. Integrating CNN-SVM and Fourier Operator: A Novel Hybrid Feature Approach for Detecting Blur in Digital Breast Tomosynthesis Images.
   - No. LY2024P03331, (2024). Intellectual Property Corporation Malaysia (MyIPO).

Awards

1. **Nur Athiqah Harron**, Siti Noraini Sulaiman, Muhammad Khusairi Osman, Iza Sazanita Isa, Noor Khairiah A. Karim, and Siti Azura Ramlan. "AI-Enhanced DBT: Blur Reduction and Improved Microcalcification Detection via Hybrid CNN-SVM Model", in 2nd Artificial Intelligence & Internet of Things International Innovation Expo 2025 (AIoTIE 2025). **Titanium Special Award Winner & Gold Medal**

2. **Nur Athiqah Harron**, Siti Noraini Sulaiman, Muhammad Khusairi Osman, Iza Sazanita Isa, and Noor Khairiah A. Karim. "Automated Blur Detection Of Digital Breast Tomosynthesis Images Using Deep Learning Approach", in Penang International Invention, Innovation and Design 2023 (PIID2023). **Silver Medal.**

3. **Nur Athiqah Harron**, Siti Noraini Sulaiman, Muhammad Khusairi Osman, Noor Khairiah A. Karim, Iza Sazanita Isa, and Syafiqah Aqilah Saifudin. "Optimization Of Blur Detection In Digital Breast Tomosynthesis Images Using Deep Learning Approach", in SIRIM Invention, Innovation & Technology Expo 2023 (Si2Te 2023). **Bronze Medal.**